# Chapter 3

# Seismic Reflection Data Acquisition and Processing

## 3.1 Introduction

Seismic reflection and refraction data are crucial in understanding the evolution of continental margins. Geoscience Australia (GA) surveys GA-228 and GA-229, the primary seismic reflection data used in this study, were completed in 2000-01 and 2001-02. Prior to this, available data acquired by surveys conducted by the Institut Francais du Pétrole (IFP) in 1982 (survey ATC82), the United States Geological Survey (USGS) in 1984 (survey L184), and the Japanese National Oil Company (JNOC) in 1982, 1983 and 1995 (surveys TH82, TH83 and TH95).

Field data from survey L184 were requested and subsequently made available by the USGS. Field data from the IFP survey ATC82 could not be obtained. However, stacked sections of Multi-Channel Seismic (MCS) data from surveys ATC82, TH82, TH83 and TH95 were obtained through the Scientific Committee on Antarctic Research (SCAR), Seismic Data Library System (SDLS) branch, at the British Antarctic Survey (BAS), Cambridge.

This chapter outlines the survey acquisition parameters and seismic processing sequence for the GA, USGS, and IFP data. The processing and interpretation of sonobuoy refraction data is also briefly outlined. The USGS MCS data were reprocessed as part of this project. This was completed in an attempt to provide increased coverage of the upper continental slope off east Wilkes Land, and to determine if imaging improvements are possible through the application of seismic processing techniques that have become common since the original processing of these data in 1984. Stacking velocities and unreversed sonobuoy refraction data were used to create velocity models to facilitate two-way-time (TWT) to depth conversion of the USGS and GA data.

## 3.2 Geoscience Australia Surveys GA-227, GA-228 and GA-229

### 3.2.1 Introduction

Geoscience Australia (GA)[1], acquired over 20 000 km of MCS, gravity and magnetic data, from 2000-2002, on the East Antarctic margin, 38-162°E. This two-season survey (GA-228 and GA-229), represents the most extensive MCS survey on the Antarctic margin. A further survey (GA-227) was completed in 2000-01 to provide bathymetric and high-speed (low-fold and small source) seismic data between the shelf edge and the southern extent of the GA-228 and GA-229 survey lines. Negotiated access to these data provides the unique opportunity to carry out an integrated geophysical study on this relatively unexplored rifted margin. The GA-228, GA-229 and GA-227 survey lines, and major geographic and morphologic features of East Antarctica are illustrated in Figure 3.1.

GA-228 and GA-229 data were acquired on transects approximately perpendicular to the Antarctic margin from the shelf edge or the surveying limits imposed by sea ice (whichever was the furthest seaward, i.e. no attempts were made to survey the continental shelf). Seismic reflection data were recorded 36 fold, and in addition, gravity and bathymetric data were recorded port-to-port and magnetic data were acquired coincident with multi-channel seismic (MCS) survey lines. Over 120 sonobuoys were also deployed during surveying, of which 99 recorded refractions and/or wide-angle reflections.

The catalyst for the acquisition of this extensive dataset was the United Nations Convention on the Law of the Sea (UNCLOS) Treaty of 1999. For Law of the Sea purposes, MCS data are required at distances of not greater than 60 nautical miles, this controlled the line density in the survey region. No tie- or cross-line was included in the survey design as under the UNCLOS treaty the lateral correlation of MCS data is not significant. No attempt was made to acquire deep seismic data landward of the shelf break in surveys GA-228 and GA-229 as these data are also not required for Law of the Sea purposes. Despite these drawbacks, this data set remains unrivalled in the realm of Antarctic geoscience and provides many exciting research opportunities.

The focus of this thesis is the Wilkes Land margin. Twelve transects across the Wilkes Land margin were completed during survey GA-228 and a number of shorter lines and line extensions were completed during survey GA-229.

[1]Formerly Australian Geological Survey Organisation (1991-2001), and the Bureau of Mineral Resources, Geology and Geophysics (pre 1991).

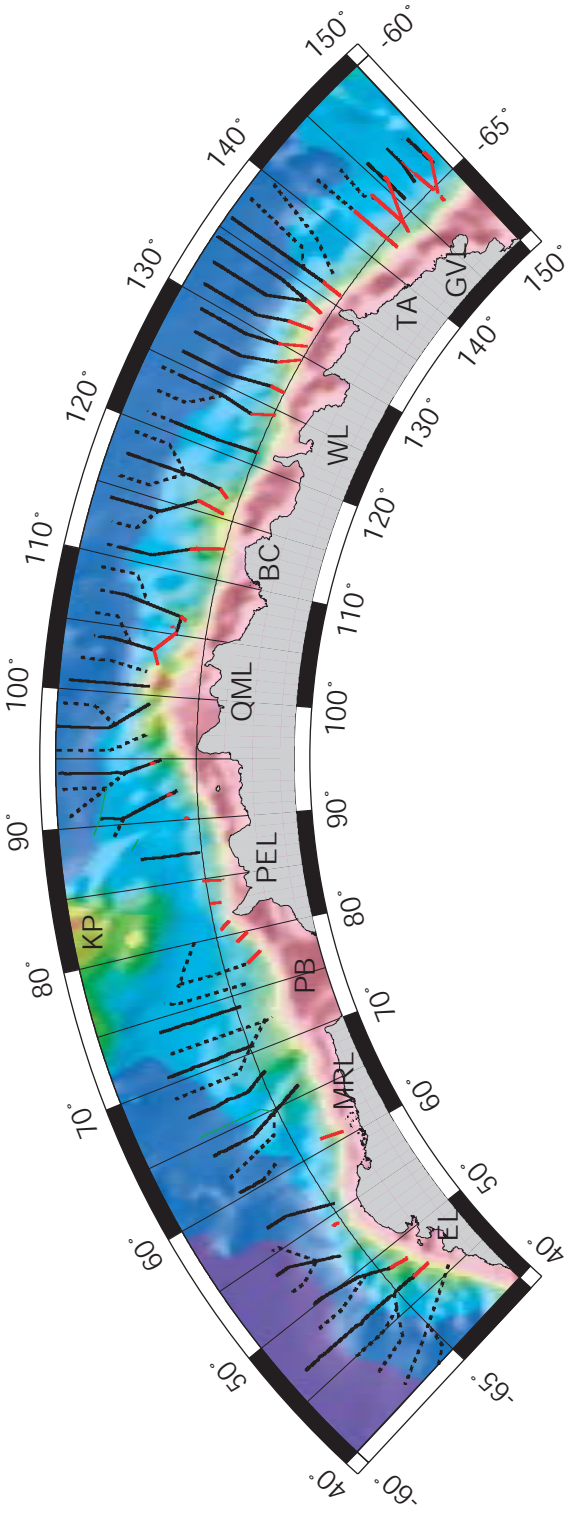


Figure 3.1: GA-228 (black), GA-229 (dashed), and GA-227 (red) survey lines on the East Antarctic margin, geographical regions are labelled. The Wilkes Land sector of East Antarctica is conjugate to the southern Australian margin. EL = Enderby Land, MRL = Mac.Robertson Land, PB = Prydz Bay, QML = Queen Mary Land, PEL = Princess Elizabeth Land, BC = Budd Coast, WL = Wilkes Land, TA = Terre Adélie, GV = George V Land.

### 3.2.2 Survey GA-227

A bathymetry survey was conducted by the *MV Polar Duke* off the Wilkes Land margin during the Austral summer of 2000-01, survey GA-227. The bathymetry survey lines extend from the shelf-break for 50-200 km downslope (average 80 km). A total of 3425 km of combined bathymetry and four-fold seismic data were recorded, Figure 3.1. A further 1183 km of bathymetry-only profiles were recorded when ice conditions prevented the deployment of seismic equipment. Survey equipment and parameters utilised during survey GA-227 are summarised in Table 3.1.

| | |
|---|---|
| recording system | 24 channel OYO digital recorder |
| streamer length | 300 m |
| group interval | 12.5 m |
| hydrophones per group | 3 |
| source | airguns |
| source volume | 6 litres |
| SP interval | 37.5 m |
| record length | 6-9 s |
| echo-sounder | Simrad EA500 operating at 12 and 18 kHz |

Table 3.1: Survey parameters and equipment utilised aboard the *MV Polar Duke* during bathymetry survey GA-227.

Survey GA-227 data were processed 'in house' at GA. A basic processing sequence was applied to these data as only very shallow penetration was achieved by the relatively small source and the short streamer. Normal Moveout Correction (NMO) was applied using a water bottom velocity function. Trace editing was also completed, and notch and dip filters applied. The data were subsequently stacked and migrated using a finite difference algorithm [F. Kroh, pers. comm.].

### 3.2.3 Surveys GA-228 and GA-229

#### Acquisition

Surveys GA-228 and GA-229 were completed during the austral summers of 2000-01 and 2001-02 respectively, aboard the *R/V Geo Arctic*, operated by geophysical contractors, *Fugro Geoteam AS*. The surveys acquired 10574 km and 9598 km of 36-fold MCS data respectively (a total 20172 km), along 73 lines (Figure 3.1). MCS Data were recorded 36-fold from a 3600 m streamer (comprising 288 channels) and a 60 litre tuned airgun

array, with a record length of 16 s, as detailed in Table 3.2. Survey geometry is illustrated in Figure 3.2.

| | |
|---|---|
| recording system | 288 channel MSX recorder |
| streamer length | 3600 m |
| group interval | 12.5 m |
| hydrophones per group | 14 |
| source volume | 60 litres |
| SP interval | 50 m |
| record length | 16 s |

Table 3.2: Survey equipment utilised aboard the *R/V Geo Arctic* during the deep-seismic surveys.

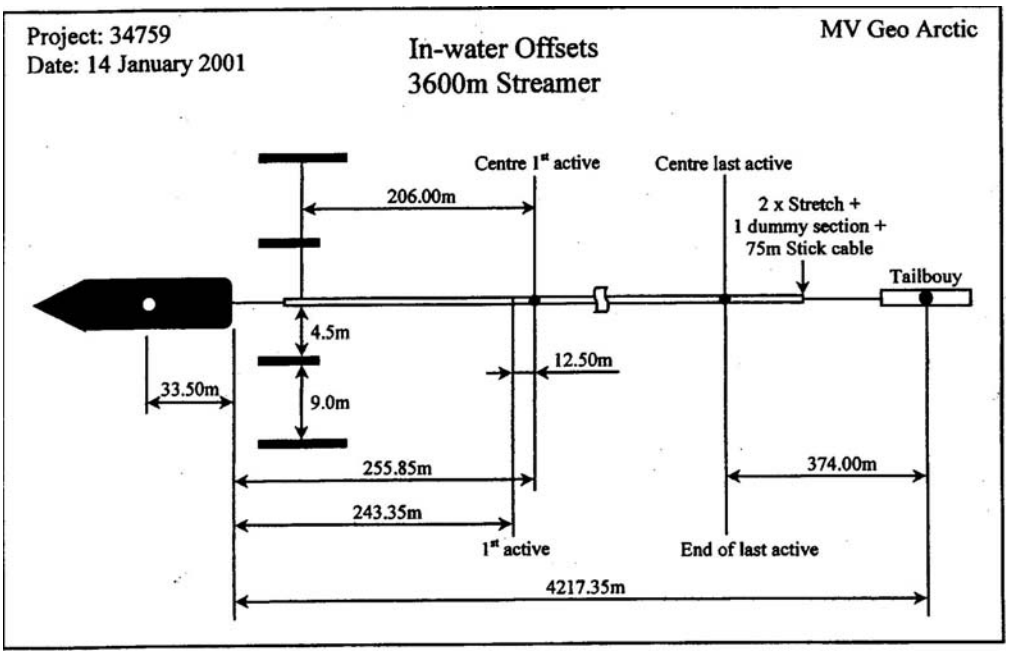


Figure 3.2: Schematic illustration of the towing configuration for surveys GA-228 and GA-229.

Twelve, approximately north-south, transects from the abyssal plain to the continental slope or lower rise of Wilkes Land (110-137°E) were completed during survey GA-228, GA-228_18 to GA-228_29. These lines are separated by ~90 km and vary in length from 300 to 450 km. A similar transect was completed during survey GA-229 off east Wilkes Land or Terre Adélie, GA-229_06, as were a number of shorter lines over the outer rise and abyssal plain which tie, at their landward extents, to GA-228 survey lines (shorter

lines were completed to satisfy particular Law of the Sea requirements).

**Processing**

Seismic data were processed on-board to stacked sections during both survey GA-228 and GA-229, Table 3.3 outlines the details of this processing. Brute stacks were created in real-time to allow quality control of data, and for analysis of regional geological setting.

| | |
|---|---|
| 1 | reformat from SEGD to Disco format |
| 2 | designature into a minimum phase wavelet |
| 3 | bandpass filter 6-90 Hz |
| 4 | resample to 4 ms |
| 5 | trace decimations (2:1 sum with NMO) |
| 6 | amplitude recovery |
| 7 | velocity analysis at 4 km intervals |
| 8 | linear mute offset 250 to 3780 m, 0-3000 s |
| 9 | 36-fold stack |
| 10 | gun and cable static correction (12 ms) |

Table 3.3: Processing stream applied on-board the *R/V Geo Arctic* to seismic reflection data during surveys GA-228 and GA-229.

Pre-stack processing, involving greater parameter testing was repeated on selected portions of a number of lines from survey GA-228. This was carried out to determine to what extent imaging improvements were possible with processing under less restrictive time constraints. Processing was completed by *Robertson Research Ltd.* with supervision from Fred Kroh, Geoscience Australia. Extensive testing of the following parameters was completed; gain recovery, demultiple techniques (F-K, F-X, Radon, Radon/F-K, Radon/F-X), predictive pre-stack deconvolution, inner and outer trace muting, dip moveout, post-stack deconvolution, migration velocities, post migration signal enhancement (i.e. Tau-p filter), bandpass filters, and post-stack scaling.

A brief outline of the applied processing steps and parameters follows. The parameters were varied spatially according to water depth for processes such as mutes, predictive deconvolution, Tau-p filter, bandpass filter and percentages of reduction in migration velocity functions. The parameters outlined below are applicable for two-way time (TWT) water bottom time at 4 s.

**Pre-Filter**

A minimum phase Butterworth filter of 5-125 Hz, with a slope of 6 dB/octave at the low

end and out at the high end was applied to the whole data set to remove low frequency noise.

**Gain Recovery**

The following gain functions were applied:

$$Gain(dB) \quad = \quad 1.0(t) + 56.0$$

and

$$Gain(dB) \quad = \quad 8.0(t)$$

where t = TWT. The gain levels were held constant after 12 s and 4 s for the first and second gain functions respectively.

**Designature**

Far signature wavelet information was supplied via GA to convert the data into minimum phase wavelet.

**Multi-Channel Filter**

A symmetrical -1250 m/s to +1250 m/s pass velocity F-K filter was applied to the data using a $4^{th}$ power cosine taper. A 43-trace operator was utilised and automatic gain control (AGC), window size = 300 ms, was applied before and removed after filtering.

**Receiver Array Simulation**

A weighted 3 trace mix was performed down normal moveout (NMO) curves. Alternative traces were output to give 144 traces with a group interval of 25 m.

**Common Mid-Point Gather**

The 144 trace array simulated shot records were sorted into 36 fold common mid-point (CMP) gathers, with a spacing of 12.5 m.

**Preliminary First Pass and First Pass Velocity Analysis**

Preliminary first pass velocities were determined using interactive *Robertson's* software. Each analysis comprised an 18-CMP stacked panel, repeated 11 times with varying NMO velocity functions ranging from ±5%, ±10%, ±16%, ±24%, and ±40% increments from a central function. The central velocity function is the interpolated value of the regional velocity trend based on water depths. Analyses were performed at 12 km intervals.

A mild F-K multiple attenuation filter was applied to enhance primary energy before further analyses, using slowed preliminary velocity functions of -12% at 0 s, -16% at 3.5 s and -24% at 6 s. This was applied for analysis only. The above velocity analysis process was then repeated using the a central velocity function as determined from the preliminary first pass velocity analysis. Analyses were completed at 4 km intervals by *Robertson's* staff.

**Radon Demultiple**

After the application of a 300 ms removable AGC function, 4 adjacent NMO corrected (using 95% of the first pass velocities) CMP gathers were merged and transformed into the Tau-p (radon) domain. An optimum transform range of -800 to 1600 ms was used to enable a complete range of the anticipated multiples' parabolic moveout to be analysed, delineated from primaries, and filtered. Modelled multiple arrival energy was then subtracted from the super-gathers to attenuate the multiples. The filtered super-gathers were then transformed back into the space-time (x-t) domain and split into their original fold gathers and the AGC and NMO corrections removed.

**F-K Multiple Attenuation**

Filtering in the F-K domain was tested as a means of multiple attenuation. However, improved results were achieved by using the F-X approach, whereby the impulse response of the F-K filter is generated by populating a model F-K space with 1's and designing a filter to attenuate the required areas of F-K space. The reverse fast fourier transforms (FFT) are applied to generate the time domain impulse response of the F-K filter. The CMP gathers can then be filtered by convolution (space domain) or multiplication (frequency domain) of the impulse response and the CMP gather. NMO was performed using the same percentages of slowed primary first pass velocity as in the Radon method.

**Dip Moveout**

Dip Moveout (DMO) achieves partial migration, whereby traces with common midpoints, but different source-receiver offsets, relate to the same sub-surface locations after DMO, for all dips. Following DMO, all reflection events appear, for the purposes of NMO correction, to have originated from horizontal reflectors. Therefore, optimum stack response for all reflector dips can be obtained from conventional moveout corrections based on velocity functions undistorted by reflector dips.

**Second Pass Velocity Analysis and NMO**

Final stacking velocities were determined using a similar process to that outlined above for the first pass analysis. However, analyses were completed at 2 km intervals and were interpreted by *Robertson's Ltd.* staff and quality controlled by Fred Kroh, GA. NMO was performed using the second pass, interpreted velocity functions.

**Mute**

A post-NMO outer trace mute was applied to remove coherent noise from outer traces, and to reduce contamination from NMO induced stretching at far offsets.

**CMP Stack**

Traces within each CMP gather were summed using $1/\sqrt{N}$ stack compensation. The maximum resulting fold was 36 with a CMP interval of 12.5 m.

**Statics**

A +13 to +17 ms static compensation for gun and cable depths was applied.

**Pre-Migration Scaling**

To compensate for large lateral variations in amplitude, a dual-window AGC of 1000 and 400 ms window lengths was used for pre-migration scaling.

**Migration**

A $3^{rd}$ order 65° finite difference algorithm was utilised for migration. The migration model velocities were based on laterally smoothed stacking velocities with the percentages of reduction outline in Table 3.4.

| Time (ms) | % of velocity |
|---|---|
| 7,000 | 100 |
| 10,000 | 90 |
| 16,000 | 75 |

Table 3.4: Percentage velocity reduction as a function of time as used for migration of GA-228 and GA-229 data.

**Post-Stack Scaling**

A dual window, time variant AGC function was used for post-stack scaling prior to display. The negative effects normally associated with AGC are avoided by employing two different window lengths to determine the amplitude model (using the minimum of the two mean amplitudes determined at each sample), then conditioning the model by a weighted mix with the amplitude model derived from a single window per trace.

Comparison of on-board processed with re-processed stacked sections indicates relatively minor imaging improvements. Further multiple attenuation was achieved, however, it was determined that this could be achieved with the post-stack processing sequence outlined above. Accordingly, post-stack processing was performed on all on-board processed data (surveys GA-228 and GA-229) to produce final, time migrated, stacked sections. It was determined that no further, significant improvements could be achieved by further processing of GA survey MCS data as part of this study.

### 3.2.4 Sonobuoy Refraction Data

Non-reversed, expendable sonobuoys were deployed to record refraction and wide-angle reflection data during surveys GA-228 and GA-229. A total of 19 sonobuoys deployed on the Wilkes Land margin successfully recorded either refractions and/or wide-angle reflections. All sonobuoys were modelled at GA using *SIGMA* ray-tracing software developed by the Geological Survey of Canada (Seismic Image Software, 1995). The modelling methodology is outlined in detail by Stagg *et al.* [in press]. An example of sonobuoy data

recorded over stretched continental crust is shown in Figure 3.3. Wide-angle reflections and refractions were used to determine velocities in the sedimentary section. Crustal velocities were typically only indicated by refractions.

Seismic reflection data and stacking velocities were utilised in the creation of a 'first-pass' velocity model. The model was then iteratively altered to fit refractions and reflections from sonobuoy data by adjusting layer velocities and depths. Due to the excellent depth penetration of the seismic reflection data, constraints were placed on the geometries of many refractors, thereby partially offsetting the shortcomings associated with the sonobuoys being non-reversed [Stagg *et al.*, in press].

In some locations, different velocities were required at the top and bottom of a velocity layer to model both wide-angle reflections and refractions. This is because wide-angle reflections provide an interval velocity for the layer above a reflection, whereas refractions provide a velocity at a velocity boundary. However, accurately constraining these gradients is not possible with unreversed sonobuoys and in the absence of velocity-depth constraints from well data. Therefore, all modelling was conducted assuming fixed interval velocity layers rather than with velocity gradients. The result of assuming discrete interval velocities in models is that interface depths are under-estimated, by up to 15% in oceanic crust [White *et al.*, 1992].

### 3.2.5 Velocity Models

Semblance analyses of common mid-point (CMP) supergathers were completed every 4 km for survey GA-228 and GA-229 data as part of the on-board processing sequence (and every 2 km for re-processed data from GA-228) as outlined above. An example of a semblance plot from Line 228_26 is illustrated in Figure 3.4. Stacking velocities were converted to interval velocities using the Dix equation (Figure 3.5). A comparison of sonobuoy derived refraction velocities and interval velocities is also shown in Figure 3.5. The independently derived velocity profiles correspond very closely for the sonobuoy located over thinned continental crust. The refraction velocities modelled over oceanic crust are slightly lower than derived from semblance analysis, this may be a function of the discrete interval velocities assumed in refraction modelling (as discussed above).

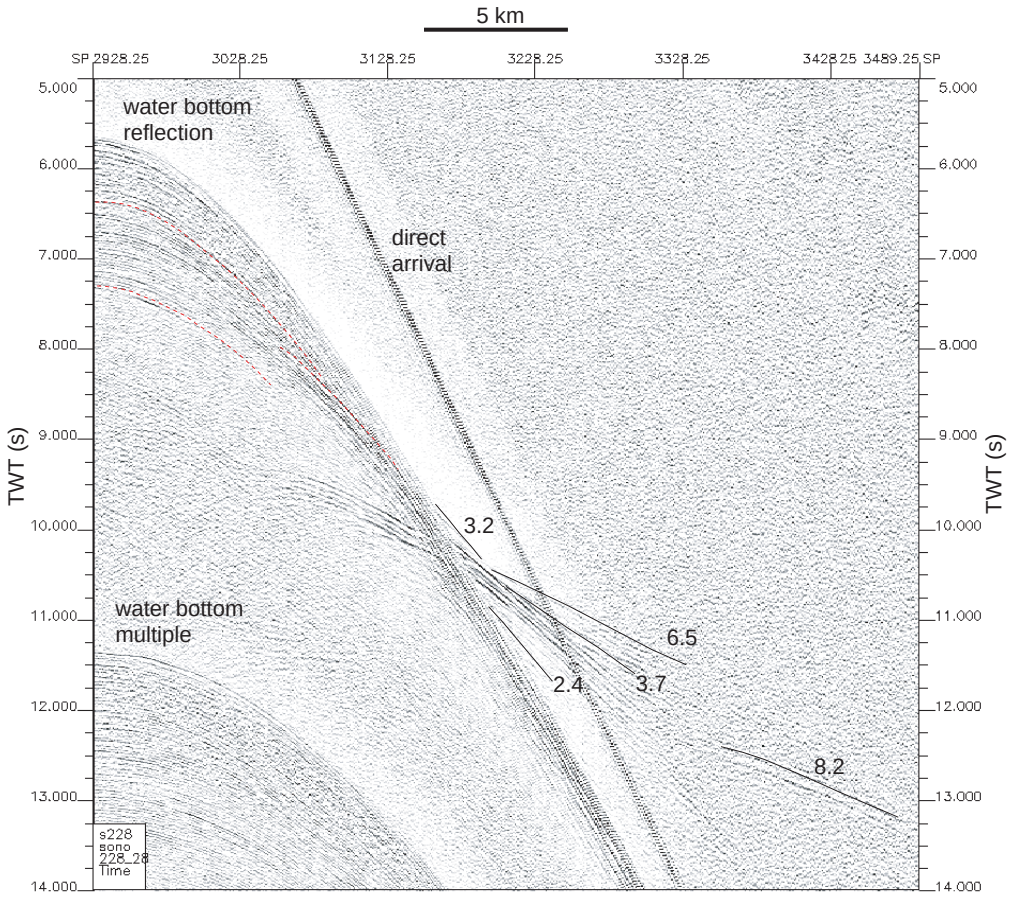


Figure 3.3: Recorded data from sonobuoy 228_21, Line 228_28. Refractions are recorded (black solid lines) along with direct arrivals, primary reflections (e.g. dashed red lines) and multiples. Refractor velocities are in $\times 10^3$m/s.

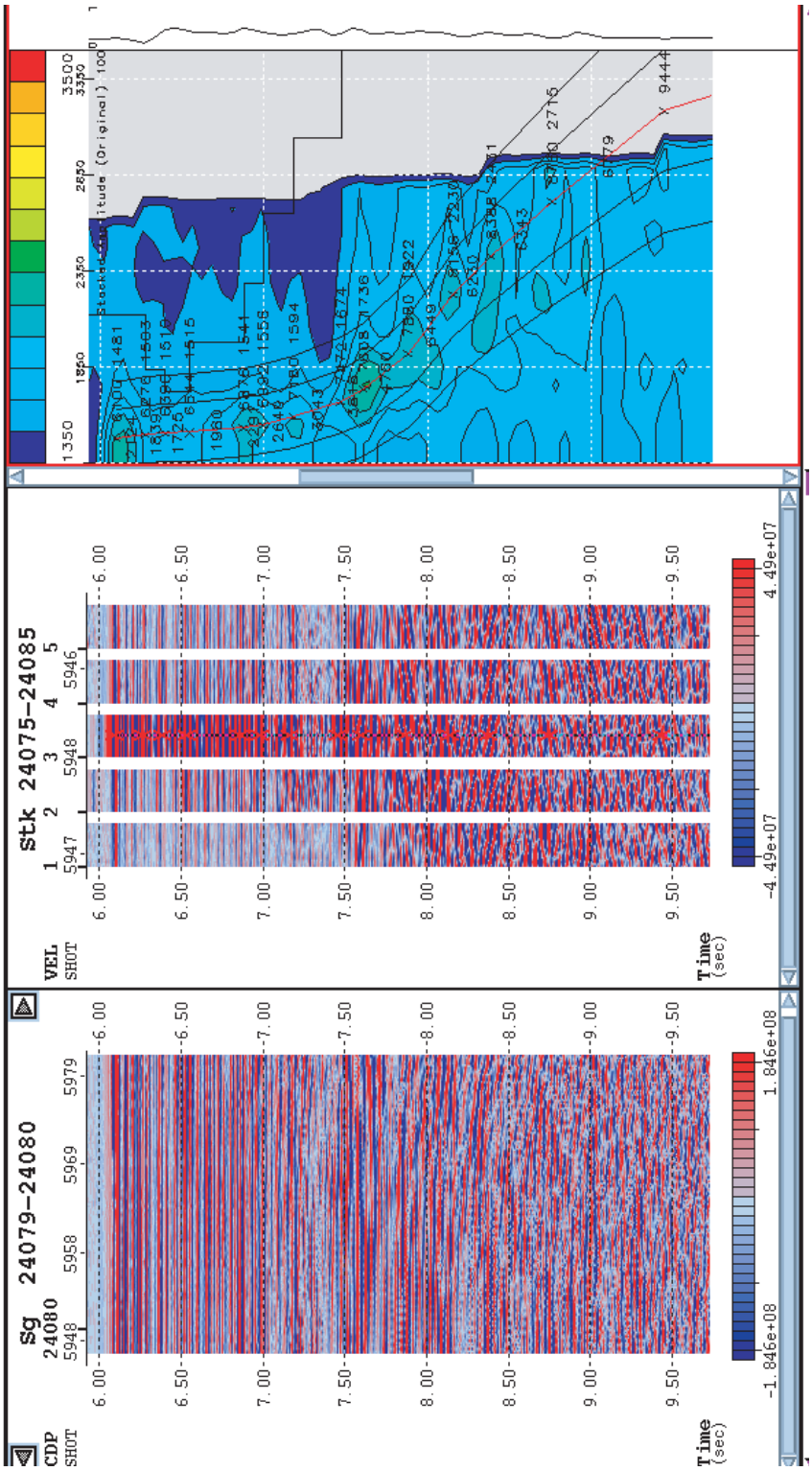


Figure 3.4: Left panel shows a 2 CMP supergather NMO corrected using the picked velocity profile, marked with X's in the right panel. The centre panel shows mini-stacks created with decreased (mini-stacks 1 and 2) or increased (mini-stacks 4 and 5) velocity functions relative to the central velocity function (mini-stack 3). The black velocity profiles, right panel, correspond to mini-stacks 1, 2, 4, and 5 from left to right respectively.

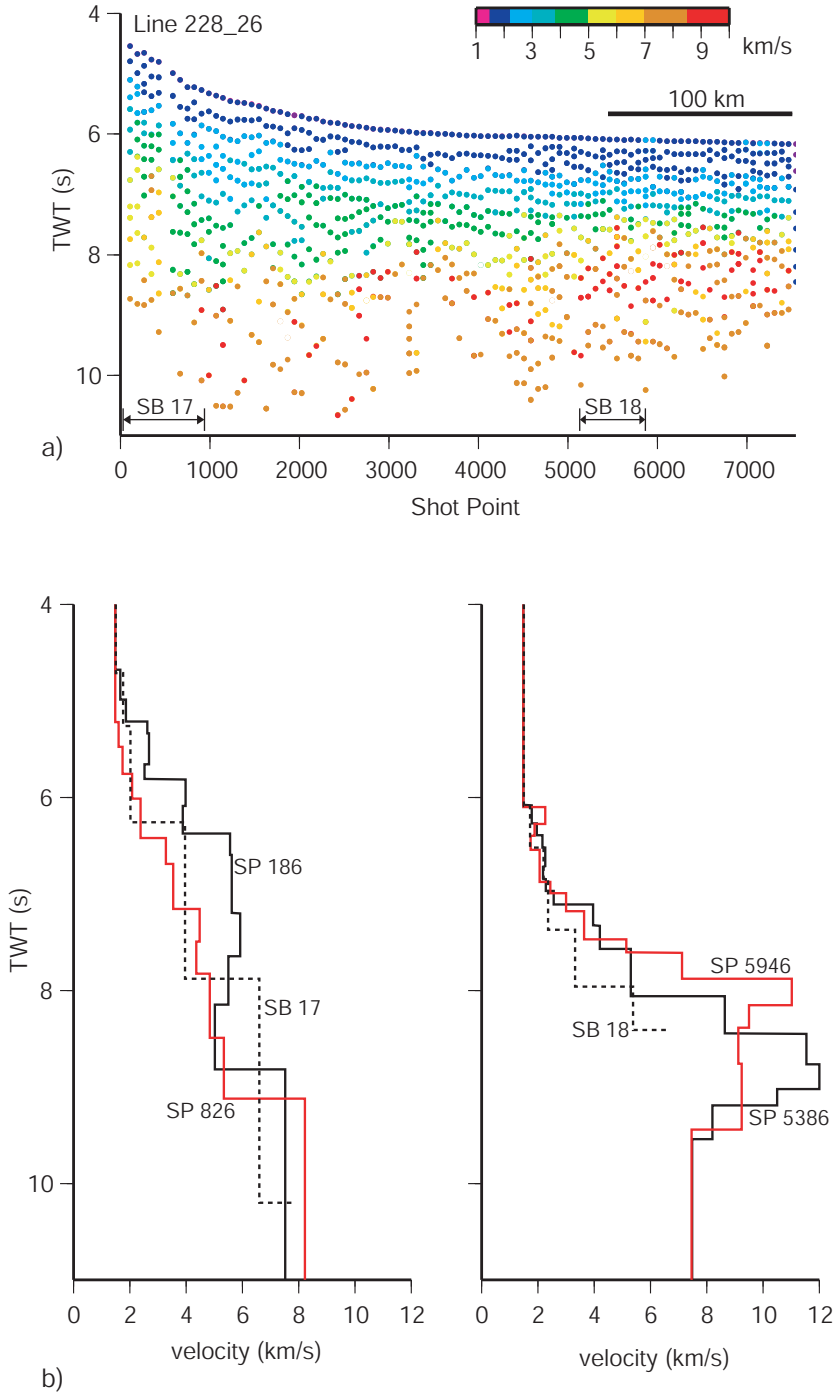


Figure 3.5: a) Interval velocities derived from stacking velocities, using the Dix equation for Line 228_26. Stacking velocities were picked from semblance analyses every 4 km. b) Comparisons of sonobuoy (SB) refraction velocity profiles, as located in (a), to two interval velocity profiles from the extreme shot points (SP) of the SB recording range. A close correlation between the velocity profiles is observed.

## 3.3 Institut Francais du Pétrole Survey ATC82

### 3.3.1 Acquisition and Processing

In January-February, 1982, IFP survey ATC82 acquired ~3000 km of MCS data on the Terre Adélie and east Wilkes Land margin of East Antarctica, between 136-154°E. Data were acquired aboard the *S/V Explora (Prakla-Seismos)* utilising a 2000 $in^3$ airgun array source and a 2400 m, 48 channel streamer [Wannesson *et al.*, 1985]. Details of the processing sequence are outlined in Table 3.5. Field data are not open file for this survey and requests for access made to the IFP were unsuccessful. Stacked sections of the IFP survey lines were obtained through the SDLS. As field data and velocity information was unavailable, these data are used only for interpretation in TWT and have not been depth converted.

| | | |
|---|---|---|
| 1 | Amplitude correction | |
| 2 | Predictive deconvolution | 160 ms operator, 20 ms lag |
| 3 | Velocity analyses | 3 per 10 km |
| 4 | Normal Moveout Correction | |
| 5 | 24 fold stack | |
| 6 | Static correction | +15 ms |
| 7 | Frequency filter | Time variant, band pass filter |

Table 3.5: Brief outline of the processing stream applied to Institut Francais du Pétrole survey ATC82 data.

## 3.4 Japanese National Oil Company Surveys

### 3.4.1 Acquisition and Processing

The JNOC conducted a number of marine geophysical surveys on sections of the Wilkes Land margin from 1983-1995. Data from these surveys are concentrated off east and west Wilkes Land. The quality of imaging achieved on these surveys is variable, however, crustal structure is not normally successfully imaged. Despite the lack of crustal penetration of JNOC data, they provide useful ties of sedimentary horizons between GA-228 and GA-229 survey lines. The 1995 survey (TH95), however, is extremely useful due to its location and improved imaging relative to other JNOC data. Survey TH95 was completed off the Terre Adélie sector of Wilkes Land and included dredging and piston-coring in conjunction with MCS data acquisition. JNOC surveys were conducted aboard the *R/V Hakurei-Maru*, survey equipment and data recording details from TH82 and TH83, and TH95 are summarised in Tables 3.6 and 3.7 respectively.

| **SOURCE** | |
|---|---|
| Volume | 9 litres |
| Shot interval | 50 m |
| **STREAMER** | |
| Group interval | 25 m |
| Phones per group | 32 |
| Streamer length | 600 m |
| **RECORDING** | |
| Sample interval | 4 ms |
| Record length | 10 s |
| Number of channels | 24 |

Table 3.6: Data acquisition parameter summary for the JNOC surveys TH82 and TH83.

| **SOURCE** | |
|---|---|
| Volume | 3.5 litres |
| Shot interval | 50 m |
| **STREAMER** | |
| Group interval | 12.5 m |
| Streamer length | 2100 m |
| **RECORDING** | |
| Sample interval | 4 ms |
| Record length | 12 s |
| Number of channels | 168 |

Table 3.7: Data acquisition parameter summary for JNOC survey TH95.

## 3.5 United States Geological Survey L184

The 1982 USGS survey off eastern Wilkes Land (survey L184) was conducted aboard the *R/V S.P. Lee* [Eittreim & Hampton, 1987]. Over 1800 km of MCS data were recorded, on 14 lines, from 130-146°E. L184 survey lines traverse the upper continental rise on a number of lines and the continental shelf on two lines.

Field data from survey L184 (pre-processed to SEGY format) were provided by the USGS to allow the data to be reprocessed and interpreted in context with the MCS data from surveys GA-228 and GA-229. This was undertaken as multiple potential benefits were identified, including:

1. The possibility of improved imaging of L184 data through the application of modern seismic processing techniques.
2. The improvement of MCS data coverage, between 130-142°E, particularly on the upper continental rise and shelf.

### 3.5.1 Acquisition and Processing

A typical processing sequence (e.g. Yilmaz [2001]) was tested on L184 survey data. Data were processed from field SEGY to fully time migrated sections using *ProMAX (v1998.6)*. Data acquisition parameters are summarised in Table 3.8, and the original processing sequence applied is outlined in Table 3.9.

The processing sequence applied was similar to that originally applied, except with the important addition of deconvolution. The three primary processes applied to reduce the noise content in the data were: deconvolution, stacking, and migration. Additional secondary processes were applied to improve the final data imaging. Where water-bottom multiple reflections obscure important reflectors additional multiple suppression techniques were also employed. Multiple suppression techniques were tested and applied on lines 11 and 12 only, the two lines that extend landward of the shelf break. A summary of the sequence of processing steps is listed in Table 3.10. The success of any seismic processing technique is dependent upon the user-defined parameterisation of the process. As such, a range of process parameters were tested on representative line sections before final application to entire lines. A detailed discussion of parameter testing undertaken, including comparative test panels is given in Appendix A. Limited imaging improvement was achieved via reprocessing. Multiple suppression techniques, particularly wave equation multiple rejection (WEMR), were successful in reducing the multiple energy to some degree. The quality of data imaging and the applicability of modern processing techniques are limited by the length of the streamer and the size of the source. The streamer length of 2400 m limited the amount of moveout, and a relatively small source resulted in relatively low signal to noise ratios at the longest offsets that were recorded. Hence, few of the techniques applied provided significant improvements beyond the basic processing steps applied.

## 3.6 Summary

All relevant, available seismic reflection data has been accessed to allow the most complete seismic interpretation possible to be completed in the following chapter. MCS data from surveys L184, GA-228 and GA-229 can also be depth converted as velocity information is available for these data.

| **SOURCE** | |
|---|---|
| Volume | 21 litres |
| Gun depth | 10.5 m |
| Shot interval | 50 m |
| | |
| **STREAMER** | |
| Length | 2400 m |
| Group interval | 100 m |
| Average depth | 12.5 m |
| Group length | 100 m |
| Phones per group | 60 |
| | |
| **RECORDING** | |
| Sample interval | 2 ms |
| Record length | 10 s |
| Recording filter | 5-110 Hz |
| Number of channels | 24 |

Table 3.8: Data acquisition parameters for the USGS L184 survey.

| | |
|---|---|
| 1 | Demultiplex |
| 2 | Trace shot edit |
| 3 | Static corrections |
| 4 | CMP sort |
| 5 | Velocity analysis |
| 6 | NMO correction |
| 7 | 24-fold stack |
| 8 | Bandpass filter |
| 9 | Automatic gain control |

Table 3.9: Process sequence applied to the L184 data during original processing.

Reprocessing of survey L184 data indicates that the limits of imaging quality are primarily a function of the original data acquisition. Although minor improvements can be achieved through modern processing techniques, the interpretation of the data is not likely to be altered due to these small improvements. The longer streamer, greater fold, and larger source implemented during surveys GA-228 and GA-229 provides the highest

| | |
|---|---|
| 1 | Preprocessing<br>- Demultiplexing (completed externally)<br>- Reformatting (completed externally)<br>- Field geometry setup<br>- Statics (DWD correction)<br>- Trace editing<br>- WEMR (Lines 11 and 12 only)<br>- Geometric spreading correction |
| 2 | *F-K filtering* |
| 3 | CMP sort |
| 4 | Predictive deconvolution |
| 5 | Velocity analysis |
| 6 | NMO correction |
| 7 | - *DMO correction*<br>- Radon filter (Lines 11 and 12 only) |
| 8 | 24 fold stack |
| 9 | Deconvolution |
| 11 | Bandpass filtering |
| 12 | Migration |
| 13 | Trace mixing |
| 14 | Gain application |

Table 3.10: General process sequence applied to survey L184 MCS data. Techniques that were tested but subsequently not applied are in italics.

quality MCS data off the Wilkes Land margin.

# Chapter 4

# Seismic Data - Interpretation

## 4.1 Introduction

Interpretation of GA-228 and GA-229 multi-channel seismic (MCS) data from the Wilkes Land margin was completed by scientific staff of GA[1] and the author. Interpretation of data acquired by the USGS, IFP and JNOC was subsequently undertaken in areas where these data could add value to the GA-228 and GA-229 interpretations. Figure 4.1 shows the location of all survey lines off the Wilkes Land margin. The line separation of ∼90 km in central Wilkes Land and varying coverage to the east and west does not allow the details of lateral facies and depositional environmental changes to be fully imaged. However, a range of depositional and erosional features, and facies changes are observed.

## 4.2 Sonobuoy Data

The MCS data interpretation presented here also integrates modelling of refraction and/or wide angle reflection data recorded with non-reversed expendable sonobuoys. Discussion of refraction velocities are included within the following interpretation sections. The locations of sonobuoy stations on the Wilkes Land margin are illustrated in Figure 4.1, and their interpreted velocities and boundary depths in two-way-time (TWT) are summarised in Table 4.1 and Figure 4.2. Unfortunately, very few sonobuoys recorded mantle velocities and accordingly there is poor control on *Moho* depth for most of the margin.

[1]Howard Stagg, Jim Colwell, Phil Symonds, Phil O'Brien, Mark Alcock, and Leesa Carson

| | **SB** | **Lat.** | **Long.** | **Line** | V1 | D1 | V2 | D2 | V3 | D3 | V4 | D4 | V5 | D5 | V6 | D6 | V7 | D7 | V8 | D8 |
|---|---|---|---|---|---|---|---|---|---|---|---|---|---|---|---|---|---|---|---|---|
| A | 229-26 | -61.43 | 110.77 | 229_14 | 1.7 | 5.59 | 1.9 | 5.80 | 2.4 | 6.02 | 2.5 | 6.64 | (3.2) | ∼6.85 | 4.9 | 7.09 | *5.9* | *7.73* | *7.1* | *8.06* |
| B | 229-19 | -61.67 | 120.87 | 229_10 | 1.7 | 5.65 | 2.0 | 6.10 | 2.5 | 6.51 | 2.8 | 6.96 | 3.7 | 7.37 | (4.5) | ∼8.02 | *6.6* | *8.73* | | |
| C | 229-18 | -60.9 | 124.23 | 229_09 | 1.7 | 5.93 | 2.4 | 6.44 | 2.7 | 6.98 | 3.4 | 7.29 | (4.9) | ∼7.86 | 6.1 | 8.04 | | | | |
| D | 228-15 | -61.83 | 127.6 | 228_24 | 1.7 | 5.88 | 2.0 | 6.23 | 2.4 | 6.63 | 3.4 | 7.45 | 5.4 | 7.74 | *6.7* | *8.78* | | | | |
| E | 228-11 | -63.95 | 128.28 | 228_24 | 1.7 | 5.05 | 2.4 | 5.74 | 2.6 | 6.16 | 3.4 | 7.19 | | | | | | | | |
| F | 228-16 | -62.92 | 129.34 | 228_25 | 1.8 | 5.83 | 2.4 | 6.65 | 3.0 | 6.94 | 4.1 | 7.34 | 5.4 | 8.27 | *7.9* | *9.98* | | | | |
| G | 228-18 | -61.63 | 130.97 | 228_26 | 1.7 | 6.09 | 2.2 | 6.52 | 2.3 | 6.87 | 3.3 | 7.37 | 5.4 | 7.96 | *6.6* | *8.41* | | | | |
| H | 228-17 | -63.88 | 131.85 | 228_26 | 1.8 | 4.71 | 2.0 | 5.26 | *3.9* | *6.26* | 6.6 | 7.88 | *7.8* | *10.2* | | | | | | |
| I | 228-20 | -60.82 | 132.65 | 228_27 | 1.8 | 6.16 | 2.2 | 6.58 | 3.1 | 6.75 | 3.9 | 7.54 | *5.4* | *8.01* | *6.7* | *8.99* | *8.2* | *9.66* | | |
| J | 228-19 | -60.69 | 132.65 | 228_27 | 1.8 | 6.17 | 2.5 | 6.67 | | | | | | | | | | | | |
| K | 228-21 | -62.87 | 134.33 | 228_28 | 1.8 | 5.67 | 2.0 | 6.22 | 2.4 | 6.42 | 3.1 | 6.71 | 4.5 | 7.42 | 6.5 | 8.70 | 8.2 | 10.21 | | |
| L | 228-22 | -60.73 | 134.33 | 228_28 | 1.8 | 6.12 | 2.1 | 6.49 | 2.8 | 6.77 | 3.0 | 7.13 | 3.8 | 7.40 | 4.9 | 7.87 | *5.7* | *8.23* | | |
| M | 228-24 | -61.79 | 136 | 228_29 | 1.8 | 5.84 | 2.3 | 6.27 | 3.0 | 6.84 | 3.9 | 7.27 | 4.4 | 8.02 | *5.5* | *8.55* | | | | |
| N | 228-23 | -60.91 | 136 | 228_29 | 1.8 | 6.01 | 2.2 | 6.62 | 3.5 | 7.26 | 4.9 | 7.65 | *6.6* | *8.21* | *8.1* | *9.16* | | | | |
| O | 229-15 | -62.97 | 136.83 | 229_07 | 1.9 | 5.29 | 2.1 | 5.78 | 2.7 | 6.22 | *4.5* | *∼7.31* | 5.6 | ∼9.75 | | | | | | |
| P | 229-13 | -62.22 | 137.42 | 229_07 | 1.9 | 5.6 | 2.0 | 6.02 | 2.3 | 6.41 | 3.3 | 7.09 | 3.6 | 7.23 | *4.1* | *8.25* | *5.6* | *8.64* | 6.6 | 9.69 |
| Q | 229-10 | -63.89 | 137.47 | 229_06 | 1.9 | 4.67 | 2.0 | 4.99 | 2.7 | 5.76 | 3.5 | 6.52 | 4.0 | 7.04 | *6.3* | *8.49* | | | | |
| R | 229-11 | -62.98 | 138.5 | 229_06 | 1.8 | 5.07 | 2.0 | 5.37 | 2.1 | 5.75 | 2.5 | 5.94 | 2.9 | 6.29 | 3.8 | 6.87 | (4.6) | ∼7.21 | 5.4 | 8.74 |
| S | 229-12 | -61.97 | 139.05 | 229_06 | 1.8 | 5.73 | 2.1 | 6.26 | 2.5 | 6.54 | 3.3 | 6.97 | *3.6* | *7.3* | *4.1* | *8.59* | 6.8 | 9.17 | | |

Table 4.1: Sonobuoy locations and solutions for surveys GA-228 and GA-229. Velocity (V) units are km/s and depth (D) is recorded in two-way-time (s) below sea level. Velocities in parentheses are assumed and depths preceded by a tilda (∼) are approximate, usually because of relief on an interface. Velocity/depth pairs in italics are solutions for interfaces that are not observed in seismic reflection data and are therefore unconstrained with regard to dip.

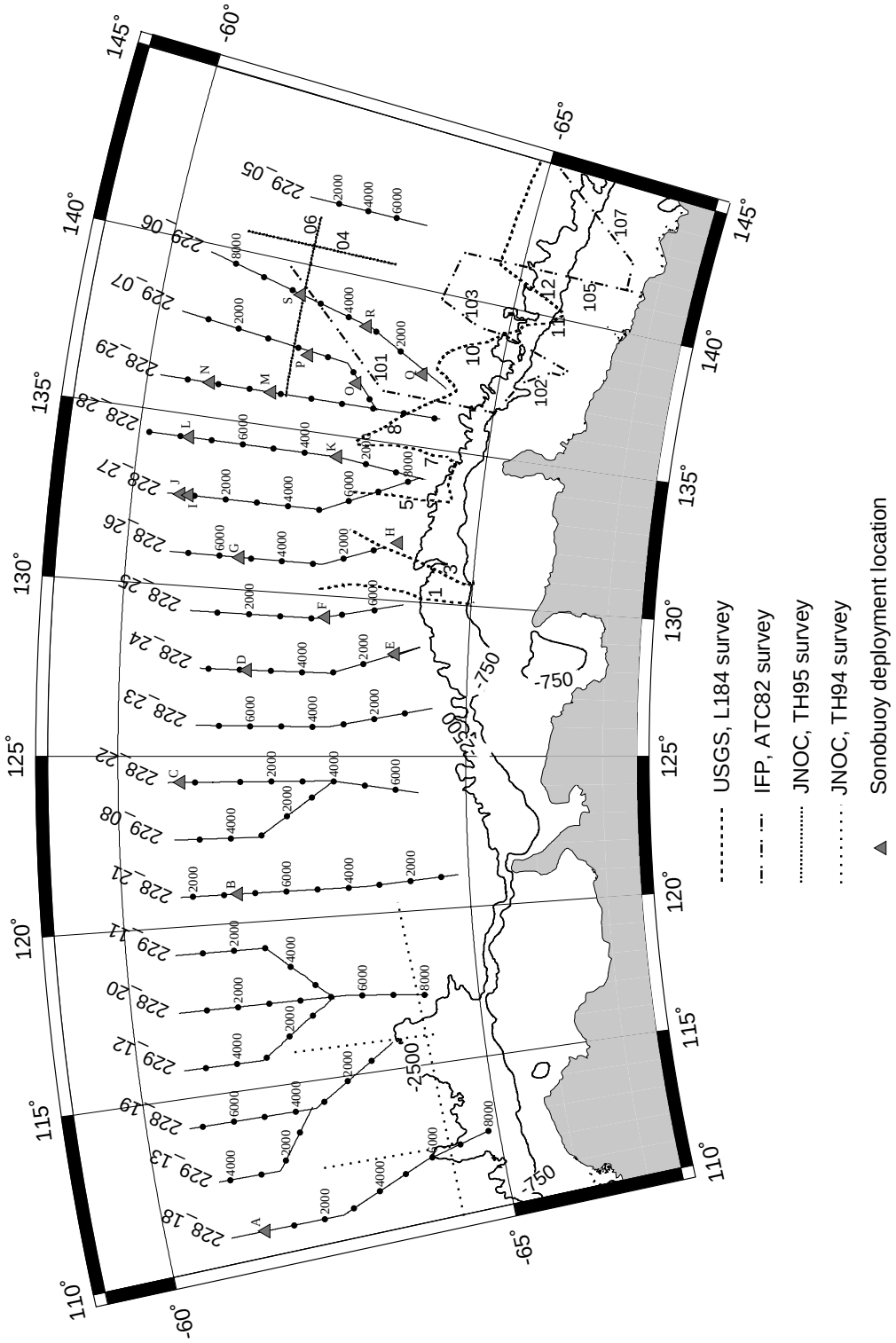


Figure 4.1: Seismic reflection survey lines from surveys GA-228, GA-229, L184, ATC82 and TH95 as labelled. Letters next to sonobuoy locations relate to Table 4.1. The 750 and 2500 m bathymetry contours from GEBCO 1-minute IOC *et al.* [2003] data are also illustrated.

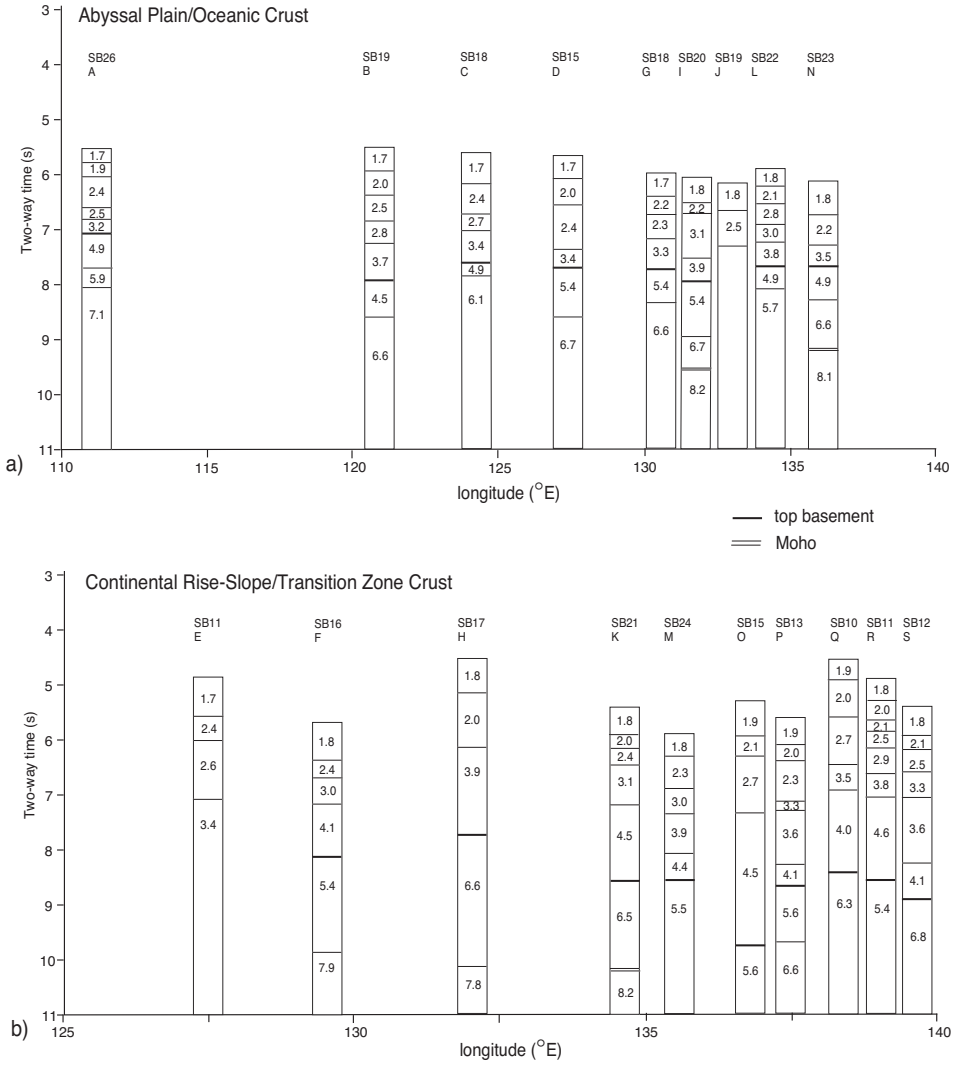


Figure 4.2: Sonobuoy refraction velocities for a) the abyssal plain, and b) the continental rise and slope. Note that the lateral scale is different in (b), as the sonobuoys are clustered off east Wilkes Land (see Figure 4.1 and Table 4.1).

## 4.3 Seismic Reflection Data

Regional seismic reflection profiles from the Wilkes Land margin, acquired during surveys GA-228 and GA-229, and their detailed interpretations are illustrated in Figures 4.3 to 4.16. Interpretations from USGS, JNOC and IFP data are illustrated selectively where they allow interpretation of features not imaged in GA-228 and GA-229 data. Isopachs are created using data from GA-228, GA-229 and USGS survey data, as velocity models are available for these data only (as outlined in the previous chapter). Seismic reflection data from the conjugate southern Australian margin is also utilised in interpretation, they provide images of an analogue system that has been more extensively surveyed and drilled.

Due to widespread ice coverage on the Antarctic margin, MCS data on the continental shelf is sparse. No GA-228 or GA-229 survey lines survey landward of the shelf break. The east Wilkes Land continental shelf was surveyed east of ~137° during USGS survey L184 (Lines 11 and 12) and IFP survey ATC82 (Lines 102, 103[2], 105 and 107). Lines L184_11, ATC82_102 and ATC82_105 are illustrated in Figures 4.17 to 4.19. No MCS data exists for the west and central Wilkes Land continental shelf.

A summary of the typical reflector patterns and geometry of each major sequence, with brief interpretations, is illustrated in Figure 4.20. Across margin variations in seismic character are illustrated by showing examples from the continental slope/rise and the abyssal plain environments. Examples from west and central/east Wilkes Land are also displayed to demonstrate the along margin variations in seismic character, which are important as the Wilkes Land margin sector extends over more than 1000 km.

Two major seismic sequences, bounded by regional unconformities labelled *eoc* and *tur*, are interpreted as sequences 1 and 2. The *eoc* unconformity is recognised as the base of onlapping reflectors beneath the continental slope and rise, it can be traced seawards confidently on all lines, except where pinch-outs against basement highs occur. The *eoc* unconformity is interpreted as Early- to Middle-Eocene (~50 Ma). The *tur* unconformity marks a transition between continuous, consistent amplitude and frequency reflectors above, and truncated, more chaotic reflector geometries below. The *tur* unconformity is interpreted to be early-Turonian (~85-90 Ma)

The top of Sequence 1 is defined by the present-day seafloor and its base by the *eoc* unconformity (landward) and the top of acoustic basement (seaward). Sequence 1 exhibits greater thickness relative to Sequence 2. Sequence 2 is observed beneath the continental slope and rise only, and does not extend to the deep abyssal plain. Both Sequence 1 and 2 thin seawards. These sequences can be further subdivided locally as

[2]Line 103 is not included in data placed with the SDLS and is therefore not publicly available

other distinct unconformities occur within them, which are interpreted as unlabelled blue lines on Figures 4.3 to 4.16. However, none of these minor sequence boundary can be correlated for the entire extent of the margin, due to the lack of a tie line and the large distance (average ∼90 km) between lines. The *eoc* and *tur* unconformities are identified from ∼110-145°E on the basis of seismic character and tie-lines provided by other data, however, they can not be confidently correlated further west or east.

A third sequence (Sequence 3) is identified off central and east Wilkes Land. Sequence 3 is highly variable with regard to thickness, seismic character, and to a lesser degree, seaward extent. Basement is interpreted, in general, to underlie Sequence 3 at the landward extent of data, to underlie Sequence 2 beneath the continental slope/rise transition, and to underlie Sequence 1 beneath the abyssal plain.

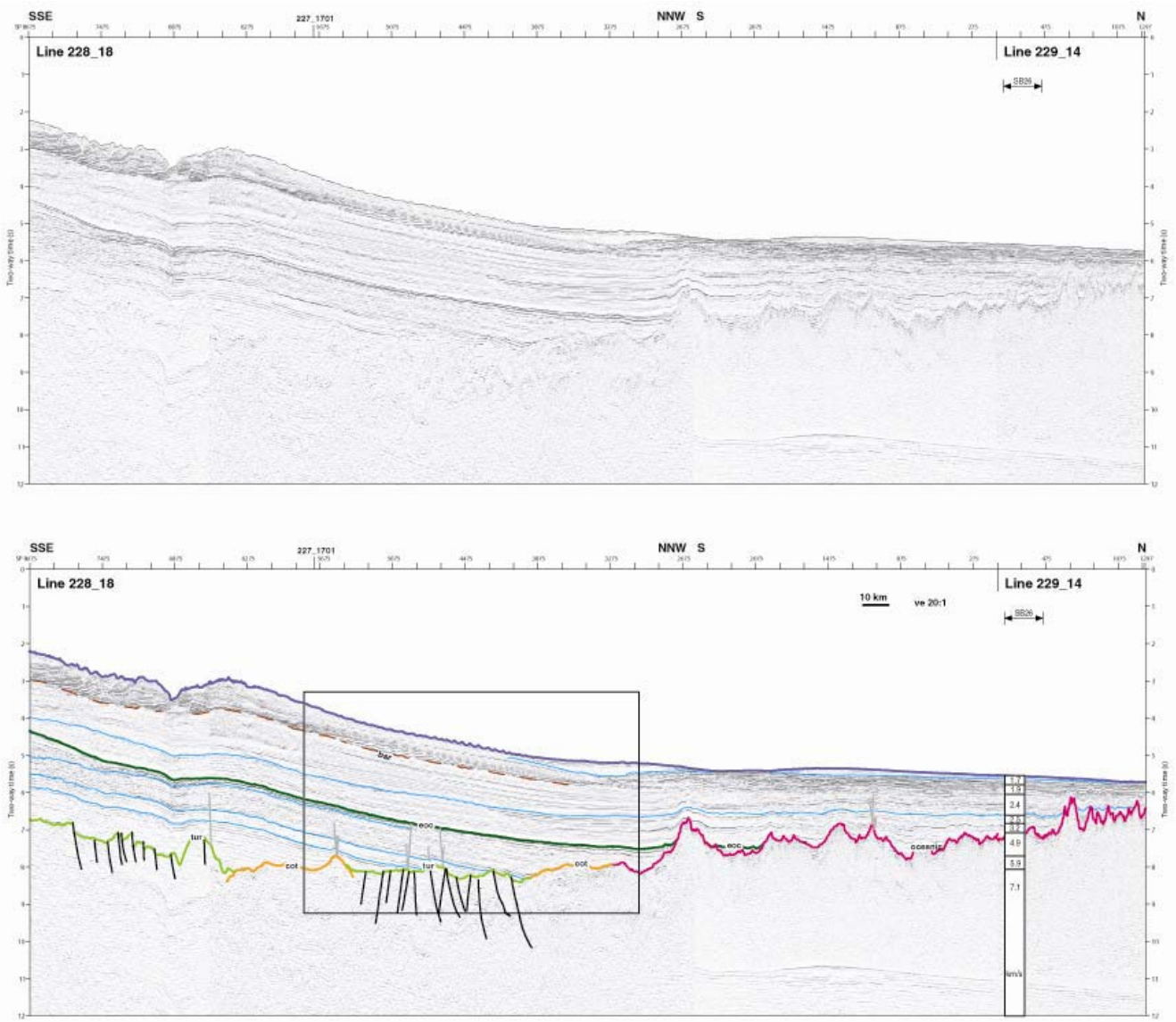


Figure 4.3. Uninterpreted and interpreted seismic reflection profiles of Line 228_18. Vertical exaggeration (ve) is calculated at the sea-floor. Boxed section is displayed in detail in Figure 4.29.

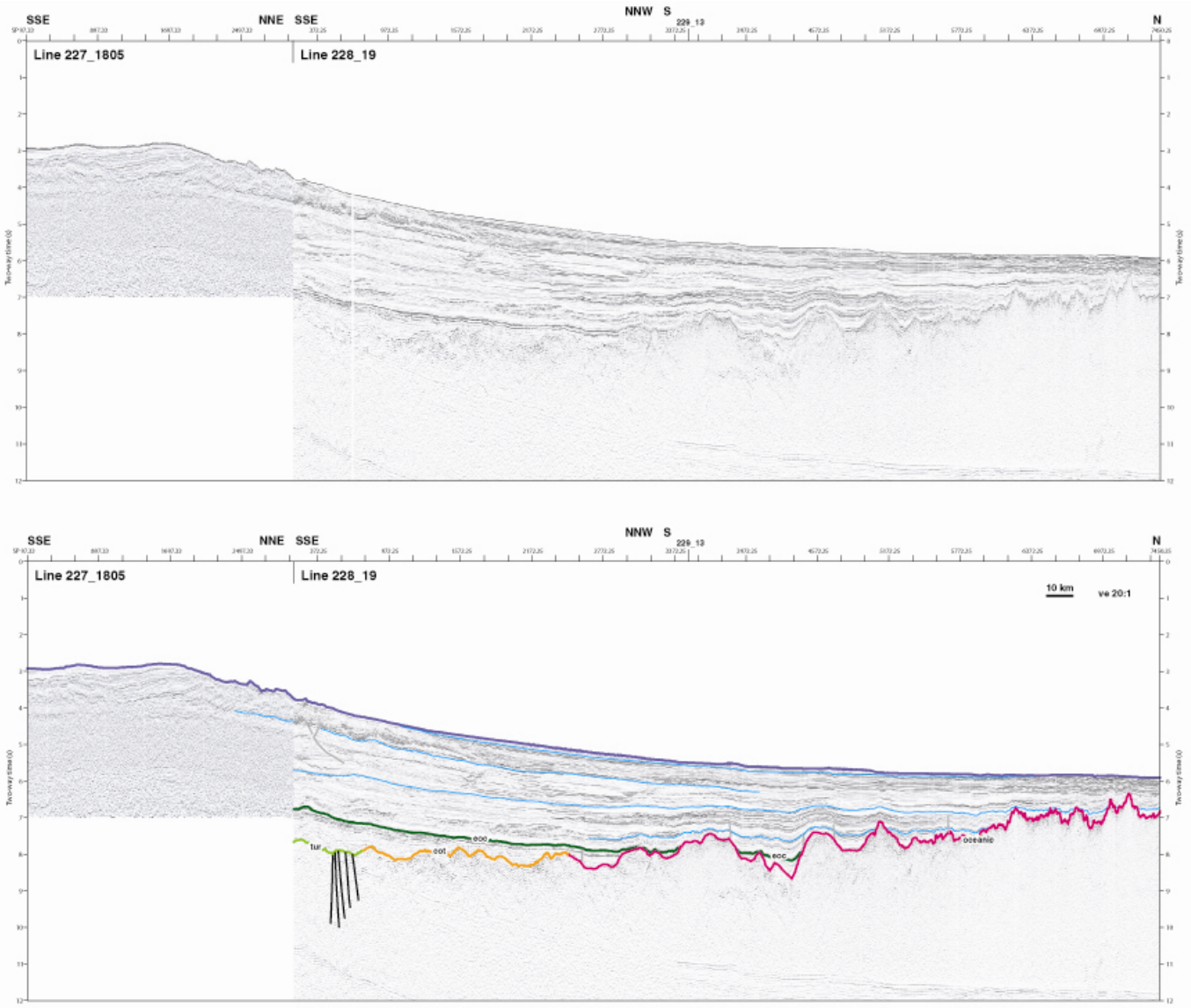


Figure 4.4. Uninterpreted and interpreted seismic reflection profiles for Line 228_19. Vertical exaggeration (ve) is calculated at the sea-floor.

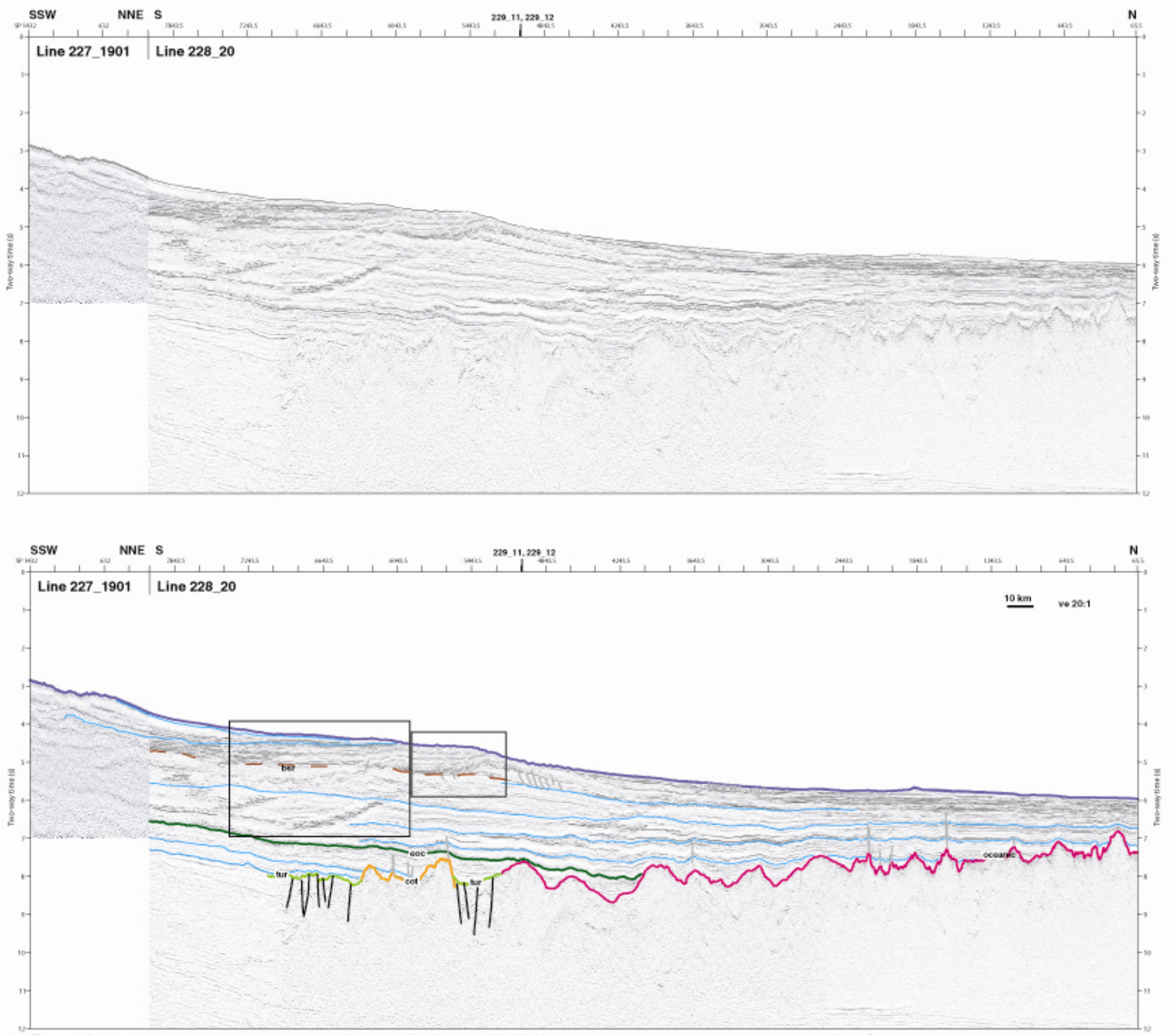


Figure 4.5. Uninterpreted and interpreted seismic reflection profiles for Line 228_20. Vertical exaggeration (ve) is calculated at the sea-floor. Boxed sections are displayed in detail in Figures 4.31 and 4.32.

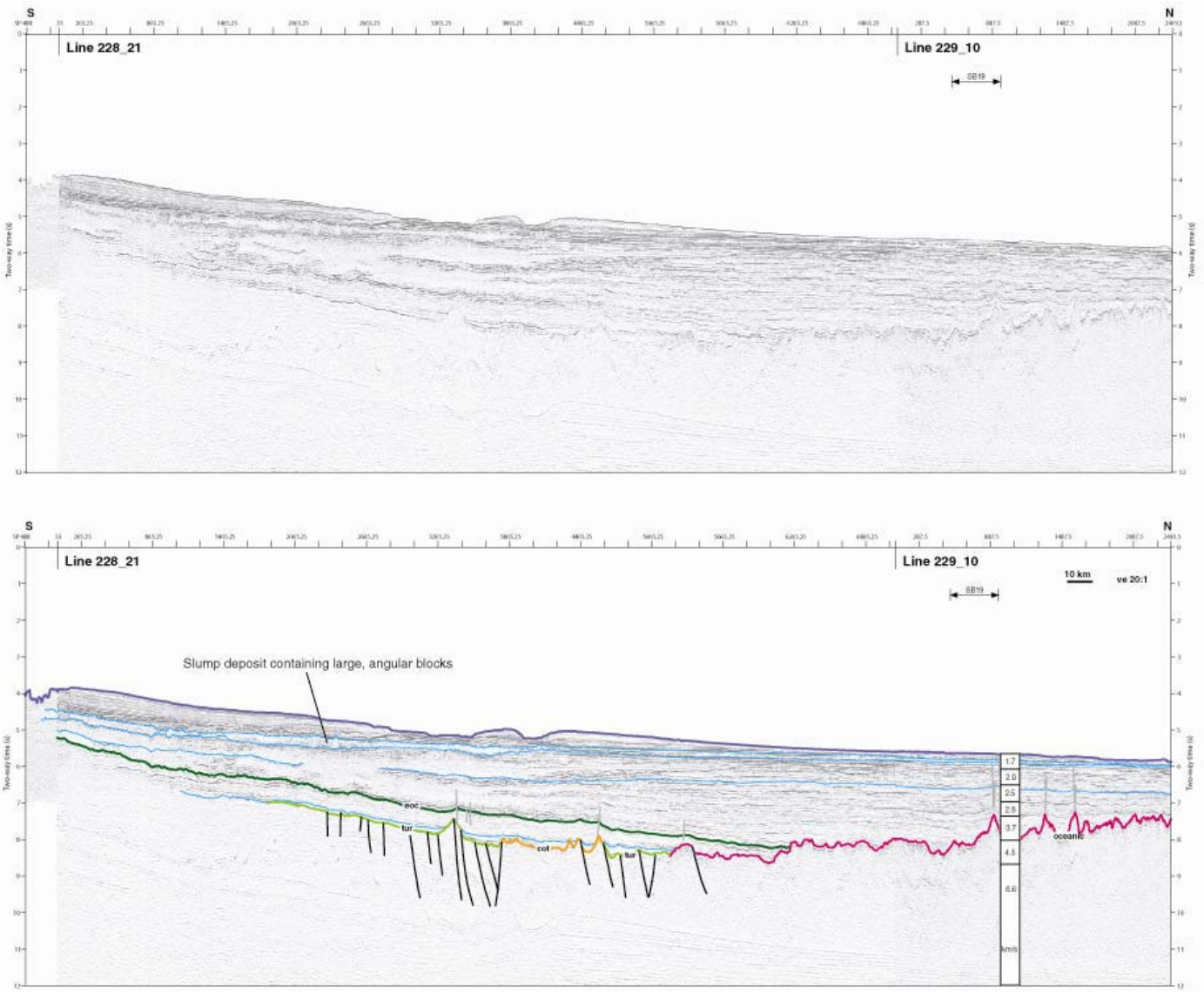


Figure 4.6. Uninterpreted and interpreted seismic reflection profiles for Line 228_21. Vertical exaggeration (ve) is calculated at the sea-floor.

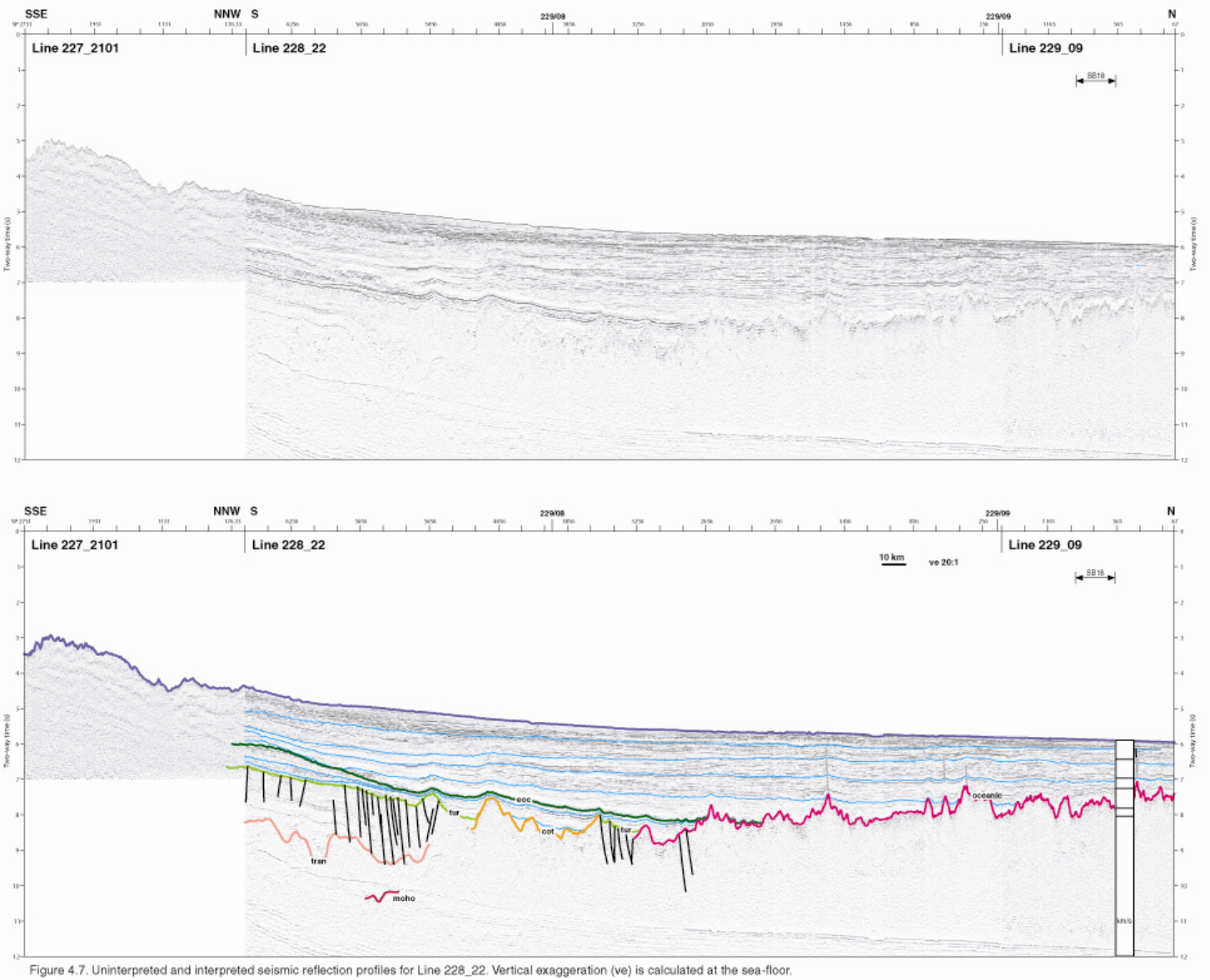


Figure 4.7. Uninterpreted and interpreted seismic reflection profiles for Line 228_22. Vertical exaggeration (ve) is calculated at the sea-floor.

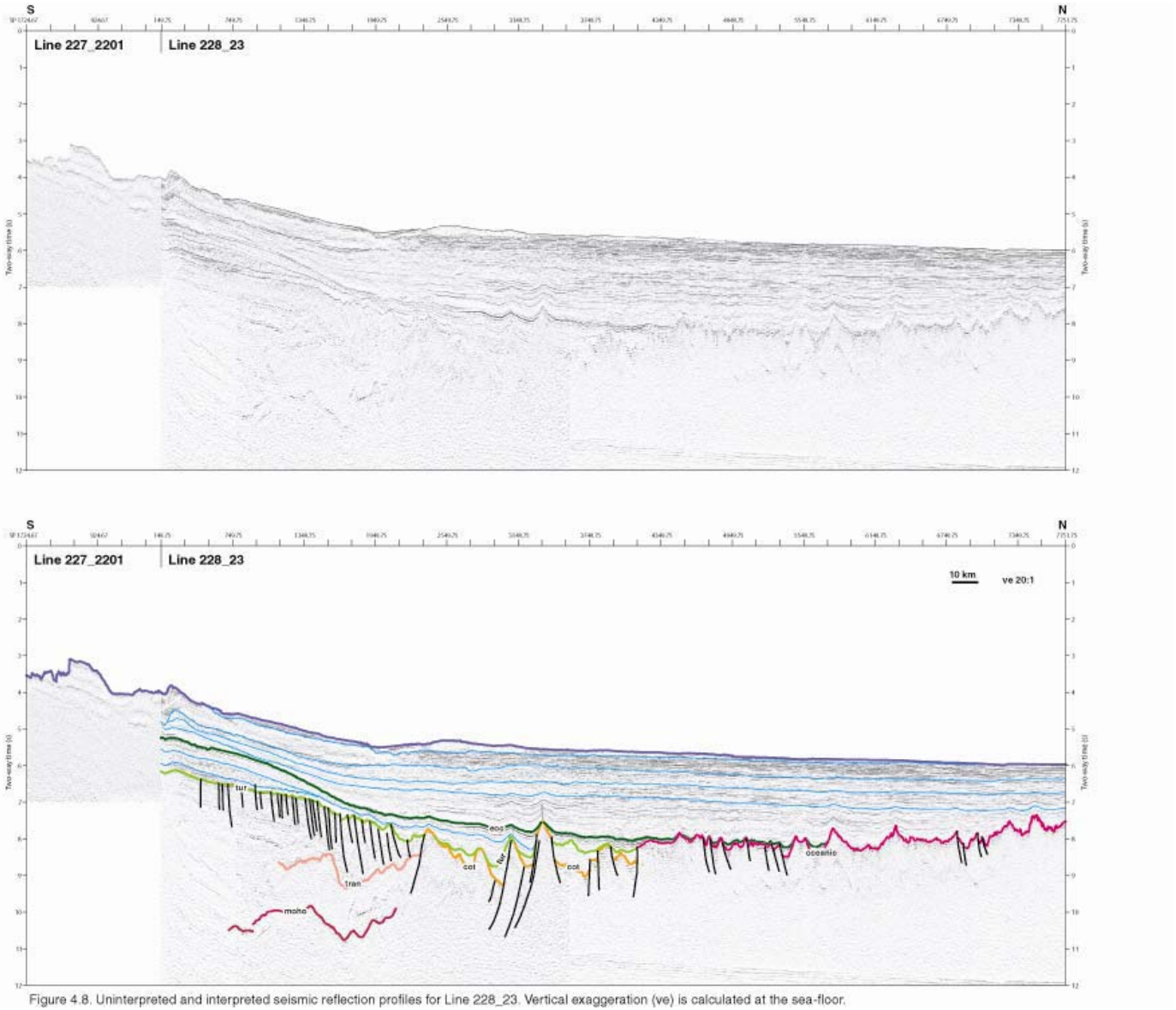


Figure 4.8. Uninterpreted and interpreted seismic reflection profiles for Line 228_23. Vertical exaggeration (ve) is calculated at the sea-floor.

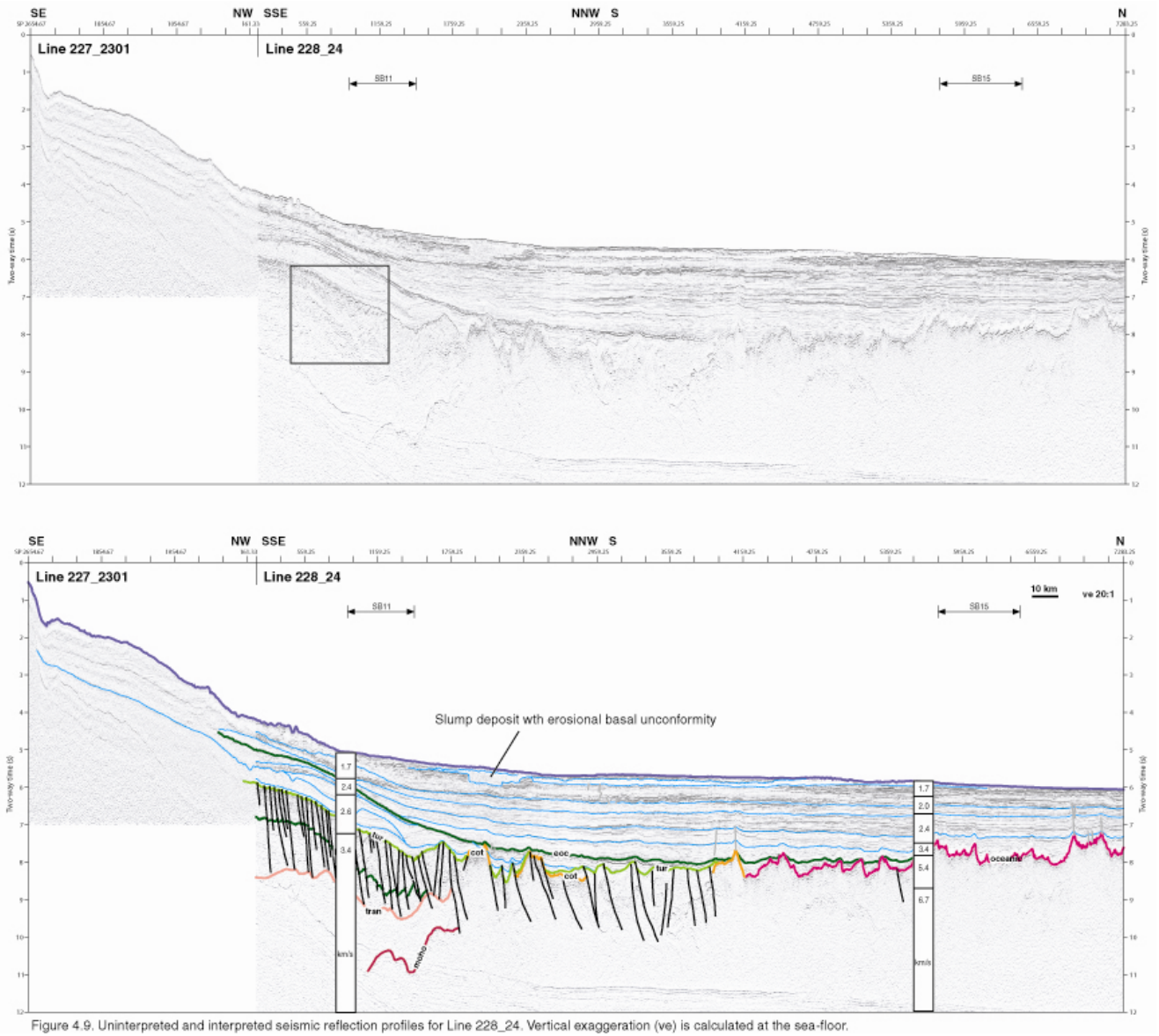


Figure 4.9. Uninterpreted and interpreted seismic reflection profiles for Line 228_24. Vertical exaggeration (ve) is calculated at the sea-floor.

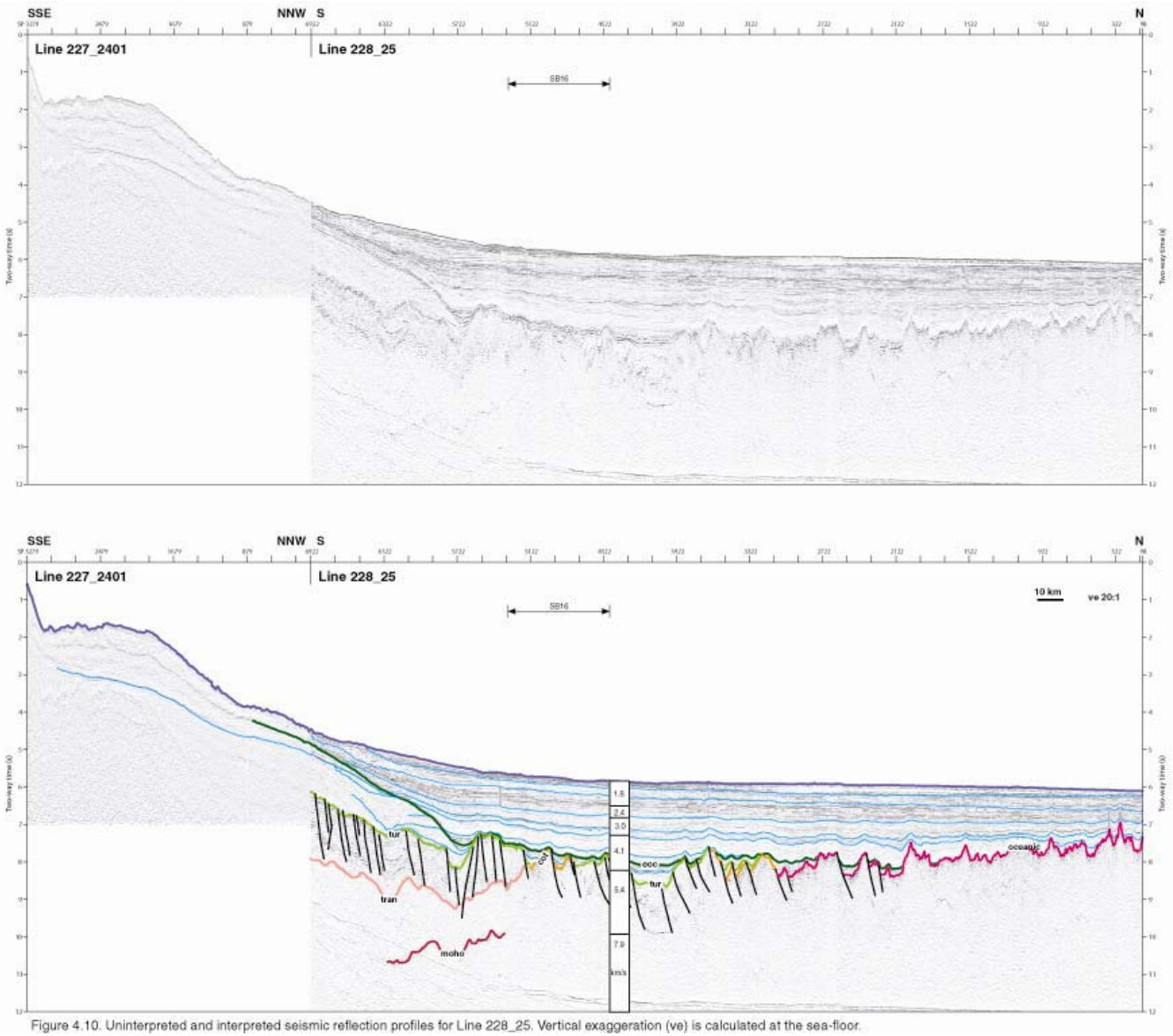


Figure 4.10. Uninterpreted and interpreted seismic reflection profiles for Line 228_25. Vertical exaggeration (ve) is calculated at the sea-floor.

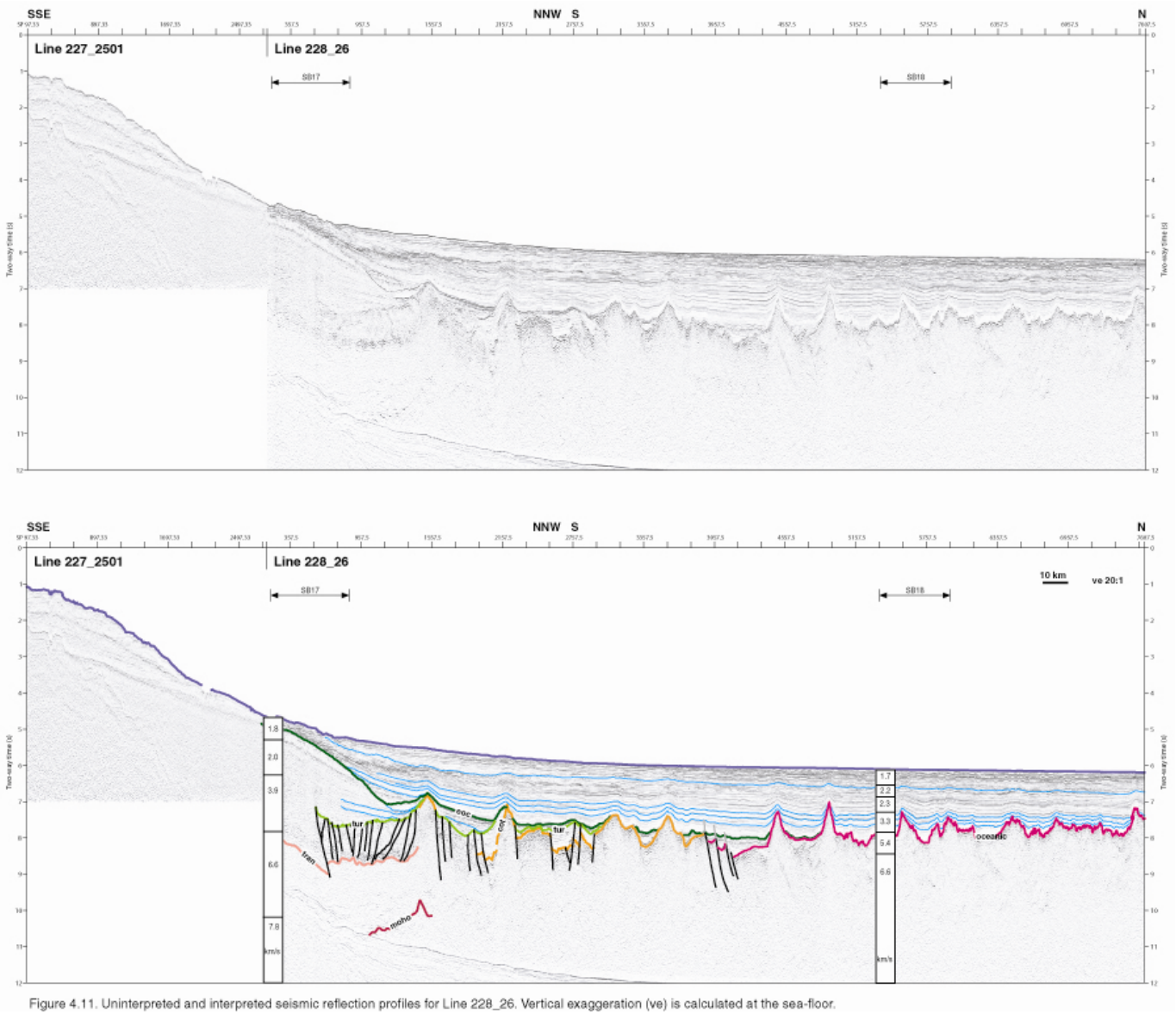


Figure 4.11. Uninterpreted and interpreted seismic reflection profiles for Line 228_26. Vertical exaggeration (ve) is calculated at the sea-floor.

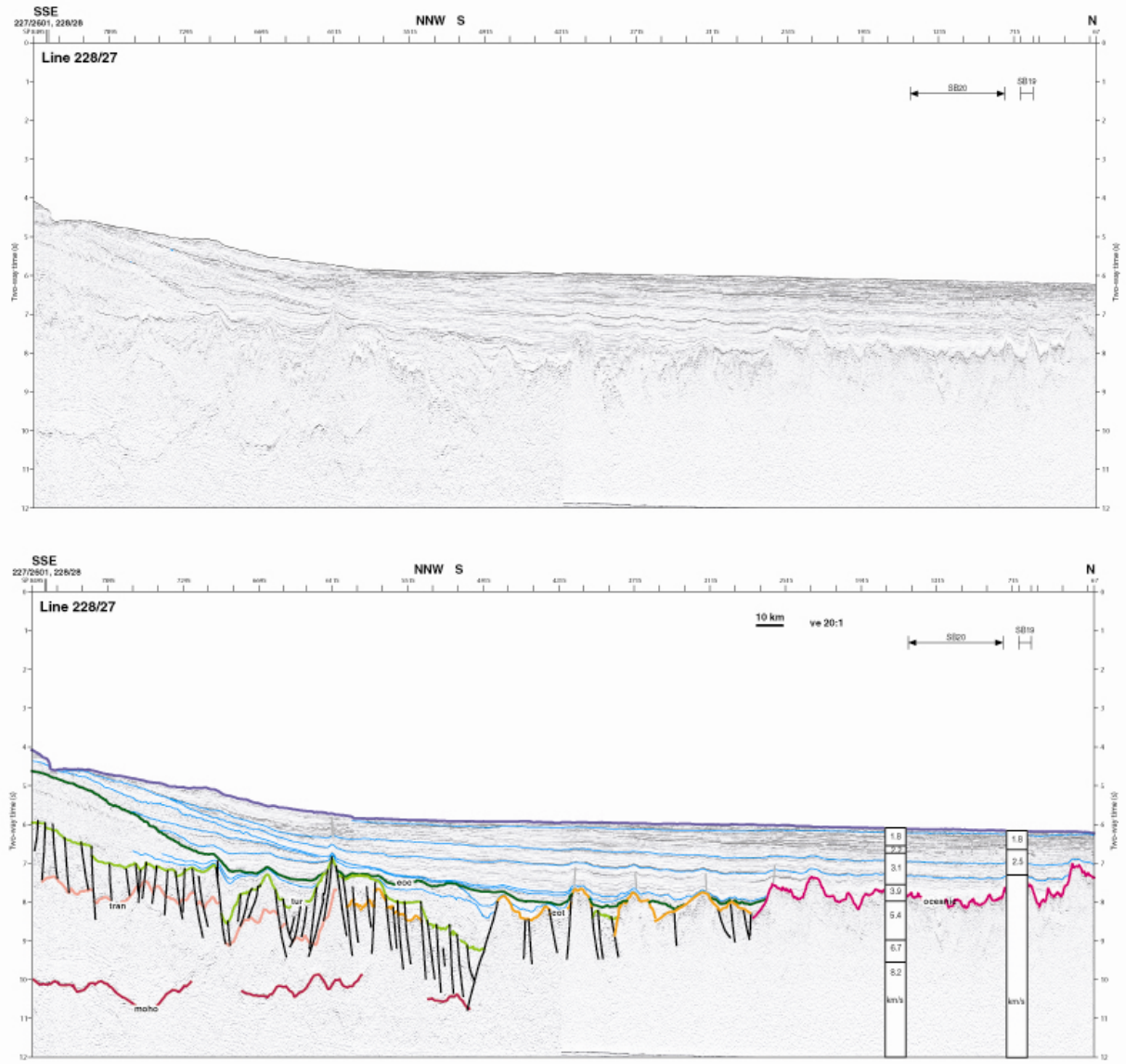


Figure 4.12. Uninterpreted and interpreted seismic reflection profiles for Line 228_27. Vertical exaggeration (ve) is calculated at the sea-floor.

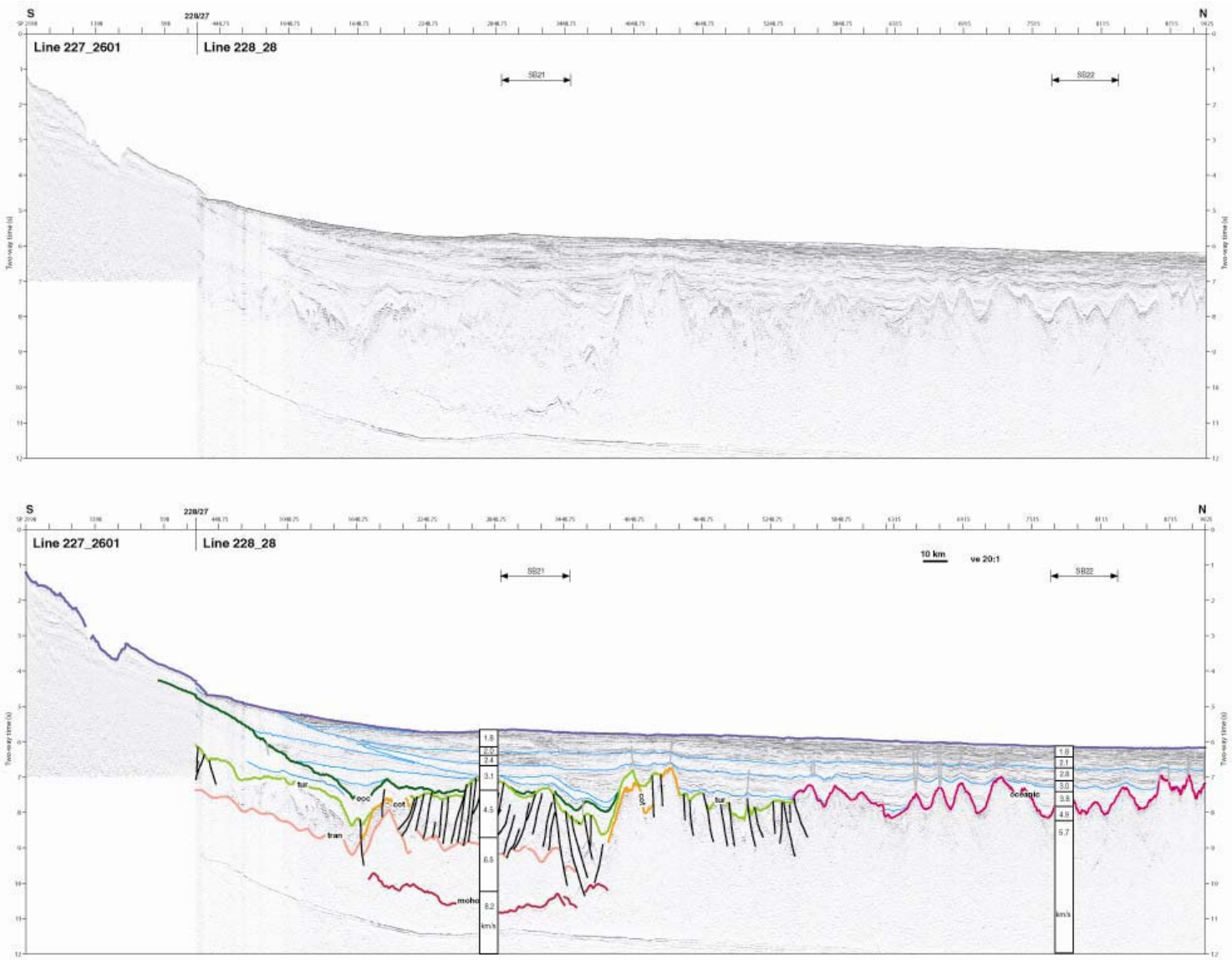


Figure 4.13. Uninterpreted and interpreted seismic reflection profiles for Line 228_28. Vertical exaggeration (ve) is calculated at the sea-floor.

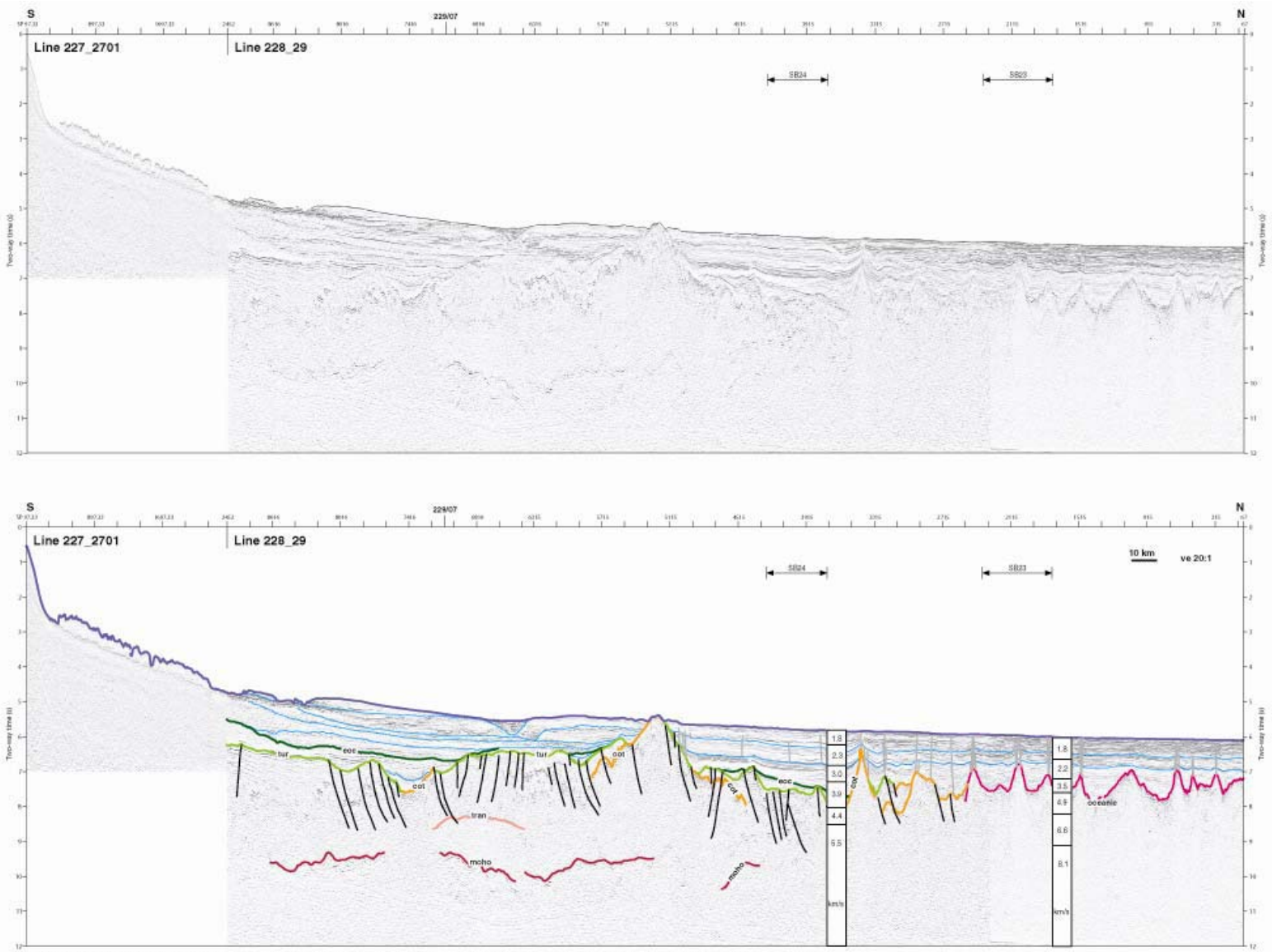


Figure 4.14. Uninterpreted and interpreted seismic reflection profiles for Line 228_29. Vertical exaggeration (ve) is calculated at the sea-floor.

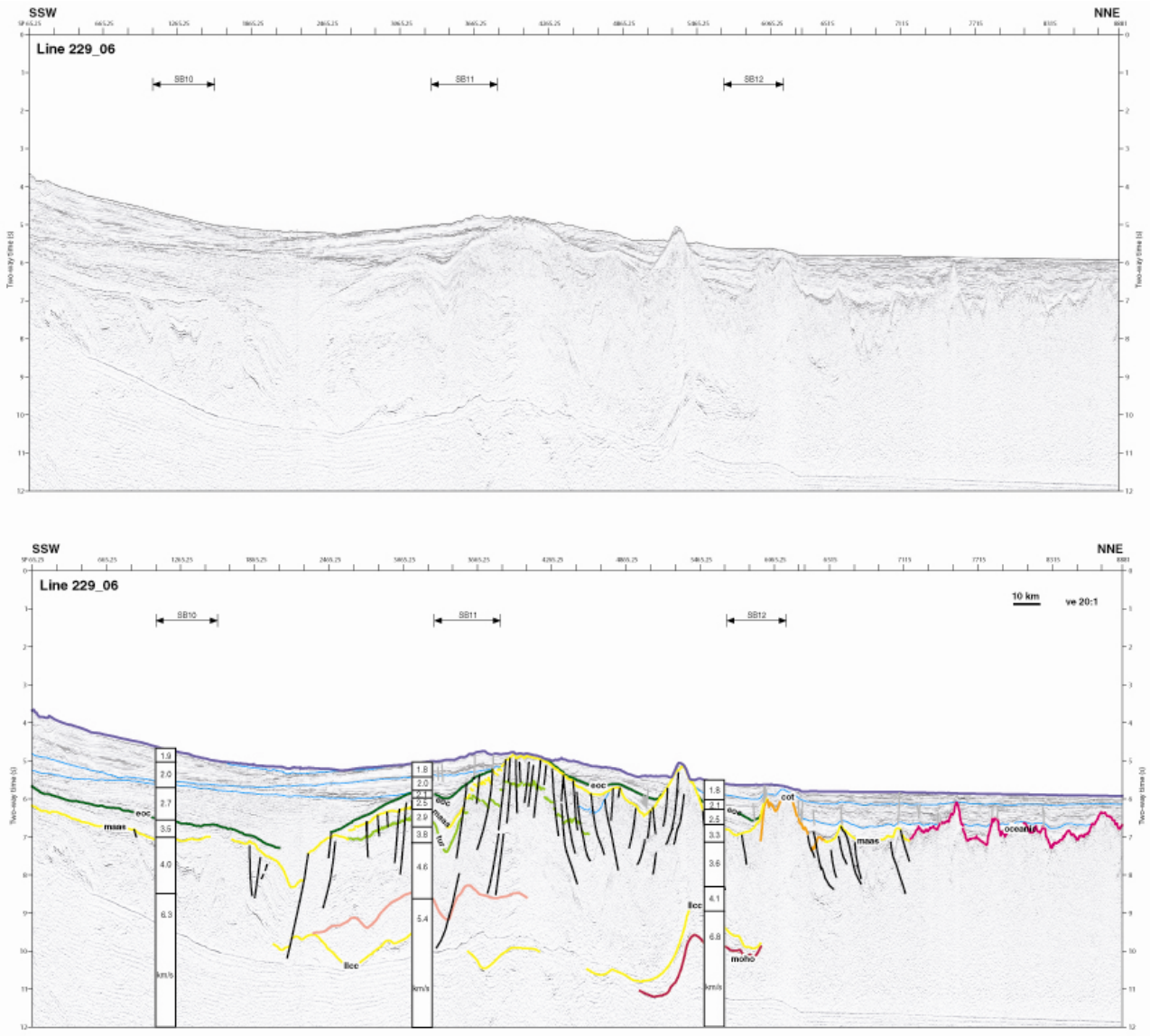


Figure 4.15. Uninterpreted and interpreted seismic reflection profiles for Line 229_06. Vertical exaggeration (ve) is calculated at the sea-floor.

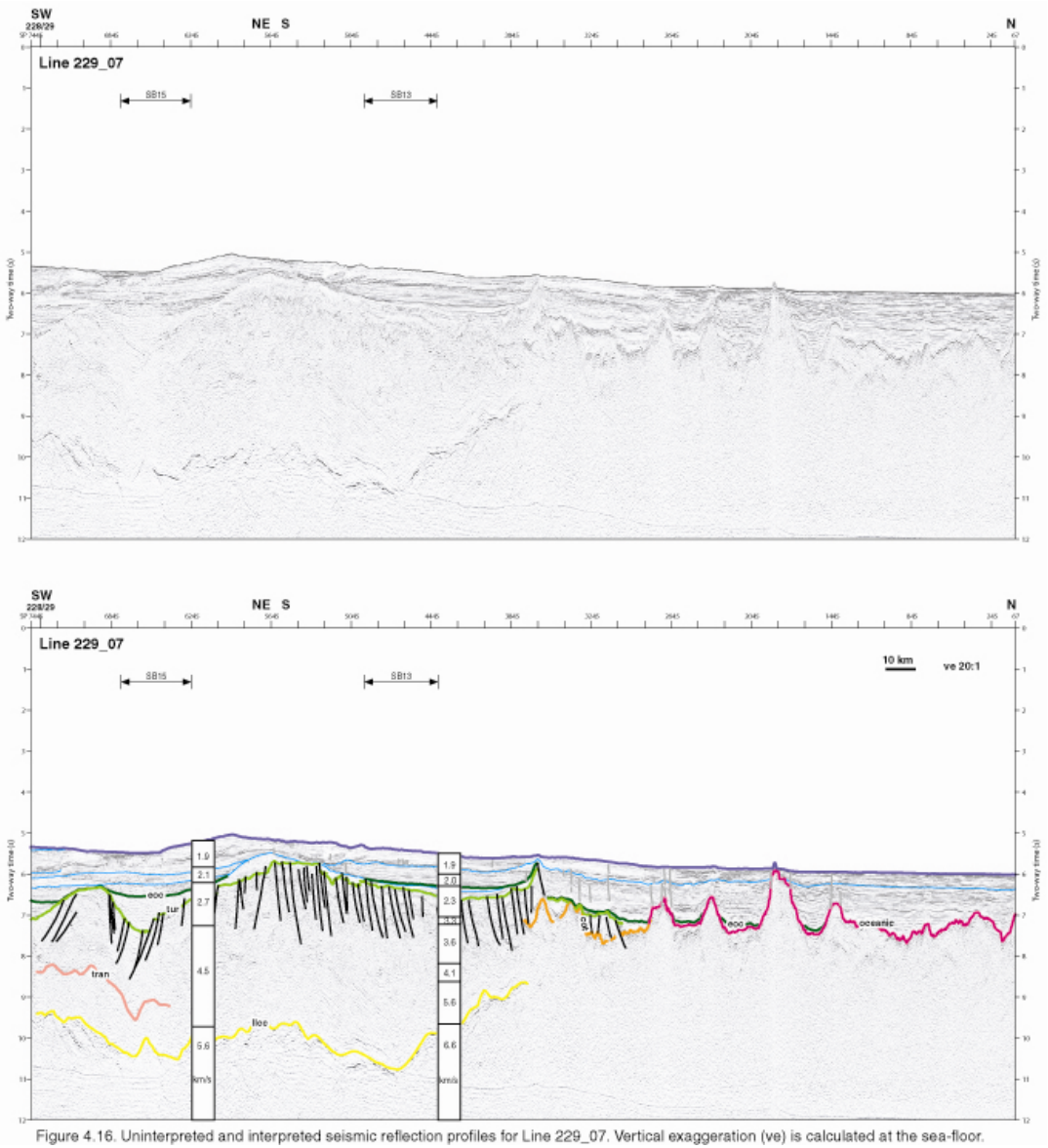


Figure 4.16. Uninterpreted and interpreted seismic reflection profiles for Line 229_07. Vertical exaggeration (ve) is calculated at the sea-floor.

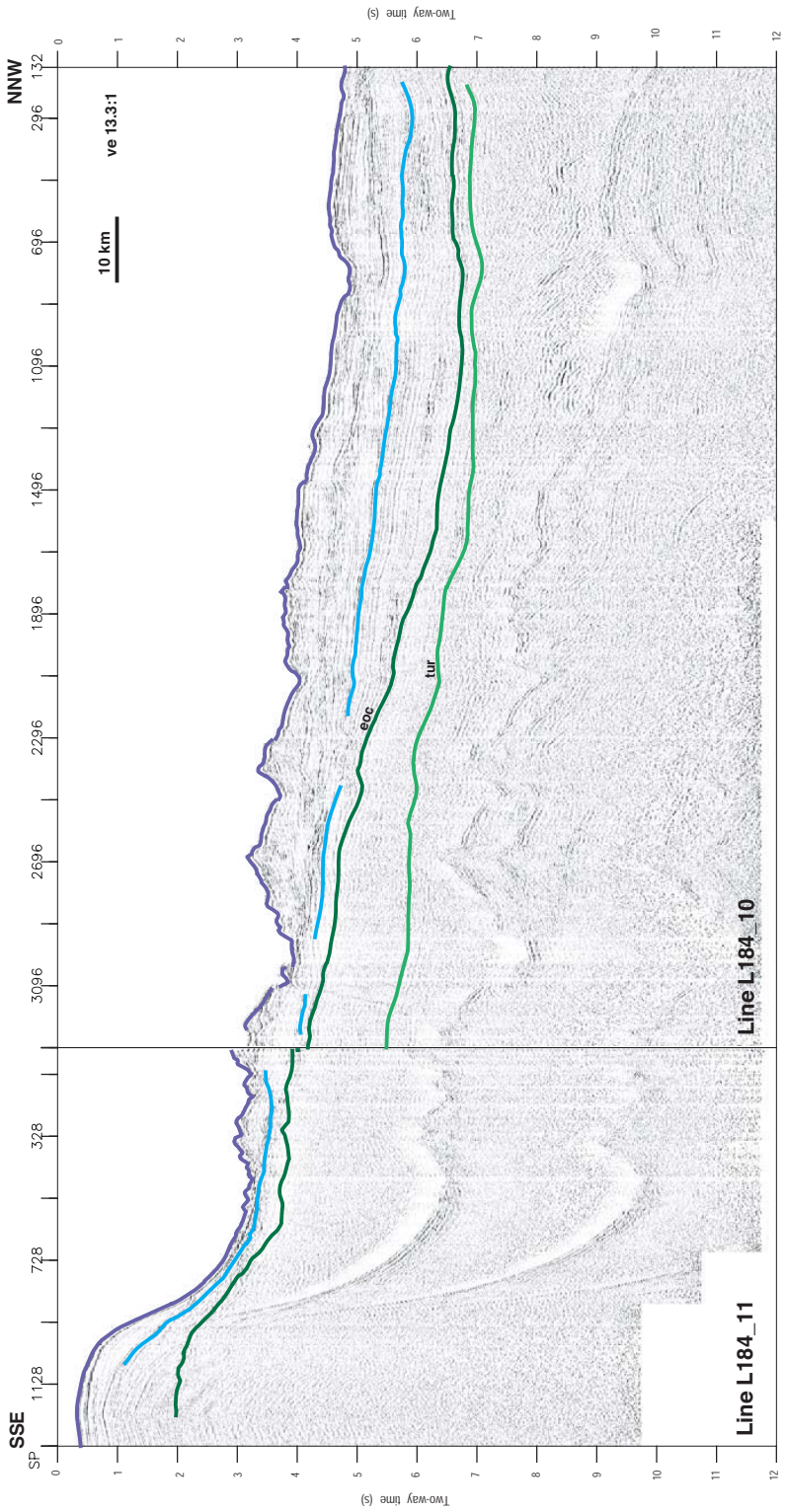


Figure 4.17: USGS, survey L184 Lines 10 and 11 as labelled. Strong multiple reflections beneath the continental slope and shelf prevent the imaging of the base of sediments.

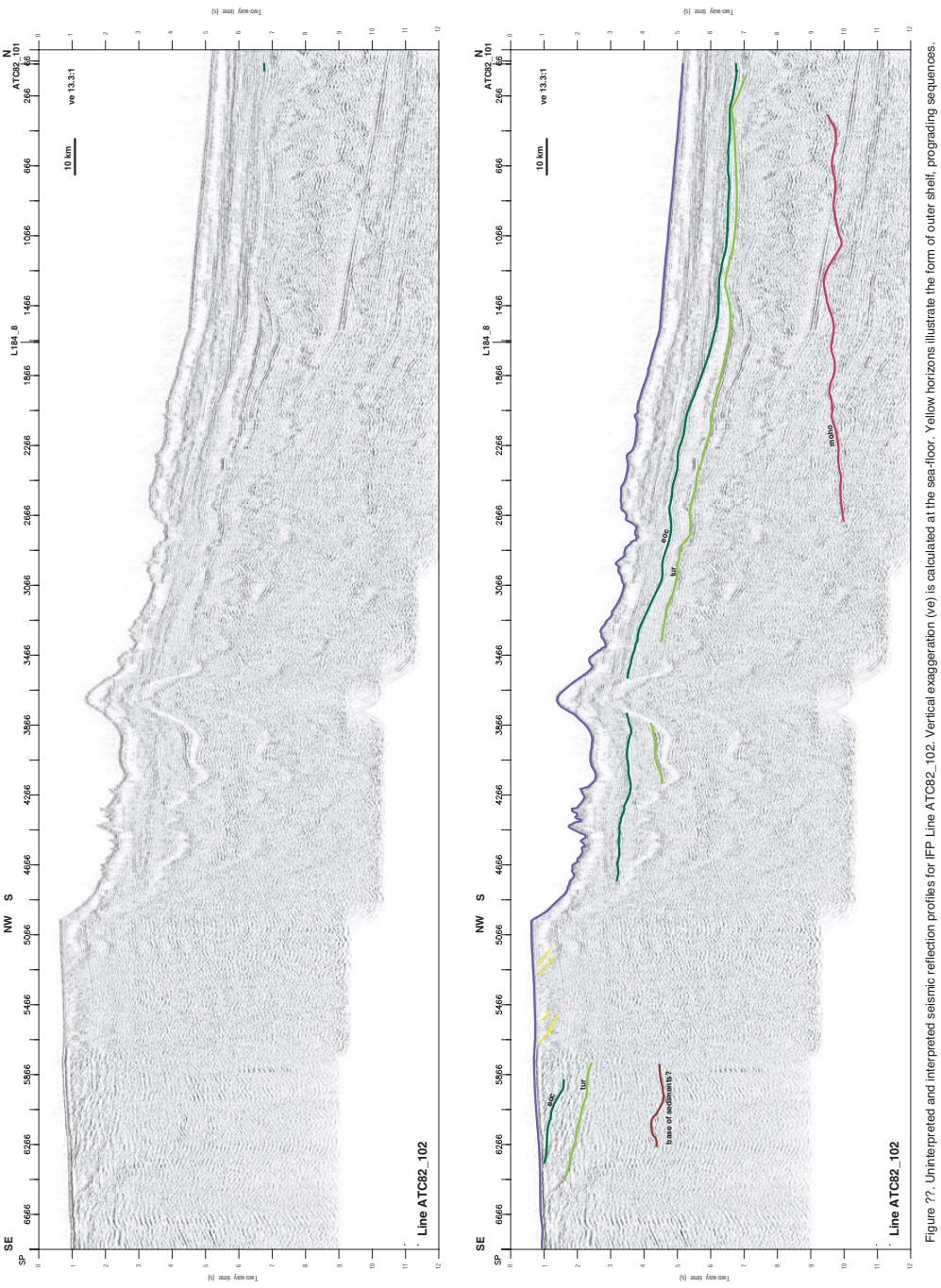


Figure ??: Uninterpreted and interpreted seismic reflection profiles for IFP Line ATC82_102. Vertical exaggeration (ve) is calculated at the sea-floor. Yellow horizons illustrate the form of outer shelf, prograding sequences.

Figure 4.18: ifp, atc82_102.

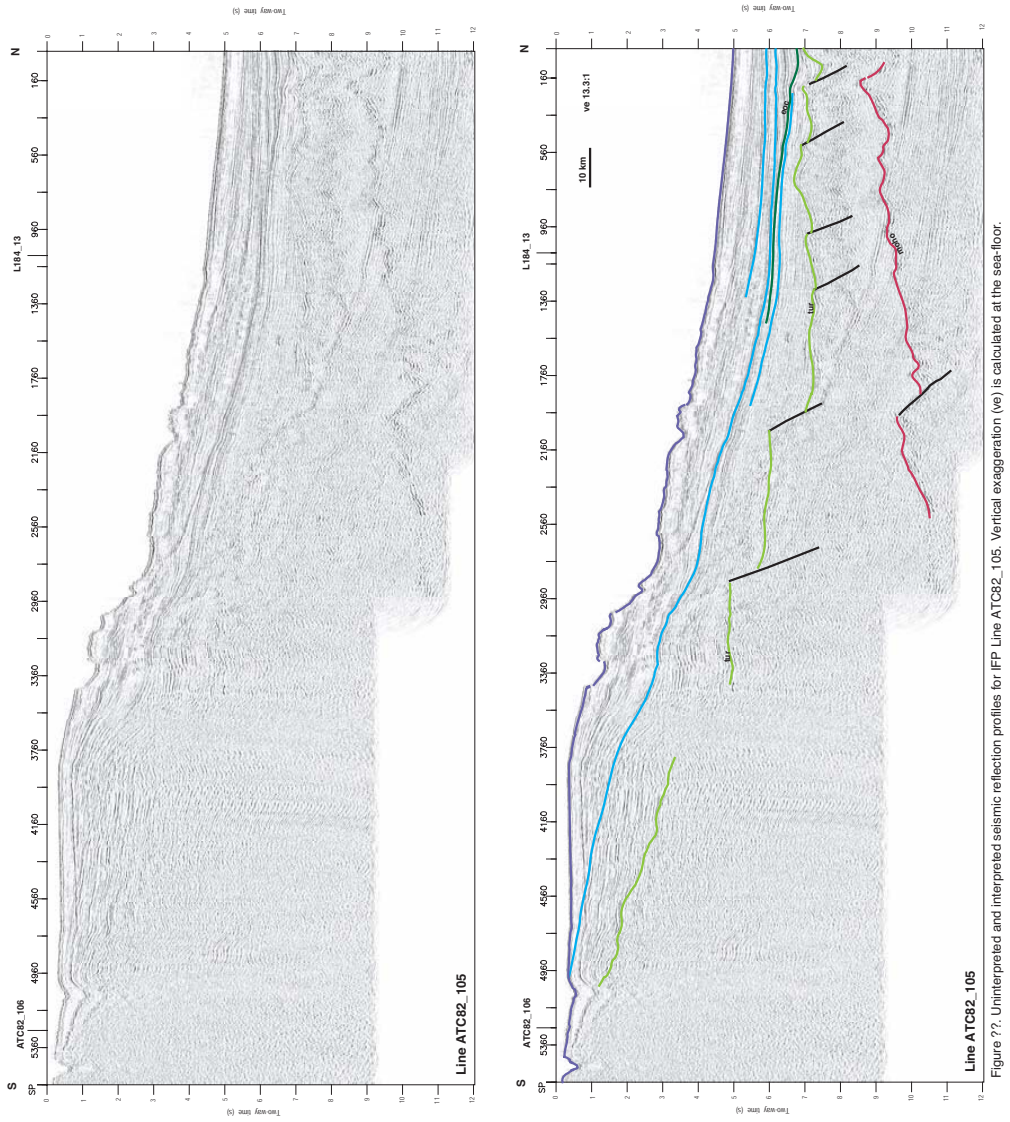


Figure 4.19: ifp, atc82_105.

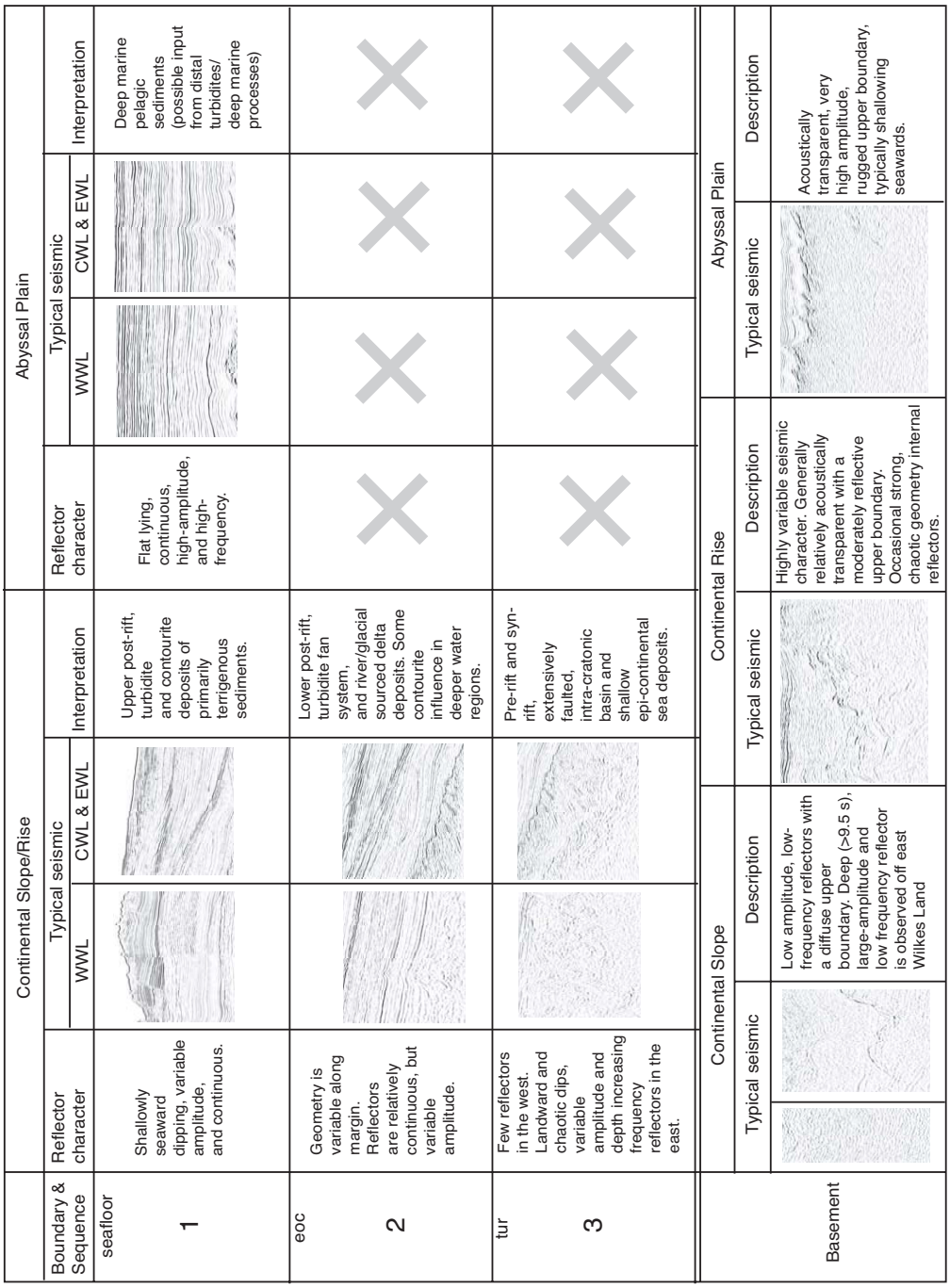


Figure 4.20: Stratigraphic summary of sequences interpreted in MCS data from the Wilkes Land margin. Variation in character and geometry of reflectors occurs along this extensive margin sector, and also across the margin with changing water depth and depositional environment.

## 4.4 Sequence 1: upper post-rift sediments

Reflector configuration and geometry of Sequence 1 are highly variable along the Wilkes Land margin. Changes in reflector character and structure occur on all scales. Clinoform reflectors are reported in survey ATC82 seismic profiles from east Wilkes Land beneath the outer shelf [Eittreim *et al.*, 1995]. Generally, however, reflectors grade from shallowly seaward dipping on the continental slope and rise to flat lying in the abyssal plain, mantling the underlying oceanic crust. Reflectors are also relatively continuous and broadly parallel, and exhibit consistently high amplitudes, except in low-amplitude zones below a bottom simulating reflector (BSR).

West Wilkes Land profiles, Lines GA-228_18 to GA-228_21, are characterised by reflectors relatively concordant with the underlying *eoc* unconformity, dipping shallowly seaward. Whereas, the central and east Wilkes Land profiles are characterised by relatively flat-lying reflectors that onlap the *eoc* unconformity landward, and offlap seaward onto oceanic crust. Lines GA-228_27 to GA-228_29 exhibit internal erosional unconformities and onlap surfaces, these are not observed off west Wilkes Land. The present-day seafloor, the top of Sequence 1, represents an angular unconformity for much of the margin, up to 1 s TWT of strata are abruptly truncated at high angles by canyons and channels, e.g. Line GA-228_18, Shot Points (SPs) 6700-6900.

The *eoc* unconformity represents the base of sequence 1 for all Wilkes Land margin sectors. Beneath the upper continental rise and continental shelf the unconformity exhibits evidence of erosion of up to 1.5 s of underlying sequence 2 strata, e.g. Line GA-228_25. The unconformity itself is often a relatively high amplitude reflector that is easily identified, however, the distinct onlap pattern of the overlying strata of sequence 1 is the most striking characteristic of this unconformable surface.

The thickness of seismic sequence 1 varies from 0 to >3 s TWT and is highly variable along the margin. A thick sequence (>3 s) is located off west Wilkes Land, predominantly between the shelf break and the abyssal plain. In contrast, sequence 1 is almost entirely absent from the outer continental slope off central-east Wilkes Land, e.g. Line GA-228_28. Refraction (from sonobuoys) and interval velocities (derived from semblance analysis) between 1.6 and 4 km/s (average $\approx$ 2.2 km/s) are recorded from sequence 1. The highest velocities in this range are recorded for the more deeply buried sediments off west Wilkes Land.

Sequence 1 is broadly interpreted as an onlap-fill sequence [Sangree & Widmier, 1977], composed primarily of turbidite, contourite, and hemipelagic deposits. Limited drilling on the outer rise, off the east Wilkes Land margin (DSDP sites 268 and 269), recovered sediment consisting of fine-grained turbidite facies and hemipelagic sediment in the lower

section, and coarser-grained turbidite facies, contourites and hemipelagic sediments in the upper section [Hayes & Frakes, 1975]. Reflector configuration and the geometry of erosional surfaces and channels are interpreted to represent a seaward migrating and laterally shifting turbidite fan system.

The modern continental slope, comprising an intricate network of downslope, broadly north-south oriented, canyons that transition into numerous channels on the continental rise, provides an analogue for the palaeo-fan system. Levee and overbank deposits form proximally to the channels, these are subject to downslope and geostrophic currents that preferentially entrain and transport different components of turbid sediment currents. The finest-grained components are likely transported laterally by along margin, contour hugging geostrophic currents, whereas larger, heavier sediment grains form the more proximal channel overbank and levee deposits.

Sequence 1 stratigraphy exhibits a wide range of erosive and constructional sedimentary structures, indicative of a dynamic and at times highly energetic depositional environment. No single, regional seismic stratigraphic feature is recognised as an indicator of glacial onset. The thick accumulation of post-Eocene sediments, however, is likely a direct indicator of wet-based, polythermal glacial erosion and sediment transport Powell [1984].

## 4.5 Sequence 2: lower post-rift sediments

Sequence 2 comprises up to 2.5 s TWT of mostly downlapping or grossly concordant reflectors of variable continuity, amplitude and frequency. The base of Sequence 2, the *tur* horizon, deepens from ∼6 s TWT beneath the outer continental slope to 8 s TWT below the abyssal plain.

Off west Wilkes Land, sequence 2 thins evenly seaward and comprises reflectors dipping shallowly seaward, downlapping onto pre-rift sediments and, transitional and oceanic crust. The overlying *eoc* horizon is relatively conformable with sequence 2 reflectors on Lines GA-228_18 to GA-228_21 and no internal unconformable reflectors are evident.

Profiles east of Line GA-228_22 exhibit greater variation in thickness and internal reflector complexity relative to west Wilkes Land. More steeply dipping, downlapping reflector sequences, are evident beneath the lower continental slope, e.g. Line GA-228_24, that grade seaward into grossly flat-lying reflectors concordant with the underlying unconformity. Internal, erosional unconformities are also inferred based on reflector termination and corresponding changes in reflector geometry. Greater amounts of stratal truncation of upper reflectors (i.e. the *eoc* unconformity) also occurs off east Wilkes Land. Sequence 2 thickens landward on Lines GA-228_26 to GA-228_28 to >2 s TWT

and is locally overlain by less than >0.5 s TWT of Sequence 1.

Sequence 2 is interpreted as a lower post-rift sequence deposited under a regime of relatively slow thermal subsidence rates associated with slow spreading from breakup until the early to middle Eocene [Cande & Mutter, 1982; Tikku & Cande, 1999]. This sequence is interpreted as post-rift for all Wilkes Land margin sectors, except off east Wilkes Land, where growth faulting is interpreted to represent syn-rift deposition.

Several phases of delta development are evidenced along the margin during deposition of this sequence. The broadly sigmoidal and downlapping reflection configuration pattern observed beneath the lower continental slope on Lines GA-228_26 to GA-228_28 is interpreted to represent continental slope (foreset) and rise (bottomset) deposits, associated with delta progradation across the broad and slowly subsiding Wilkes Land margin after breakup. Internal unconformities likely indicate sea level changes and erosion during this initially slowly subsiding environment. The non-marine and continental shelf components of this delta are not imaged in GA-228 and GA-229 survey data, however, aggradational, nearly flat-lying shelf deposits are imaged on Lines ATC82_105 and ATC82_107. Hampton *et al.* [1987] interpret toplap terminations high in the continental slope section to represent either a lowering in sea level or an excess sediment supply relative to subsidence rates that allowed sediment to by-pass the shelf and continue to grow the slope. Along margin erosional channels, e.g. Line GA-228_25, SPs 6100-6300, support the occasional seaward migration of the delta-fan channel system during the deposition of sequence 2.

The geometry of sequence 2 changes off east Wilkes Land. The *tur* unconformity does not represent the base of extensional faulting, and the *tur* horizon shallows seaward from the base of the continental slope before deepening again further seaward, e.g. Line GA-229_06. Sequence 2 is subdivided off east Wilkes Land by the *maas* horizon. Reflectors from the underlying sequence exhibit seismic character and structural similarities to the Late Cretaceous Sherbrook Group and the upper part of the Early Cretaceous Otway Supergroup of the Otway Basin, southeast Australia [Moore *et al.*, 2000]. The unconformity at the top of this sequence (*maas* horizon) is therefore interpreted as being Maastrichtian (∼71-65 Ma) in age. Reflectors within the sequence, bounded below and above by the *tur* and *maas* horizons respectively, exhibit divergence towards fault footwalls, indicating that crustal extension continued between eastern Wilkes Land and the southeast Australian margin until the Maastrichtian.

Refraction velocities of 2.30 to 2.71 km/s were recorded from this sequence at sonobuoy GA-228-11 in central Wilkes Land and from sonobuoys GA-229-13 and GA-229-15 in east Wilkes Land. The range of interval velocities inferred from stacking velocity conversion shows a greater variation of 2 to 5 km/s. The higher interval velocities are inferred for

the more deeply buried sequence off west Wilkes Land.

## 4.6 Sequence 3: Pre-Breakup Sediments

Imaging quality of Sequence 3 is poor off west Wilkes Land relative to central and east Wilkes Land. Sequence 3 thickness reaches up to ~2.6 s TWT (~5 km) below the continental rise off central Wilkes Land, this decreases seaward and typically pinches out entirely against the landward extent of transition zone crust. The lower Sequence 3 reflectors exhibit variable amplitude and dip, and are relatively discontinuous. Upper Sequence 3 reflectors are more continuous, higher frequency, and generally lower and more consistent amplitude.

Sequence 3 is bounded above by the *tur* unconformity and below by the more diffuse *tran* horizon, interpreted as the top of crystalline basement. The *tur* horizon ubiquitously terminates against transition zone or early oceanic crust. The seaward extent to which this horizon is mapped is subjective, particularly as basement topography creates pinch-outs of the underlying reflectors on almost all lines. Many of the basement highs that cause the pinch outs are acoustically transparent, and are likely intrusive igneous bodies or possibly exhumed mantle; their character and genesis are discussed later in greater detail. Distinctly layered and truncated reflectors of Sequence 3 occur seaward of some basement highs, although they are isolated from unequivocal Sequence 3 reflectors, e.g. Line GA-228_24.

Extensive faulting is interpreted within Sequence 3, it is most easily identified in the upper sequence 3, e.g. Lines GA-228_22 and GA-228_23. Faults are almost entirely seaward dipping normal faults, along which rotation of fault blocks has occurred, Figure 4.21. Landward dipping faults, however, are also imaged.

A number of sonobuoys record the seismic velocities of Sequence 3. Velocities recorded in all but the upper-most sequence range from 3.66 to 4.61 km/s. This velocity range correlates closely to the pre-rift sequence from the conjugate southern Australian margin (e.g. Veevers [1987] and Sayers *et al.* [2001]). It also encompasses the range of seismic velocities measured from Beacon Supergroup rocks of 4.1 to 4.4 km/s [Bentley & Clough, 1972]. On the basis of seismic velocity correlations, and the extensive faulting relative to overlying sequences, Sequence 3 is interpreted to represent a pre- and syn-rift sequence that was highly stretched and deformed by extensional rifting processes. By analogy with the pre- and syn-rift geological record of southern Australia, Sequence 3 likely comprises both siliciclastic and cool-water carbonate sub-sequences. Salt sequences (common to rift margins) are not observed in well data from the southern Australian margin, and it is unlikely, given the more southerly location of the Antarctic margin, that evaporites


Figure 4.21: Detail of Line GA-228_24 illustrating reflector truncation and offset associated with faulting. Rotation along faults (e.g. dashed-dot lines), causing landward dips (e.g. dashed lines), is also evident. The top of faulted and extended crust is interpreted as the base of the post-rift sequence.

formed on the Wilkes Land margin. High amplitude, concordant but discontinuous reflectors (e.g. Line GA-228_28, SPs 1100-1600) are likely intrusive sills associated with extensive Jurassic volcanism. The Beacon Supergroup is extensively intruded by Jurassic dolerites [Quilty, 1986], and likely correlates to basal sub-sequences of Sequence 3.

No clear rift-onset unconformity, as defined by Falvey [1974], is evident within Sequence 3 on the Wilkes Land margin. This is likely a function of the complex rift history indicated by subsidence studies on the southern Australian margin [Hegarty *et al.*, 1988; Totterdell *et al.*, 2000]. Modelling indicates 1-2 km of subsidence due to an intracratonic rifting event in the Late Jurassic, 160-140 Ma. This event occurred contemporaneously with extensive igneous activity in Gondwana; represented by the Karoo province in southern Africa and the Jurassic dolerites of south-eastern Australia and Antarctica. Rifting is also inferred at this time between East Antarctica and Africa/South America, ∼150 Ma [Rabinowitz & LaBreque, 1979].

Relatively subdued thermal subsidence followed intracratonic extension and there is no evidence of oceanic crust emplacement. A second extensional rifting event, is inferred from subsidence modelling on the southern Australian margin at ∼100 Ma. Slow thermal subsidence recommences at ∼85-90 Ma and this correlates to the earliest known seafloor spreading anomalies in the Australia-Antarctic Basin (AAB) [Cande & Mutter, 1982].

Slow thermal subsidence is interpreted to relate to the slow (<5 mm/yr HSR) rates of seafloor spreading following breakup [Cande & Mutter, 1982; Tikku & Cande, 1999].

The multiple rift event history and subsequent slow thermal subsidence violates the simple assumptions of Falvey [1974]. Hence, no rift-onset unconformity is identified along the Wilkes Land margin. However, an unconformity within Sequence 3, e.g. Line GA-228_24 (dark green horizon, SPs 0-1500), is inconsistently observed on seismic profiles from central and east Wilkes Land. This horizon represents a change in seismic character from the overlying relatively high frequency, landward dipping reflectors bounded by normal faults, to the underlying, more chaotic reflection patterns. This horizon likely represents an unconformity associated with either the Late Jurassic or mid-Cretaceous rifting events and correlates to the *K2* reflector of Eittreim & Smith [1987], which they interpreted as a rift-onset unconformity. The horizon may represent the erosional, upper boundary of the Beacon Supergroup.

Evidence of syn-rift deposition is sparse, reflector divergence and growth faulting can be inferred on Line GA-229_06 only. Wilson *et al.* [2001] note similar broad absences of syn-rift sediments, as represented by stratal divergence towards fault footwalls, on the west Iberian margin also. They suggest this may be due to resedimentation of syn-rift sediments, a lack of hanging-wall rotation, or the syn-rift interval being too thin to resolve in MCS data.

Although some intrusive igneous activity is interpreted in the pre-rift sequence, very little evidence of extrusive volcanism, in the form of seaward dipping reflector sequences, is evident in the late pre-rift and syn-rift sequence. The absence of such evidence supports the contention that the southern Australia-East Antarctic rift margins are non-volcanic (e.g. Nichols *et al.* [1981] and Totterdell *et al.* [2000]).

## 4.7 Regional Unconformities: Ages and Correlations

Although many local unconformities are evident in seismic reflection data, only two are correlatable along the entire Wilkes Land margin. These two unconformities separate Sequences 1, 2, and 3 as described above. The *eoc* unconformity forms the base of a sequence of clearly onlapping strata. It is interpreted here to represent a change in tectonic setting of the Wilkes Land margin at early to middle Eocene time (∼50 Ma). The lower of the two regional unconformities (*tur*) is marked by a strong reflector that represents the upper limit of the pre-rift sedimentary sequence for the west and central Wilkes Land sectors. However, extension and syn-rift sedimentation continues above this unconformity off east Wilkes Land and Terre Adélie.

These unconformities are identified as U3 and U2 by Wannesson *et al.* [1985], and T

and K1 by Eittreim & Smith [1987] and Hampton *et al.* [1987] on the east Wilkes Land-Terre Adélie margin. Tanahashi *et al.* [1994] sought to simplify the nomenclature used for the Wilkes Land seismic stratigraphy and renamed the U3/T and U2/K1 unconformities as WL2 and WL3 respectively. De Santis *et al.* [2003] again redefined the nomenclature and provide a detailed stratigraphy for the post-rift sedimentary sequence of the east Wilkes Land-Terre Adélie margin. Analysis of line ties between GA-228, L184 and ATC82 survey data indicates that the WL3 and WL2 unconformities correspond to the *tur* and *eoc* unconformities respectively. The WL2 unconformity was initially interpreted by Hampton *et al.* [1987] as the result of a relative sea-level drop at ∼65 Ma. However, a second, less favoured interpretation that associated the unconformity with a global plate re-organisation at ∼42 Ma was also considered. The WL3 unconformity is interpreted by Wannesson *et al.* [1985] and Eittreim & Smith [1987] as the breakup unconformity, this accords with our interpretation that *tur* is associated with breakup.

More recent interpretations by Eittreim *et al.* [1995] and Escutia *et al.* [1997] suggest that the WL2 surface is an erosive unconformity caused by glacial downcutting at ∼40 Ma. These workers invoke fast-flowing ice streams, grounded as far as the shelf break, to erode the pre-glacial continental shelf. De Santis *et al.* [2003] suggest that the unconformity does not have a glacial origin and we accord with this re-assessment. Several lines of evidence contraindicate a glacial erosive genesis and 40 Ma timing for the *eoc* or WL2 unconformity.

The margin wide extent of the *eoc* unconformity requires that if it is associated with glacial erosion, glaciation would necessarily have been continent wide at 40 Ma. The relative importance of the contributing factors to Tertiary polar glaciation, such as declining $CO_2$ concentrations, opening of deep water pathways around the entire continent and the presence of high elevation areas, is not well constrained. The timing of the rapid onset of glaciation extending beyond isolated highland areas, however, near the Eocene-Oligocene boundary (∼34 Ma), is well constrained by Ocean Drilling Project (ODP) data (Legs 188) (as discussed in Chapter 2). This evidence precludes the possibility of a glacially controlled *eoc* unconformity at 40 Ma.

A further problem to a glacial origin is the continuity of the *eoc* unconformity surface, from the lower continental rise to the continental shelf, which suggests a relatively synchronous formation. To fulfil this timing criteria and invoke a glacial genesis for this unconformity, erosion on the slope and rise is required contemporaneously with a glacial advance across the shelf; there is no *a priori* reason why such events should be synchronous. Clearly the *eoc* unconformity can not have a direct glacial origin beyond the shelf break, as grounding ice on the continental slope is not feasible.

We suggest an early to middle Eocene timing, and tectonic origin for the *eoc* uncon-

formity. Comparison of Wilkes Land and southern Australian margin MCS data reveals an almost symmetric stratigraphic pattern from the breakup unconformity until the middle Tertiary. The prominent onlap surface (*eoc* horizon) is dated as early Eocene on the basis of its correlation with similar onlap surfaces in the Great Australian Bight (base Dugong sequence, Figure 4.22, [Totterdell *et al.*, 2000]), in the Otway Basin (base Nirrinda Group, [Moore *et al.*, 2000]) and in the Sorell Basin on the west coast of Tasmania (unconformity U5, [Hinz *et al.*, 1986]). The unconformity is dated in a number of wells on the southern Australian margin as early to middle Eocene (∼50 Ma) [Totterdell *et al.*, 2000]. The stratigraphic position and characteristic onlap pattern of the *eoc* boundary is compelling evidence of a synchronous event in a relatively narrow oceanic basin (<400 km, based on spreading rates of Tikku & Cande [1999]).

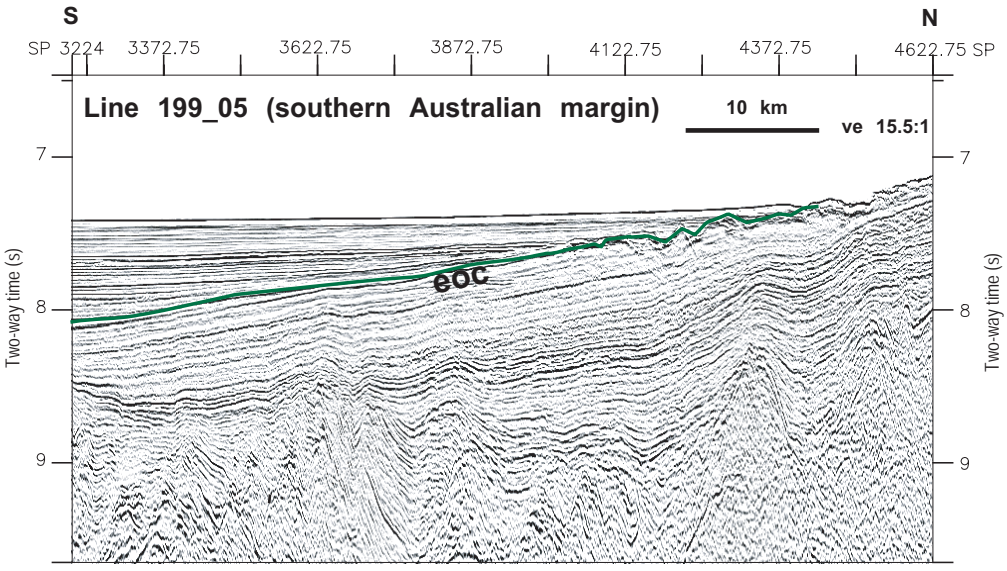


Figure 4.22: This strong onlap surface on the southern Australian margin (dark green horizon) is interpreted to correlate to the *eoc* horizon on the Wilkes Land margin. Seismic and well data from the Australian margin indicate an Early- to Mid-Eocene age for this unconformity.

The inferred timing of the *eoc* unconformity corresponds to the end of ultra-slow (∼1.5 mm/yr half rate) seafloor spreading rates, [Tikku & Cande, 1999]. Associated with this spreading rate increase is an increase in the thermal subsidence in wells on the southern Australian margin at ∼50 Ma [Totterdell *et al.*, 2000]. The result of an increased subsidence and spreading rate is a wider, deeper ocean basin that could have allowed the initiation of deep water, erosive currents and resulted in the formation of the *eoc* unconformity. Increased subsidence may have increased the gradient of the continental slope, and also have destabilised shelf and upper-continental slope sediments, resulting

in widespread slumping and erosion on the continental slope.

The *tur*, angular unconformity represents the top of extensional faulting and structuring off Wilkes Land. Accordingly, it is interpreted to represent breakup and the transition from intracratonic, continental stretching to sea floor spreading. This horizon can be correlated for over 1500 km along the margin, it is marked by a strong reflector which exhibits significant topography (0.5-1 s TWT) and fault-plane, ridge surfaces. The timing of this unconformity is constrained broadly through interpretation of seafloor isochrons as 83-95 Ma.

On the Southern Australian margin, the base of the post-rift sequence (base Hammerhead sequence of Totterdell *et al.* [2000]) is estimated as Santonian (∼85 Ma). This is underlain by the syn-rift Tiger Sequence. No clear syn-rift sequence is interpreted on the Wilkes Land margin, but the reflection and structural character of the *tur* unconformity is similar to the base Tiger sequence unconformity of Totterdell *et al.* [2000] [Colwell *et al.*, in press]. Identification of *P. mawsonii* spore-pollen in well data, from the southern Australian margin, dates the oldest sediments above this unconformity as early Turonian (∼90 Ma) [Totterdell *et al.*, 2000]. Therefore, the *tur* unconformity represents an erosional unconformity at ∼90-85 Ma.

The identification of the *tur* and *eoc* unconformities on the Wilkes Land margin allows an insight into the broad scale, post-rift depositional history of the Wilkes Land margin. The post-rift stratigraphy provides the fullest record of margin evolution since rifting. Stratigraphic interpretation of this sequence is of particular interest as it records the global transition from greenhouse to icehouse conditions, adjacent to the continent where this transition initiated. The distribution of post-rift sediments and structures imaged within Sequences 1 and 2 are discussed later in this chapter.

## 4.8 Continental Crust

Continental crust is interpreted at the landward extent of all MCS profiles, beneath the continental shelf and slope, and extended continental crust is interpreted to extend beneath the continental rise on a number of profiles. Strong water bottom multiple reflections, ubiquitous on the Antarctic margin Larter *et al.* [1990], prevent clear imaging through sediments in continental shelf data. However, it is possible to estimate a minimum sediment thickness in L184 and ATC82 data. Sediment thickness reaches at least 4 s TWT (∼5-7 km) below the shelf on line ATC_102, and total depth to this surface is ∼5 s TWT. Line drawings of line ATC_103 indicate a similar thickness of continental shelf sediments [Eittreim *et al.*, 1995]. Crustal or *Moho* reflections are not imaged beneath the shelf in MCS or seismic refraction data, hence no constraint on crustal structures

or the thickness of relatively unstretched continental crust is available from seismic data alone. The basement likely comprises metamorphic rocks of the continental shield, as the most common coastal and highland rock outcrops along the Wilkes Land margin are Proterozoic metamorphic rocks as discussed in Chapter 2.

Large-scale downfaulting of the crystalline basement is inferred beneath the outer continental shelf and continental slope. Combined sediment and water thicknesses of over 10 s TWT overlie the basement beneath the continental rise; >5 s TWT deeper than beneath the continental shelf. Strong water bottom multiples and a lack of data from the upper continental slope and continental shelf prevent the direct imaging of these fault structures. Basement faults at similar relative location and of similar offset are also interpreted on the conjugate southern Australian margin [Totterdell *et al.*, 2000].

Seaward of the shelf-slope fault zone, deeply subsided, stretched continental crust extends for up to 250 km. Determining the extent of continental crust is subjective, it is based on seismic character, and to a degree the presence of faulted pre-rift crust/sediments. Imaging of crustal structure in MCS data is variable along the margin. The relatively thinner sedimentary section off east Wilkes Land allows clear imaging of crustal structure. *Moho* reflections are also interpreted in MCS data from central and east Wilkes Land (Lines GA-228_23 to GA-228_29). Sonobuoy refraction data provides constraint on *Moho* depth for east Wilkes Land only, and even then only beneath stretched continental, and oceanic crust (sonobuoys GA-228-23, GA-228-21, GA-228-20). The only MCS *Moho* reflection that coincides with a refraction interpreted mantle velocity occurs on Line GA-228_28, here they correlate to within ∼0.3 s TWT.

The interpreted *Moho* is characterised by a high amplitude, long wavelength reflector beneath stretched continental or transitional crust and oceanic crust. However, on lines GA-229_06 and GA-229_07, a sequence of planar reflectors, similar in character to the *Moho* reflector occur; these are marked by the *llcc* horizon (laminated lower continental crust). Whether the top or base of these reflectors represents the *Moho* is unclear. This sequence of reflectors, therefore, indicates either altered upper mantle, or anomalous lower crust. Upper mantle reflectors are known from the Enderby margin of East Antarctica [Stagg *et al.*, in press], however, their genesis is uncertain. Refraction velocities associated with these reflectors are variable. At sonobuoys GA-229-12 and GA-229-13 refractor velocities of 6.82 and 6.57 km/s correlate to the *llcc* horizon. Landward on Line GA-229_07, however, at sonobuoy 15, a refractor velocity of 5.63 km/s correlates to the *llcc* horizon. These velocities are in the range determined for transition zone, upper mantle peridotites on the west Iberian margin [Dean *et al.*, 2000]. However, these possible 'transition zone' velocities occur beneath stretched continental crust on the east Wilkes Land margin, whereas they commonly form the top of basement between stretched continental

and oceanic crust on the Iberian margin.

Offsets in the *Moho* reflector (e.g. Line GA-228_28, shot-point (SP) 3400 and Line GA-228_27, SP 5200), indicate that faulting and brittle deformation occurred within the lower crust and upper mantle during or since rifting. The detailed orientation of these faults can not be determined, as the relatively acoustically transparent mantle and crustal character prevents faults being interpreted on the basis of reflector terminations and offset. The *Moho* reflector also exhibits some long wavelength relief. For example, on Line GA-228_27 (SPs 7900-7600) the *Moho* reflector deepens from 10 s to ∼10.75 s TWT (∼2-2.5 km) over a distance of ∼20 km, before shallowing again northwards.

Overlying the *Moho* reflector, within stretched continental crust, is an acoustically transparent zone (e.g. Line GA-228_25, SPs 5200-6900). The top of this zone is marked by an indistinct change in character (the *tran* horizon), and is interpreted as top of crystalline lower crust. Faults are typically not imaged within these lower crustal rocks, however, this again may be a function of the acoustically transparent rock character rather than an indicator of entirely non-brittle deformation. Sonobuoys GA-228-17, GA-228-21 and GA-229-11 recorded deep crustal refraction velocities of 6.60, 6.51 and 5.39 km/s respectively, coincident with the interpreted *tran* horizon. These velocities are consistent with the presence of continental crust [Stagg *et al.*, in press]. Higher velocity crustal refractions were also recorded at sonobuoys 288-16 (7.89 km/s) and GA-228-17 (7.84 km/s). These velocities are approaching typical mantle velocities of >8 km/s and likely represent altered upper mantle rocks.

The lower crustal sequence, bounded above and below by the *tran* and *Moho* horizons respectively, thins massively seaward as the *tran* horizon deepens and the *Moho* shallows. For example, on Line GA-228_24 if the *Moho* horizon is extrapolated landward, the lower crust thins from over 3 s to ∼1 s TWT (∼9 to ∼3 km) over a distance of 75 km. Large amounts of faulting in the overlying Sequence 3 accompanies the lower crustal thinning. The lack of lower crustal faulting imaged within this massive sequence indicates that much of the lower crustal thinning occurred through relatively ductile stretching.

The *tran* reflector can typically only be traced within unequivocal continental crust and wedges out against the onset of the interpreted transition zone crust. The *Moho* reflector is also not imaged as consistently seaward of the onset of transition zone crust (e.g. Line GA-228_24). A similar phenomenon is observed on the Iberian margin, where one of the identifying characteristics of transition zone crust is the lack of an identifiable *Moho* in seismic reflection and refraction data [Dean *et al.*, 2000].

## 4.9 Oceanic Crust

Unequivocal oceanic crust is observed at the seaward extent of all GA-228 and GA-229 seismic profiles. It is characterised by a relatively transparent acoustic character and rough, rugged topography. The velocity structure inferred from refraction modelling is also characteristic of oceanic crust. Although some variation in seismic character and crustal structure is observed, the oceanic crust remains the most uniform crustal type identified on the Wilkes Land margin. It is overlain, almost entirely, by mantled layers of high frequency reflectors, likely indicative of deep marine, pelagic deposition, with minor input from distal turbidites.

The top of oceanic crust is observed at depths of 6 to 8.5 s TWT, typically shallowing northwards. Greatest shallowing is observed on western lines (Lines GA-228_18 and GA-228_19) where the largest thickness of terrigenous sediments is observed, here oceanic crust shallows from >8 to 6.5 s TWT. This contrasts with the central Wilkes Land sector where over comparable distances the top of oceanic crust maintains a consistent depth of ∼7.5 s. The wavelength and amplitude of oceanic crust topography is also variable. Broadly speaking, the roughness of topography increases eastwards, towards the Spencer, Tasman and George V fracture zones. However, oceanic basement highs are observed on all profiles. Some are relatively broad, e.g. Line GA-228_18, SPs 2900-2200 (35 km), whereas others are very narrow, e.g. Line GA-228_26, SPs 4900-5150 (12.5 km). The wide spacing of the lines prevents correlation of any of these features along the margin.

Changes in topographic character are observed on a number of lines. For example, oceanic crust on Line GA-228_21 (including extension Line GA-229_10) exhibits relatively subdued topography from SP 6200 (Line GA-228_21) to SP 700 (Line GA-229_10), however, seaward of this point average basement depth is ∼0.5 s shallower and is characterised by rough topography. The topographic highs indicate a variable relationship between magma discharge at the South-East Indian Ridge (SEIR) spreading centre and extension and/or seafloor spreading. Volcanic buildups at the spreading centre may equally represent an increase in magma discharge or a decrease in spreading rates of the Australian and Antarctic plates. Slow seafloor spreading rates typically result in rough basement topography [Macdonald, 1982]. As changes in seafloor spreading rates are known to be variable for the Australia-Antarctic Basin from breakup until the early Eocene [Tikku & Cande, 1999], it is possible that changes in oceanic basement level (e.g. Line GA-228_19, SP ∼6000) correlate to major changes in seafloor spreading rates.

Faulting of oceanic crust is inferred on a number of lines. Faulting is likely more widespread than interpreted, however, due to the lack of internal reflectors and the

relatively homogeneous nature of oceanic crust, imaging of the faults is difficult. Faults that offset the top of oceanic crust are most easily interpreted, e.g. Line GA-228_23. Slow spreading rates are thought to be associated with greater amounts of mechanical extension within oceanic crust [Mutter & Karson, 1992], and therefore with extensional, normal faulting. Abundant evidence of large extensional faults is observed at the slow spreading Mid-Atlantic Ridge [Kong *et al.*, 1988]. As very-slow seafloor spreading rates (1.5 to 10 mm/yr half-spreading rates [Tikku & Cande, 1999]), are modelled for the Australia-Antarctic Basin for ∼50 Ma following breakup, faulting of oceanic crust is not surprising.

Reflections from the upper-most section of oceanic crust exhibit some layering, particularly adjacent to basement highs. These roughly laminar reflector sequences, e.g. Lines GA-228_23 and GA-228_24, are likely basaltic lava and pyroclastic flows, or slides of basaltic rock from adjacent crustal peaks. Again, the occurrence of these sequences indicate intermittent periods of magma discharge excess to rates of extension. Discontinuous, internal oceanic crustal reflections are also observed, e.g. Line GA-228_20. These internal reflections are most common in the oldest sections of oceanic crust. Shallowly dipping internal reflections, e.g. Line GA-228_24, SPs 4600-5300, may represent relic magma chambers, oceanic layer transitions (i.e. pillow basalts to sheeted dykes to massive gabbro), or layers of successively intruded sills. However, evidence from Cretaceous ocean crust in the Atlantic suggests it is likely that some of these internal reflectors are normal faults generated at or near the spreading axis [Morris *et al.*, 1993; Collier *et al.*, 1998].

Sonobuoy refraction data typically record two velocity layers within oceanic crust, and mantle velocities also at two locations. The uppermost crustal layer, layer 2, is characterised by velocities of 4.47 km/s (sonobuoy GA-229_19) and 4.93 km/s (sonobuoys GA-229_14, GA-229_18, GA-228_22). These velocities are at the lowest end of the 'average' velocity range for 'normal' layer 2 crust [Raitt, 1963; White, 1984; Bratt & Purdy, 1984]. At sonobuoys GA-228_15, GA-228_18 and GA-228_20, the top of oceanic crust (as determined in MCS data) correlates to a refraction velocity of 5.36 to 5.39 km/s, this velocity range is more typical of layer 2 oceanic crust.

Layer 3 oceanic crust P-wave velocities typically range from 6.5 to 7.0 km/s [Raitt, 1963; White, 1984; Bratt & Purdy, 1984]. Velocities between 6.56 and 6.72 km/s were recorded by sonobuoys GA-229_19, GA-228_15, GA-228_18, GA-228_20 and GA-228_23, indicating the presence of a distinct oceanic Layer 3. sonobuoys GA-229_18 and GA-229_26 recorded seismic velocities of 6.12 and 7.11 km/s respectively, these are outside the range of 'normal' oceanic layer 3 velocities, but are likely still representative of deep oceanic crust. The thickness of overlying layer 2 crust ranges from 1.3 to 2.6 km, which

is a typical range [Raitt, 1963; White, 1984; Bratt & Purdy, 1984].

Mantle velocities were recorded on only two sonobuoys over oceanic crust, sonobuoys GA-228_20 and GA-228_23. Velocities of 8.18 and 8.14 km/s were recorded at these locations respectively. At sonobuoy GA-228_20 the thickness of the overlying layer 3 crust is only 1.68 km, this is less than half the average layer 3 thickness of ∼4.6 km [Raitt, 1963]. The total oceanic crustal thickness indicated at this sonobuoy is 4.9 km. The thickness of layer 3 at sonobuoy GA-228_23 is 3.0 km, again significantly thinner than average layer 3 crust. The overall crustal thickness indicated at sonobuoy GA-228_23 is 4.96 km. Average oceanic crustal thickness, not affected by fracture zones and hotspots, is 7.1 km [White *et al.*, 1992]. The trend of 4.5 to 5 km thick oceanic crust inferred at sonobuoys GA-228_20 and GA-228_23 indicates oceanic crust off the Wilkes Land margin is less than 75 % the thickness of average oceanic crust.

Oceanic crust formed at spreading rates slower than <10 mm/yr is known to exhibit a sharp reduction in the thickness of crust formed [Bown & White, 1994]. Mutter & Mutter [1993] use seismic refraction data to demonstrate that variations in layer 3 thickness are the primary control on varying oceanic crust thickness. Refraction data from the Wilkes Land margin supports the hypothesis that thinner than average crust is associated with slow spreading, and also that layer 3 exhibits the greatest departure from average thickness.

The landward extent of oceanic crust can not be defined trivially. Although the seismic and morphologic features, and velocity structure of oceanic crust are characteristic, its most landward extent remains a subjective interpretation. On each seismic profile a continent-ocean transition zone is interpreted that separates unequivocal oceanic and continental crust.

## 4.10 Transitional Crust and the Continent-Ocean Boundary

The extent of continental and oceanic crust at continental margins is of fundamental importance to understanding rifting and plate tectonics. The continent-ocean boundary (COB), however, remains an enigmatic feature that can rarely be defined unequivocally at passive rift margins. The most diagnostic data for COB definition are seismic reflection and refraction, and gravity and magnetic anomaly data. Typically, a continent-ocean transition (COT) zone is defined at passive rift margins, which separates unequivocal continental and oceanic basement.

The width of transition zone crust of North Atlantic and Labrador Sea region rifted margins (a good analogy to the Wilkes Land and southern Australian margin due to

their non-volcanic character and slow-spreading history), varies from <10 to 170 km (see Dean *et al.* [2000] for references). The transition zone crust of the North Atlantic and Labrador Sea region is, in part, rigourously constrained by P-wave velocity structure. Where greater widths of transition zone crust are identified, the amount of extended continental crust is limited such that the sum of extended continental and transition zone crust is 100 to 200 km [Dean *et al.*, 2000]. The west Iberian margin (Galicia Bank and the southern Iberian Abyssal Plain) transition zone also includes a peridotite ridge that has been variably hydrated and serpentinised [Boillot *et al.*, 1980].

Refraction velocity data is far too sparse on the Wilkes Land margin to attempt to define a COT on the basis of P-wave velocity structure. The case for an indistinct, variable extent COT zone, however, can be demonstrated by the high quality, deep-penetrating seismic reflection data of surveys GA-228 and GA-229. The *cot* horizon is used to define the upper limit of pre-rift rocks that are not clearly continental or oceanic in structure and character. This zone represents some of the most deeply subsided crust on the Wilkes Land margin, reaching depths of up to 9 s TWT, and ranges in width from <30 to >100 km.

The belt of deeply subsided crust seaward of faulted and rotated continental crustal blocks is characterised by the presence of shallow-crustal and/or basement sub-cropping crystalline bodies. Seismically, these bodies are internally transparent relative to continental crust, however, they typically exhibit greater internal character than oceanic crust. Up to 1 s TWT of topography of the *cot* horizon is evident, through both faulting (e.g. Line GA-228_23), and crystalline basement uplift (e.g. Line GA-228_28). Imaging of the COT zone is inherently more difficult off west Wilkes Land where much greater post-rift sediment deposition has occurred. Variation in broad-scale topographic character of COT zone crust, however, can be inferred. The COT zone off west Wilkes Land is relatively subdued, whereas rough topography is observed in the COT zone off east Wilkes Land. A basement high on Line GA-228_29 penetrates the water column.

Crystalline basement highs may represent shallow, intrusive igneous bodies associated with Jurassic magmatic activity. However, it is possible that crystalline basement highs represent peridotite ridges or exhumed mantle. The coincidence in central and east Wilkes Land of the transition zone basement ridges and the termination of the *Moho* horizon in MCS data indicates that massive lower crustal thinning has occurred, unroofing the upper-mantle and forming a basement comprised of upper-mantle peridotites. A lack of typical mantle velocities, and therefore also a 'seismic *Moho*', characterises the transition zone crust of the Iberian Abyssal Plain margin [Dean *et al.*, 2000]. If the basement ridges observed off the west Wilkes Land margin are in part exhumed mantle, then they are likely serpentinised peridotite ridges similar to those interpreted off the Iberian margin.

A basement ridge on the conjugate southern Australian margin has been interpreted by Sayers *et al.* [2001] as a peridotite ridge. However, this can not be determined for the Wilkes Land margin on the basis of seismic reflection data alone.

The seaward and landward extents of the *cot* horizon, interpreted here on the basis of seismic and structural character, are interpreted to represent the extents of unequivocal oceanic and continental crust respectively. Sections of COT crust which are bound seaward by blocks of continental crust may represent abandoned seafloor spreading ridges, e.g. Line GA-228_18 and GA-228_22. The along strike extent of the COT zone is indicated in Figure 4.23. However, to consider either 'edge' of COT crust as a definitive determination of the COB is not realistic.

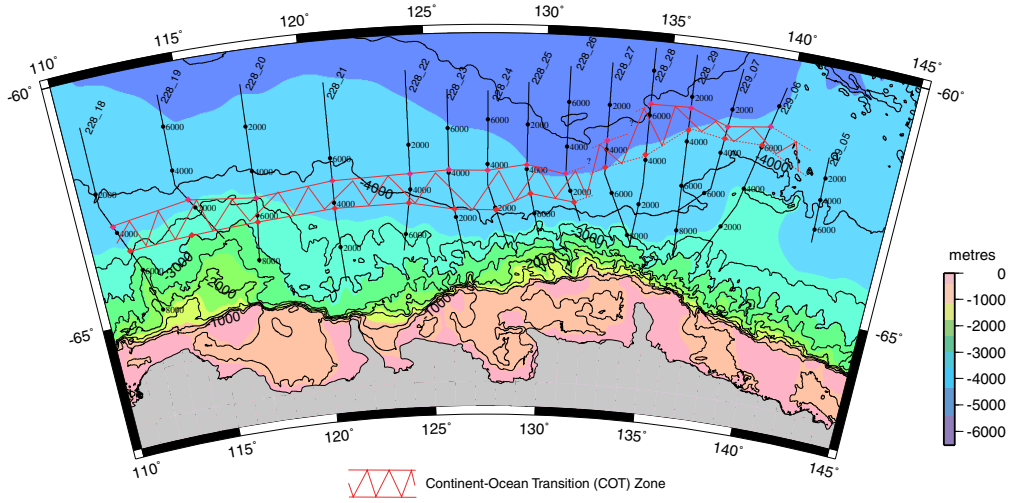


Figure 4.23: Continent-Ocean Transition (COT) zone along the Wilkes Land margin. The COB is interpreted to lie within this zone on the basis of crustal seismic character and velocity structure.

The similarity in crustal character of the crystalline bodies typical within the COT crust and oceanic crust precludes simplistic interpretation of a COB based on crustal identification. This is particularly true off west Wilkes Land due to the greater sediment thickness. Also, as radical changes in seafloor spreading rates occur for ~40 Ma post rifting, changes in oceanic crustal structure and character would be expected. Therefore, changes in crustal character may not necessarily indicate transition from stretched continental/transitional crust to oceanic crust. Initial interpretation of these data by Colwell *et al.* [in press] typically places the COB at a point of rapid change in crustal character, e.g. Line GA-228_19, SP 5000. However, on the basis of MCS data alone, there is nothing that precludes a COB up to ~180 km further landward for this transect, i.e. SP 1000. The COB interpreted by Colwell *et al.* [in press] for this line is located ~30

km seaward of the interpreted base of Eocene sediments, therefore implying an onset of seafloor spreading at <50 Ma.

The transition zone, as located in Figure 4.23, typically occurs ∼200 km from the shelf break and the COB typically <100 km further seaward. However, it steps out significantly off east Wilkes Land and Terre Adélie where the COB is located at ∼450 km from the shelf break. The interpreted width of COT crust also decreases in this region. This interpretation is discussed and defended in the following section.

## 4.11 Ocean Basin, Continental Crust, and Mantle Peridotites: The east Wilkes Land - Terre Adélie Margin

A group of seamounts, a basement ridge, and a broad bathymetric shallowing occurs at the edge of the abyssal plain off the east Wilkes Land margin, from 137-140°E, Figure 4.24. The seamounts and basement ridge reach heights of over 1000 m above the average ∼4000 m deep seafloor. The basement ridge forms the seaward extent of the broad zone of relatively shallowed bathymetry. The ridge reaches a maximum height at its eastern extent, and plunges to the west, continuing for ∼75-100 km above the seafloor. The seamounts and basement ridge are located south of the Spencer fracture zone, and ∼100 km west of the George V fracture zone.

An un-named, northwest-southeast trending basement structure (fracture zone?) can be inferred, from free air gravity anomaly data, directly east of the seamounts, Figure 4.25. The seamounts and basement ridge correlate to positive free air gravity anomalies. However, the regional gravity field is anomalous in this region; the broad edge-effect low, typical of the central Wilkes Land continental slope/rise transition, is replaced by a positive free air anomaly and an outer, negative free air anomaly.

MCS data have been acquired in this region by the IFP, USGS, JNOC and GA. In-situ peridotite blocks were also dredged during JNOC survey th95 from seamount B (Figure 4.24). A number of interpretations of this region of shallowed bathymetry and anomalous basement features have been presented. Wannesson *et al.* [1985] interpreted this region as an anomalous oceanic zone, similarly, Eittreim & Smith [1987] interpreted volcanic basement associated with early oceanic crust emplacement. In contrast, Tanahashi *et al.* [1997] suggest that basement in the region comprises either metamorphosed continental or igneous (but not oceanic basalt) crust.

Geochemical analyses of recovered peridotite samples indicate the seamounts have a fertile sub-continental mantle origin [Yuasa *et al.*, 1997]. The existence of sub-continental mantle material does not definitively indicate the presence of continental crust around the seamounts. However, it can be inferred that oceanic crust was not being produced in the region of the seamounts during their formation. As the seamount samples were recovered seaward of oceanic crust interpreted by Wannesson *et al.* [1985] and Eittreim & Smith [1987], the mineral chemistry analyses support the conclusions of Tanahashi *et al.* [1997].

MCS data from the IFP (ATC82) and USGS (L184) surveys do not penetrate sufficiently to image structures within pre-rift rocks. However, MCS data from the th95, GA-228 and GA-229 surveys confirm that basement is comprised of continental crust beneath this bathymetric anomaly, and that the ridge is not composed of oceanic crust.

These data indicate a stretched crystalline lower crust, overlain by up to 3 s TWT of extensively faulted pre- and syn-rift metasediments/sediments. The thickness and structures of the faulted and deformed sedimentary sequence, beneath <0.5 to 2 s TWT of deep marine sediments, precludes the possibility of oceanic crustal basement, Figure 4.26. This region of deeply subsided but clearly continental crust is labelled the Adélie Rift Block by Colwell *et al.* [in press], and we follow this protocol here.

The basement ridge is traversed by line th95_04, SPs 350-1000 (Figure 4.27) where the ridge core forms a north-facing scarp. The more gently dipping southern ridge-flank is overlain by ∼1 s TWT of sediments, which dip conformably with the underlying crystalline basement. This structure likely represents a large-scale, rotated fault, that has exposed the lower crust. The dipping sediments are overlain by an angular unconformity above which flat-lying, marine sediments onlap.

The westward, thinly sediment covered, extent of this basement ridge is traversed by Line GA-229_06, SPs 3500-4500. The ridge is significantly broader and deeper at this location and the crystalline basement occurs below an even greater thickness of pre- and syn-rift sediments (up to 3 s TWT). The top of crystalline lower crust (*tran* horizon) is not evident until a depth of ∼8-9 s TWT. Growth faulting occurs in the upper sedimentary sequence, indicating active extension during deposition. Both landward and seaward dipping fault blocks are imaged, suggesting a spatially variable locus of extension during rifting.

The landward extent of the basement ridge, on Line GA-229_06, correlates to a large-offset (∼0.5 s TWT) normal fault that penetrates through the upper-crustal, pre-rift sediments, into the laminated lower crust. This point is also the location of greatest crustal thinning imaged on this line. Assuming the thickness of the laminated lower crust is <1 s TWT (as it is farther north on this line), less than 3 s TWT of the total pre-rift crustal thickness remains. This region corresponds to a positive free air gravity anomaly that is interpreted to represent very shallow level mantle rocks associated with the crustal thinning, Figure 4.25. At the seaward extent of the basement ridge a crystalline basement high occurs in the upper-crust, and the laminated lower crust and *Moho* reflections terminate at depth. This is typical of the transition zone crust of central Wilkes Land. An isolated rift basin of 30-50 km width separates the *cot* body from oceanic crust.

Although the ridge structure becomes diffuse and less clearly imaged to the west, e.g. Lines GA-229_07, GA-228_29 and GA-228_28, the depth of the pre-rift upper surface remains elevated (average ∼6 s TWT) in the Adélie Rift Block relative to central Wilkes Land (average ∼7.5 s TWT). The Adélie Rift Block exhibits similar characteristics to the "extensional allocthons" observed in the Alps, which are interpreted to be separated from underlying exhumed mantle rocks by low-angle detachments [Manatschal, 2004].

These extensional allocthons are also interpreted to have formed within a slow spreading ridge environment.

Rough crustal topography, comprising basement highs independent of the basement ridge, is also evident in MCS data from the Adélie Rift Block. A crystalline basement high remains a consistent feature at the transition from stretched continental to oceanic crust in this region. However, the along strike extent of the basement highs is equivocal. An along-strike transect recorded during survey th95, Line th95_06, exhibits rough basement topography (Figure 4.27). This indicates that basement highs surveyed on north-south profiles may represent either ridge or seamount structures. The thickness of the post-rift sediments and height of the individual basement highs dictate whether they have a bathymetric expression.

Line th95_04 and th95_06 MCS data show seamount flank gradients of ~7.5-15%, e.g. Line th95_06, SPs 900-1400. The seamounts are characterised by a lack of coherent internal reflections. Basement highs, similar in morphology and seismic character to the observed seamounts, are observed partially or entirely sub-seafloor at a number of locations, e.g. Lines th95_06 (SPs 2900-3200), GA-228_29 (SPs 3200-3600). These features typically correlate to positive free air gravity anomalies (Figure 4.25). Interpolating between the known locations of seamounts and/or basement highs of similar character using the free air gravity data indicates an arcuate belt of similar features as illustrated in Figure 4.25. As in-situ mantle peridotites have been dredged from one of these seamounts, we suggest this belt represents a zone of extreme crustal thinning and a zone of exhumed continental mantle that forms the seaward extent of the Adélie Rift Block.

Modelling results of Pérez-Gussinyé *et al.* [2001] indicate that serpentinisation of the upper mantle occurs preferentially in cratonic rift margin environments characterised by stretching factors of 3-4. These stretching factors are observed and exceeded for most of the Adélie Rift Block. A second key factor that contributes to the presence of shallow level and exhumed, serpentinised mantle rocks is low melt production; which is also characteristic of slow spreading ridges [Bown & White, 1995]. The Adélie Rift Block exhibits many of the key factors optimal for mantle serpentinisation, as outlined by Pérez-Gussinyé *et al.* [2001]. Under these rift conditions brittle, full-crust faulting allows water to penetrate and serpentinise the mantle. Given the modelling results of Pérez-Gussinyé *et al.* [2001] and the similarities between the Adélie Rift Block and the west Iberian margin, it is likely that the upper mantle beneath the stretched continental crust of the COT zone of east Wilkes Land is, at least partially, serpentinised.

The interpreted COB location, based on MCS data and the geochemical analyses of recovered basement samples, on the east Wilkes Land margin, occurs over 450 km from

the shelf break. This is ~220 km further seaward than the interpreted COB in central Wilkes Land. This indicates that following the commencement of seafloor spreading in the central Australia-Antarctic Basin, continental crust to the east continued to stretch. Points of massive crustal thinning, as observed on Line GA-229_06, indicate that the continental crust stretched to <20% of its original thickness (assuming an initial crustal thickness of 31 km) without failing and allowing seafloor spreading to commence. This point of maximum stretching and crustal thinning occurs at a similar distance from the shelf break as the interpreted COB to the west. It is likely that this point represents a failed rift as continental crust extends seaward for up to 250 km from this point of extreme thinning before oceanic crust is encountered. Bassi [1995] demonstrates that the increased cooling associated with slow stretching causes the crust to become brittle, and the locus of maximum strain rate to move laterally and induce widened rifts. However, although widened rifts are predicted at slow rifts, modelling by Bassi [1995] also indicates it is not possible to stretch, brittle continental crust to the extent observed here.

Extensive terranes of submarine continental crust, such as the Campbell Plateau, New Zealand, and Exmouth Plateau, Australia, are well known [Nur & Ben-Avraham, 1982], however, they typically occur at relatively shallow depths (<1000 m). Stretched continental crust is inferred at greater depths at other passive rifted margins, e.g. West Iberia [Dean *et al.*, 2000], Labrador Sea [Chalmers & Pulvertaft, 2001], West Africa [Rosendahl & Groschel-Becker, 2000], East Coast U.S.A [Mohriank & Talwani, 2000], southeastern Brazil [Bassetto *et al.*, 2000], South China Sea [Huchon *et al.*, 2001], and southern Australia [Sayers *et al.*, 2001]. However, at none of these locations is the COB located at distances of greater than ~250 km from the shelf break. The Rockall Trough is an example of a failed rift that is interpreted to be floored by massively stretched continental crust (~6 km thick) that is now subsided to great depths [Pérez-Gussinyé *et al.*, 2001]. However, the width of Rockall Trough stretched crust is ~200 km, still less than half the total width of massively stretched crust off the east Wilkes Land margin.

The Wilkes Land margin, and the Adélie Rift Block in particular, share a number of similar characteristics to the west Iberian margin, e.g. slow spreading ridge, non-volcanic rifting, presence of massively thinned crust, and exhumed and serpentinised mantle peridotites. However, the zone of exhumed mantle off Wilkes Land, as interpreted from MCS and free air gravity anomaly data, is much narrower than off West Iberia. In contrast, the extent of unequivocal continental crust at abyssal depths, off east Wilkes Land in the Adélie Rift Block is greater than observed off West Iberia (or any other well-studied passive rift margin). The identification of the COB at this location adds further complexities to tectonic reconstructions in an area where continental overlap is already noted in reconstructions [Tikku & Cande, 1999; Royer & Rollet, 1997].

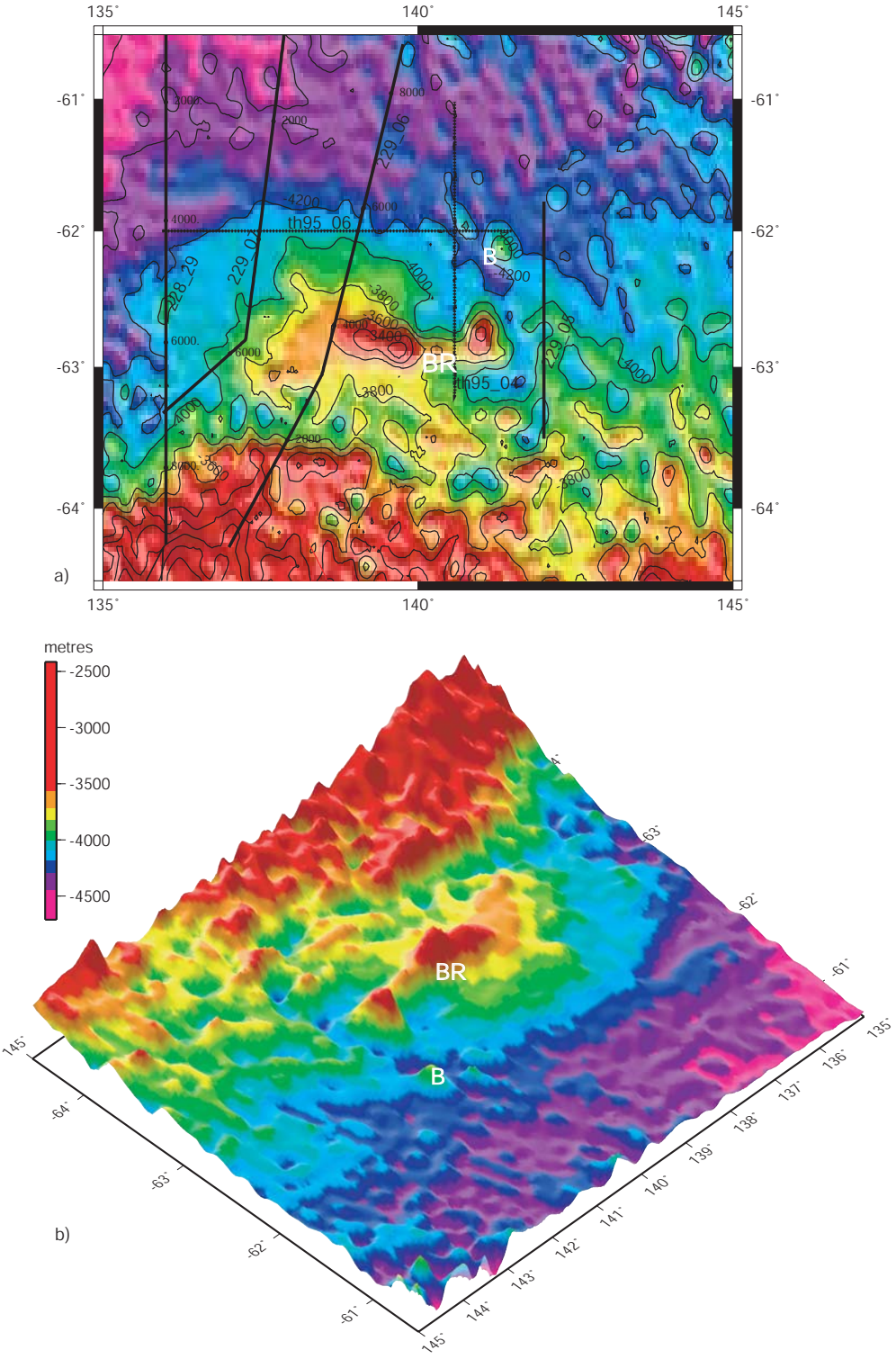


Figure 4.24: Bathymetry detail of the east Wilkes Land margin in a) map and b) perspective view. An east-west trending basement ridge (BR) and northwest-southeast trending seamounts form the seaward limit of an anomalously shallow region. B is seamount B as defined by Yuasa *et al.* [1997]. Bathymetry data from Smith & Sandwell [1994].

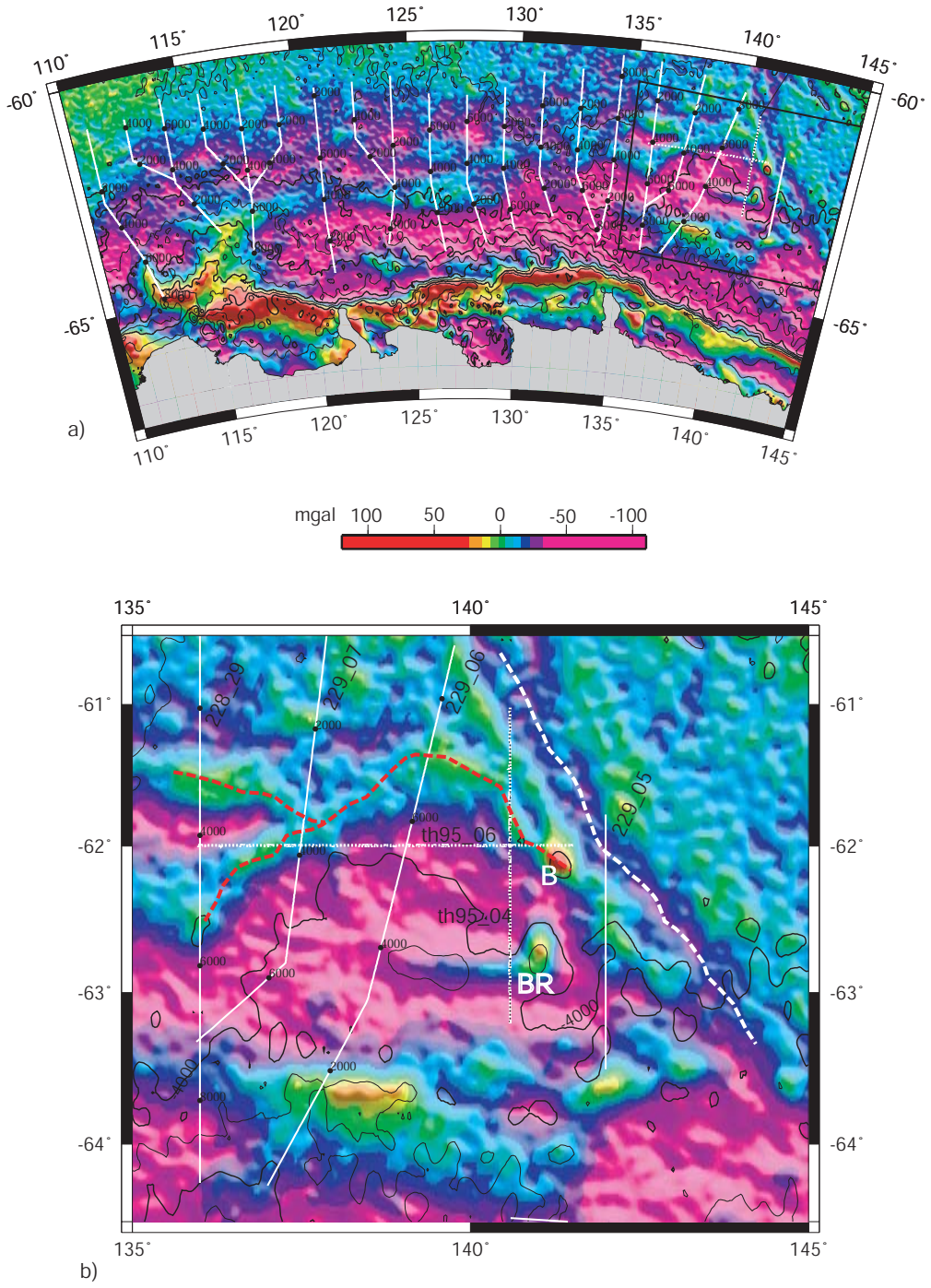


Figure 4.25: Free air gravity anomaly data overlain with bathymetry contours for a) the Wilkes Land margin, and b) the region of anomalous bathymetry off east Wilkes Land. The free air edge effect anomaly is disturbed off east Wilkes Land in the region of the basement ridge (BR) and shallowed bathymetry. B is seamount B as defined by Yuasa *et al.* [1997]. White dashed line traces the northwest-southeast trending fracture zone(?). Red dashed line traces belt of positive free air anomalies associated with outcropping or sediment covered seamounts/basement highs.

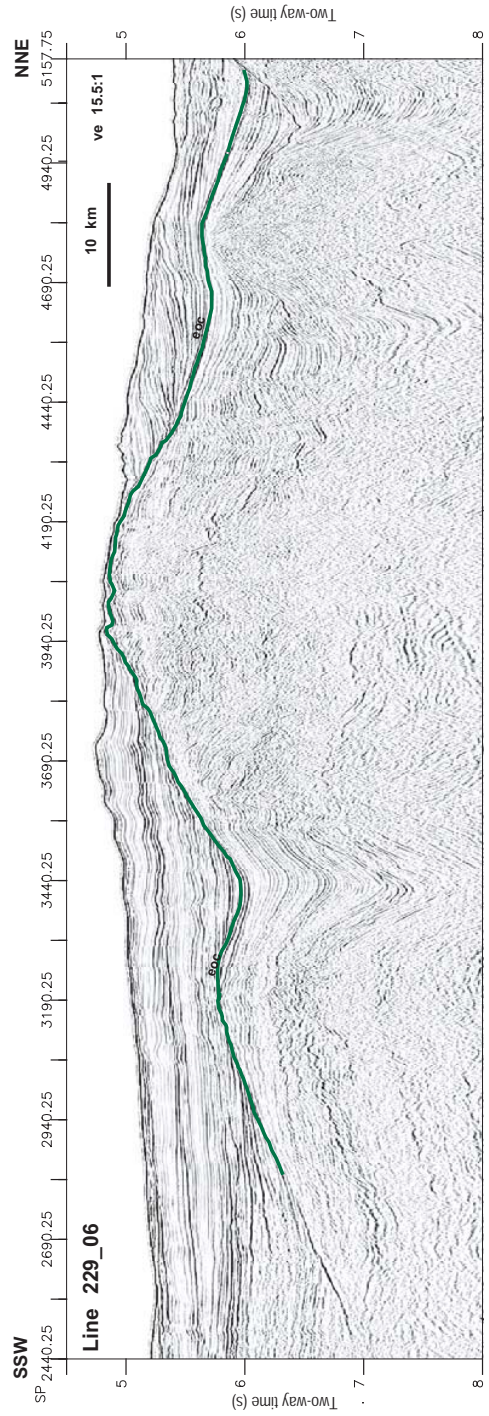


Figure 4.26: Detailed section of Line GA-229_06. The *eoc* horizon is marked for reference. Reflector geometry and structure beneath the *eoc* horizon are typical of structured sedimentary/metasedimentary rocks and precludes the possibility that the underlying crust is oceanic.

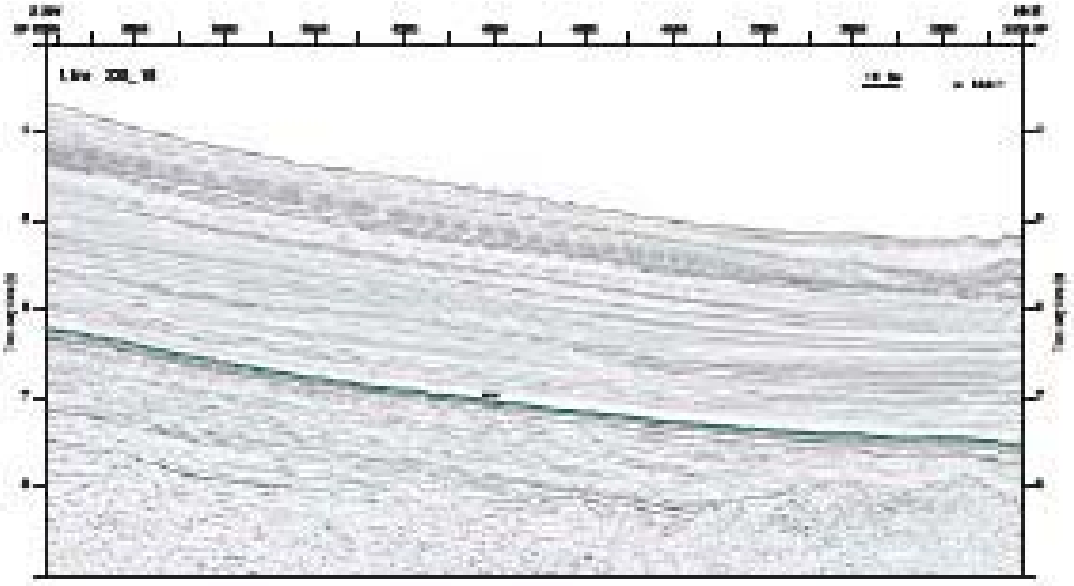

## 4.12 Sediment Distribution

Compilation of post-rift sediment thickness, based on the identification of the *tur* and *eoc* horizons, provides the first regional sediment isopach for the Wilkes Land margin, Figure 4.28. Although data is located on lines separated by up to 90 km, gridding of the two-dimensional sediment thickness data provides insight into the broad-scale sediment distribution. A previously unrecognised major sedimentary basin is identified off west Wilkes Land, we label this basin the Budd Coast Basin (BCB). The BCB comprises a delta and glacial sourced sediment thickness of greater than 5 s TWT (∼9 km). The volume of sediments within this basin is comparable to the major river deltas of other continents, such as the Niger and Amazon deltas.

The Sequence 2 isopach illustrates a sediment depocentre off west Wilkes Land, and a secondary, minor depocentre off east Wilkes Land. Central Wilkes Land is characterised by a thin veneer of sequence 2 sediments. The total sediment isopach demonstrates that total sediment distribution is primarily a function of variation in sequence 1 thickness. The distribution of the thickest sequence 1 sediments is distinctly asymmetric, seaward of ∼64°S the axis of thickest sediments is deflected west to east. This distinct west to east asymmetry of the BCB indicates that deep marine processes have been an important control on sediment transport and deposition on the East Antarctic margin since at least the onset of regional Antarctic glaciation. The locus of thickest sediments occurs offshore of the termination of the Totten glacier, one of the widest and highest velocity, 'fast-flow features' [Bamber *et al.*, 2000] in East Antarctica. This indicates that major ice-streams and/or flowing glaciers may be very long lived despite observations of short term (<100 years) changes in glaciomorphological features [Domack & Anderson, 1983].

The contrast in post-rift sediment volumes between sequences 1 and 2 indicates a significant change in rates of onshore erosion and sediment transport to the Wilkes Land margin. The onset of temperate-glacial climatic conditions are likely the catalyst for the much greater volumes of sequence 1 sediments. This is supported by the relative absence of Tertiary sediment on the southern Australian margin [Totterdell *et al.*, 2000], where no glaciation has occurred. If this assumption is true, then the majority of the sequence 1 thickness has been deposited since the onset of glacial conditions at ∼34 Ma. Further, as the current polar-glacial conditions can be observed to be relatively static in terms of erosion and sediment transport, we can attribute the majority of the sediment flux to have occurred prior to stable, frozen-base, glacial conditions. ODP results from the continental rise offshore from Prydz Bay show a seven-fold reduction in sedimentation rates (70-10 m/My) in the late Miocene (∼9 Ma), relative to peak sedimentation rates in the early Miocene [Cooper & O'Brien, in press]. This reduction is interpreted to indicate

close to peak glacial conditions being reached. Extrapolating the regional importance of this event suggests that the majority of Wilkes Land sedimentation occurred from ~34-9 Ma.

To infer sedimentation rates for the ~34-9 Ma interval it is necessary to estimate the thickness of sediments deposited between the *eoc* unconformity and the onset of glaciation, and since the late Miocene stabilisation of glacial extent. No unconformity or stratigraphic horizon can be recognised in regional MCS transects to be representative of glacial onset. Hence, sedimentation rates for the *tur-eoc* interval were extrapolated to 34 Ma to determine the thickness of post-*eoc* sediments not attributed to glacial erosion and/or transport. Sedimentation rates since the late Miocene of 20-25 and 10 m/My have been reported from DSDP 269 (east Wilkes Land) and ODP 1165 (Prydz Bay) sites respectively. However, this is likely to be higher during times of glacial expansion.

On the basis of the above, it is not likely that more than 250-500 m of post-*eoc* sediments is younger than late Miocene. Restricting the post-*eoc* sediment thickness, using these simple assumptions, provides an estimate of the 34-9 Ma interval sediment thickness for GA-228 survey lines that traverse the locus of thickest sediments; lines 18, 19 and 20. A thickness of 5-6 km of sediment is inferred for these lines.

Using the interval and thickness outlined above, sedimentation rates of between ~160-200 m/My are inferred for the Budd Coast Basin (BCB). This average is comparable to modern rates observed in the temperate glaciers of the Gulf of Alaska [Powell, 1984]. However, peak sedimentation rates achieved during times of glacial expansion are likely much higher than the 25 Ma average. Alley *et al.* [1989] modelled sediment flux rates of 100-1000 $m^3$/yr per metre width of the grounding line for Antarctic wet based glaciers, these rates are orders of magnitude higher than typical glacial sedimentation rates [Powell, 1984] and the average sedimentation rate determined here for west Wilkes Land. The peak rates modelled by Alley *et al.* [1989] could only be sustained for short periods and would overwhelm all other sources of sediment [Eittreim *et al.*, 1995].

The estimated total volume of BCB sediments (assuming a baseline sediment thickness of 2 km) is 450,000 $km^3$. This is comparable to the volume of the Niger Delta (500,000 $km^3$, Hospers [1965]), and greater than the volume of the Amazon Cone (140,000 $km^3$, Watts [2001]). The Amazon Cone is located on the passive rift margin of northern Brazil and formed between the Miocene and the present, ~100 Ma after rifting [Kumar, 1978]. Similarly, the BCB formed in a time interval of ~25 Ma, some 50 Ma after rifting. Hence, both the Amazon Cone and BCB represent massive loads on old, tectonically subsided, passive rift margins.

The locus of thickest sediments within the BCB occurs offshore of the Totten Glacier discharge region of west Wilkes Land. The Totten Glacier is one of the widest, fast-flow

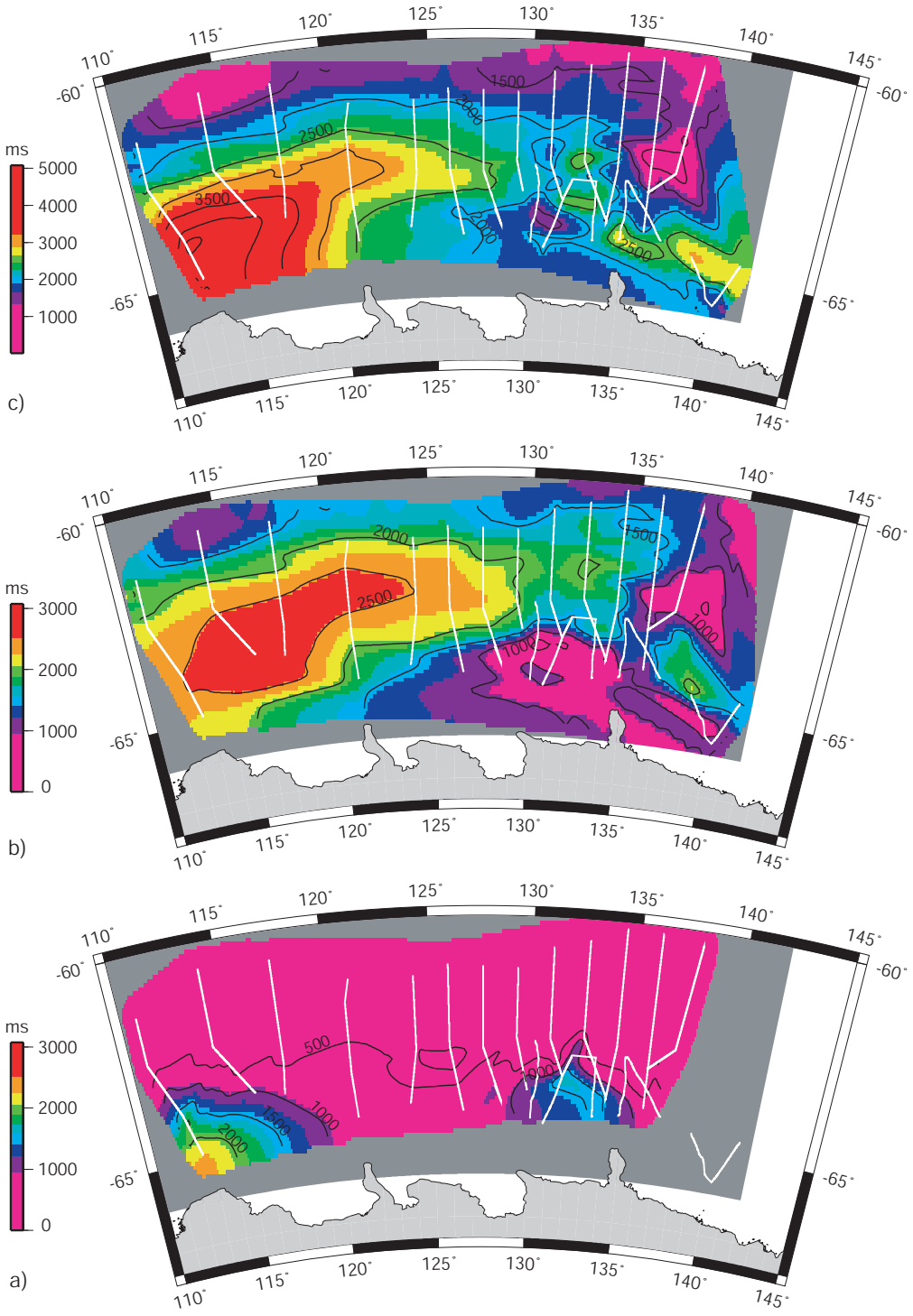


Figure 4.28: Two-way-time isopachs for a) sequence 2, b) sequence 1, and c) total post-rift sediment thickness. White lines indicate line data used in gridding. Note that isopach (c) is plotted with a different scale for improved resolution of spatial distribution.

features (outlet glaciers or ice-streams) in East Antarctica [Bamber *et al.*, 2000]. Bamber *et al.* [2000] model a peak discharge velocity of almost 800 m/y, and average velocities of greater than 50 m/y are inferred for glacier sections over 200 km wide. Analysis of the bedrock topography of the Wilkes Land interior (BEDMAP project, Lythe *et al.* [2000]) suggests that the catchment area of the Totten Glacier includes the Aurora Basin, a major depression that may be, at least in part, an erosive feature. The spatial correlation of thick offshore sediments and the Totten Glacier provides evidence that some fast-flow features maintain relatively static discharge points on long time scales (>10 My).

The west to east asymmetry of the axis of thickest sediment off Wilkes Land indicates a long-lived, marine transport process. Lateral, deep-water currents on the East Antarctic margin are interpreted as the most likely mode of along margin sediment transport. We infer that west to east deep-water currents existed for most (if not all) of the interval from ∼34-9 Ma. Measurements of bottom current velocity off the Wilkes Land margin, however, indicate an east to west direction for the geostrophic current south of ∼65°S [Bindoff *et al.*, 2000], and show no consistent trend in the deeper waters of the continental rise and abyssal plain. The only strong eastward current noted by Bindoff *et al.* [2000] occurs between 90-100°E, just south of the southern boundary of the Antarctic Circum-polar Current (ACC), where a recirculation of the westward slope current and a weak cyclonic gyre is suggested. The absence of a modern analogue current to that inferred from the distribution of Miocene sediments indicates a change in ocean circulation patterns around East Antarctica since the late Miocene.

Although the initiation of the ACC is interpreted to have occurred soon after the opening of the Tasman Gateway and Drake Passage between 34-29 Ma, the bottom water currents important in Southern Ocean and global ocean circulation likely only date back in their current (or approximately current) form to ∼9 Ma, when the ice sheet began to stabilise towards its current configuration. Therefore, palaeo-current direction could have been in the opposite sense prior to the influence of bottom water associated with continental glaciation, and these palaeo-geostrophic-currents could have provided the required transport mechanism. A second possibility is that the ACC existed south of its modern latitude range (50-60°S), from ∼34-9 Ma, and was the primary agent for the observed sediment distribution. The narrower Antarctic-Australia ocean basin and more southerly latitude of the Tasman Gateway [Lawver & Gahagan, 2003] could have forced the ACC far enough south such that it deflected the down-slope transported turbid sediment to the east off the Wilkes Land margin.

Sedimentary structures, such as wavy bedforms, do indicate the presence and influence of along margin, deep water currents. However, it is not possible to infer an absolute direction or timing of onset of these currents from two-dimensional transects of

the sedimentary section. A number of features within the post-rift sediment sequence are discussed and analysed in detail in a later section.

## 4.13 Sedimentary Structures

Dynamic depositional environments on the Wilkes Land margin are indicated by the range of sedimentary structures and lateral facies changes observed in MCS data. Features common to other sectors of the Antarctic margin, such as levee and channel structures, sediment drifts and mounds, and sediment waves, are evident. Down-slope gravitational and lateral-current induced forces are inferred to exert varying amounts of influence over depositional environments. Long lived, erosion-deposition cycle features, comparable to enigmatic reflectors reported by Rebesco *et al.* [1997], are imaged in fine detail. Bottom simulating reflectors (BSR) are also evident below the continental slope and rise on a number of lines.

### 4.13.1 Sediment Waves

Wavy bedforms are recognised in varying forms and extent along the Wilkes Land margin. The thickest and most longitudinally extensive sequence of migrating sediment waves yet discovered occurs off west Wilkes Land, Figure 4.29. This sequence is over 1.5 s TWT (∼1.5-2 km) thick and extends for ∼100 km from the continental rise to the abyssal plain. Migrating sediment waves are generally regarded as a primary indicator of contour-current deposition [Damuth, 1979]. Sediment waves in this sequence appear to migrate up-slope, however, as they are imaged in two dimensions, it is not possible to absolutely determine their direction of migration. Donda *et al.* [2003] report that sediment wave crests on channel levees observed off east Wilkes Land are generally parallel with the bathymetric contours and appear to migrate up-slope.

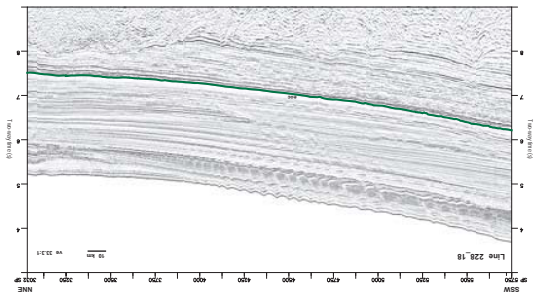

Figure 4.29: Thick sequence of sediment waves from Line GA-228_18. Waves appear to be climbing up-slope.

Contour and geostrophic currents flow in a broadly margin parallel sense, which is

grossly east-west or west-east for Wilkes Land. If the observed sediment waves formed under the influence of contour current, it suggests a long-lived (>10 My - assuming sedimentation rates derived above) interaction between deep current systems and sediment discharge from the west Wilkes Land margin. Although the presence of long lived west to east contour currents is indicated by the observed sediment distribution, the geometry of the sediment waves does not support construction due solely to west to east (or east to west) current flow.

Migrating sediment waves identical to those created by contour currents have been observed on the levees of large deep-sea channels [Embley & Langseth, 1977] and on levees of deep-sea fan valleys [Damuth, 1979], in regions interpreted to have been absent of strong or long lived contour currents. Migrating waves on channel levees, in the absence of contour currents, suggest that the channel overflow of down-slope, turbidity currents create these bed forms also. A second plausible source of down-slope currents on the Wilkes Land margin is Antarctic bottom water (ABW). ABW is saline, dense and particulate rich water produced on the Antarctic continental shelf in response to sea-ice formation [Eittreim *et al.*, 1972], it then spills over the shelf break and down the continental slope and rise. This suggests a possible alternative mode of genesis, not associated with contour currents, for sediment waves observed off west Wilkes Land. Normack *et al.* [1980] suggest that sediment waves associated with down-slope turbidity currents exhibit a down-slope decrease in amplitude, this trend is evident in this sequence of sediment waves off west Wilkes Land.

The occurrence of sediment waves in the upper-most sedimentary sequence, and the consistent form of these bedforms throughout the sequence, indicates that the genetic processes producing these bed forms have been continuous and are maintained in modern times. Whereas, comparison of modern bottom current directions and those inferred from pre-Pliocene sediment distribution indicates a change in ocean circulation patterns around the Wilkes Land margin. This ambiguity in current directions through time and the stratal patterns identified (i.e. up-slope migration and increasing amplitude) indicate that the turbidity overflow mode of genesis is more likely to represent the primary control on the observed pattern of sediment waves. This does not discount some influence from laterally flowing contour currents. Swath bathymetry of the region would allow the areal extent and true geometry of this sediment wave field to be determined, and the importance of the contrasting influences of contour current and gravity driven turbid flow to be established. If a diagonal migration direction is identified in three-dimensional data, then a contour current influence is likely.

Despite the large thickness of sediment waves imaged on Line 18, adjacent lines show little (west) or no (east) evidence of such bed forms. This is interpreted primarily as a

function of line location in relation to morphology. Whereas Line 18 traverses the ridge of a sediment levee adjacent to a major channel, adjacent lines to the east (Lines GA-228_19 and GA-228_20) are located on the flanks of levee structures, Figure 4.30. This suggests that whether their genesis is contour current or turbidity flow related, migrating sediment wave formation is also a function of morphology in glacimarine, turbidite fan systems.

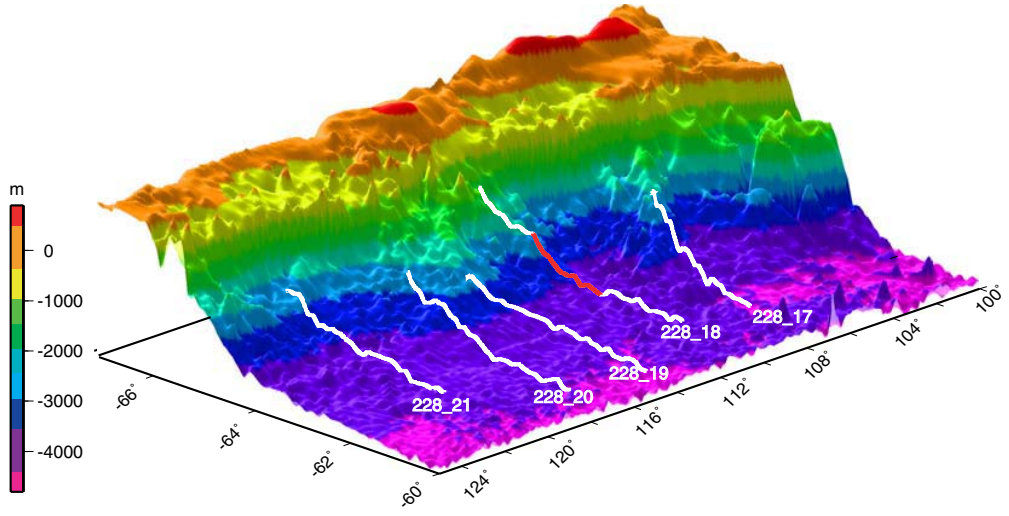


Figure 4.30: Perspective view from the northeast of the west Wilkes Land margin. The laterally isolated occurrence of the thick sequence of sediment waves on Line GA-228_18 (location marked in red) may, in part, be a function of physiography.

### 4.13.2 Deep, Stacked-Channel Reflections

Strong, concave reflectors are imaged on a number of lines off west Wilkes Land, e.g. Line GA-228_20, SPs 6000-7500. These reflectors occur at varying depths and on different scales, however, they share common, characteristic stratigraphic patterns. The gross geometry of these features closely resembles the enigmatic reflectors (labelled X by Larter *et al.* [1997]), identified west of the Antarctic Peninsula. Rebesco *et al.* [1997] consider the possibility that the reflectors represent bottom-current erosion, however, they reject this interpretation due to the magnitude (>1500 m) of erosion required at abyssal depths. Their favoured interpretation suggests that the reflectors represent the traces of local, diachronous hiatuses of limited temporal extent associated with the migration of abyssal currents.

We propose an alternative origin of formation for these reflectors, based on meso-scale stratigraphic relationships, involving palaeo-channel surfaces. Detailed analysis reveals that not all reflectors terminate down-dip against this 'apparently' cross-cutting reflector

surface, Figure 4.31. This suggests the reflector represents a migrating facies change from channel to overbank deposits, and comprises a 'stack' of erosional unconformities. The channel fluctuates through stages of erosion and deposition, presumably depending on the magnitude of individual turbidity currents. This removes the requirement that 1500 m of erosion occurs during a single interval and does not necessarily require bottom current erosion, the two main factors that Rebesco *et al.* [1997] used to argue against an erosional genesis.

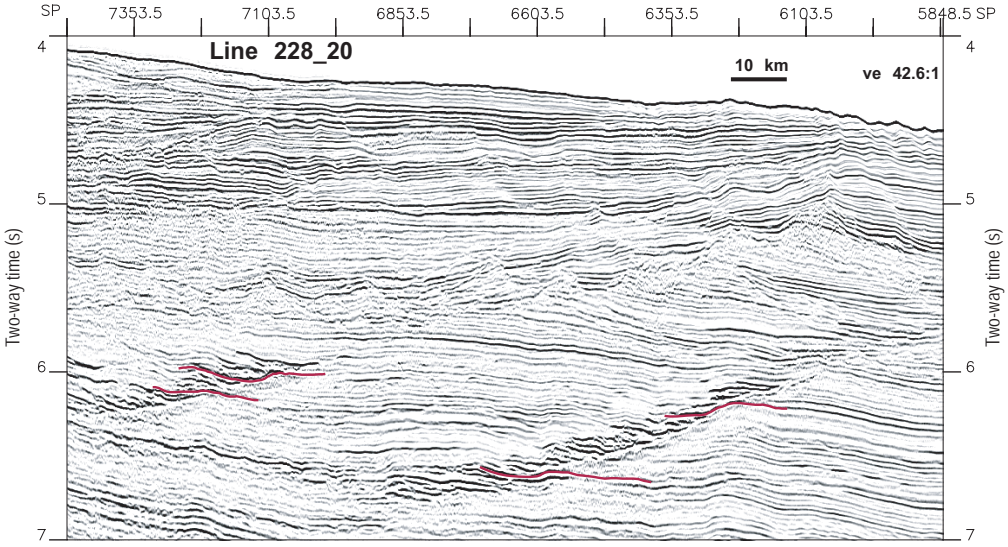


Figure 4.31: Enigmatic reflectors that appear to cross-cut the stratigraphy on Line GA-228_20. This detailed section illustrates the continuity of reflectors (e.g. red form lines) across this 'apparent erosive surface'.

The possibility that reflectors such as these represent low-angle gravity-induced slip surfaces is not supported by these data. Reflector offset, an expected association with structural, or gravity-slip origins is not evident. The erosional and onlap patterns also preclude a structural origin.

### 4.13.3 Multi-Scale Slumping

Three very large slump deposits are identified on the Wilkes Land margin that extend over 200 km from the base of the continental slope. These deposits exhibit a relatively transparent acoustic character and variably rough, unconformable, lower boundaries. One of these deposits is recognised as a lobe deposit, formed at the edges of a laterally spreading slump on the lower rise. The flow-axis deposit of two other slumps are also recorded from the slope to the lower rise, these deposits contains large slide blocks. Large slumps are known on almost all continental margins and also around oceanic islands,

however, they have not been reported previously on the Wilkes Land margin.

The slump-lobe deposit imaged on Line GA-228_18 exhibits a relatively conformable (i.e. only minor erosion of underlying strata) lower contact. The deposit reaches a maximum thickness of ~250 m and extends for over 50 line kilometres. It is not possible to determine the direction of propagation from this two dimensional transect or its farthest extent from the base of the continental slope.

Much more chaotic slump deposits are imaged on Lines GA-228_21 and GA-228_24. The deposit identified on Line 21 extends for over 200 km, achieving a maximum observed thickness of ~350 m at more than 100 km from the base of the continental slope. The lower contact of this deposit is rough and strongly erosive. The upper surface is also very rough and exhibits angular surface reflections from large blocks entrained by the slump. This slump clearly evidences a high-energy, and large volume displacement of sediment from the continental shelf or upper continental slope.

Smaller-scale, channel-bank slump deposits are also evident in the submarine fan system that exists on the Wilkes Land margin. Figure 4.32 illustrates a reflector interpreted as a low-angle failure surface where the sense of failure is oblique to the survey line direction. Chaotic reflector geometries are observed within channel bank and levee deposits and around palaeo-channels, where gravity-induced sediment slumping has occurred. Such processes have clearly been an almost continuous process through the life of the fan system.

### 4.13.4 Bottom Simulating Reflectors

Bottom simulating reflectors (BSR) are observed in MCS data on the Wilkes Land margin. They typically occur at sub-seafloor depths of ~500-700 m and represent a major change in reflector amplitude. Reflector amplitudes decrease significantly below BSR, e.g. Lines GA-228_18 and GA-228_20. BSR are recognised in many marine environments where they are commonly interpreted as the basal boundary of frozen gas hydrates. We interpret Wilkes Land BSR as representative of a diagenetic, silica phase transition. Prydz Bay ODP site 1165 results Cooper & O'Brien [in press] document a transition from sediments with diatoms (opal-A) above 606 m below sea level (mbsl), to sediments with silicified horizons (inferred opal-CT and/or chert) below this depth.

Corresponding to the depth of this silica transition are abrupt shifts in downhole logging measurements such as velocity, density, porosity and resistivity Cooper & O'Brien [in press]. The physical changes associated with this diagenetic transition cause the change in reflector amplitude noted in MCS data. The depth at which the transition occurs is a function of temperature and the ratio of terrigenous to biogenic silica concentrations,

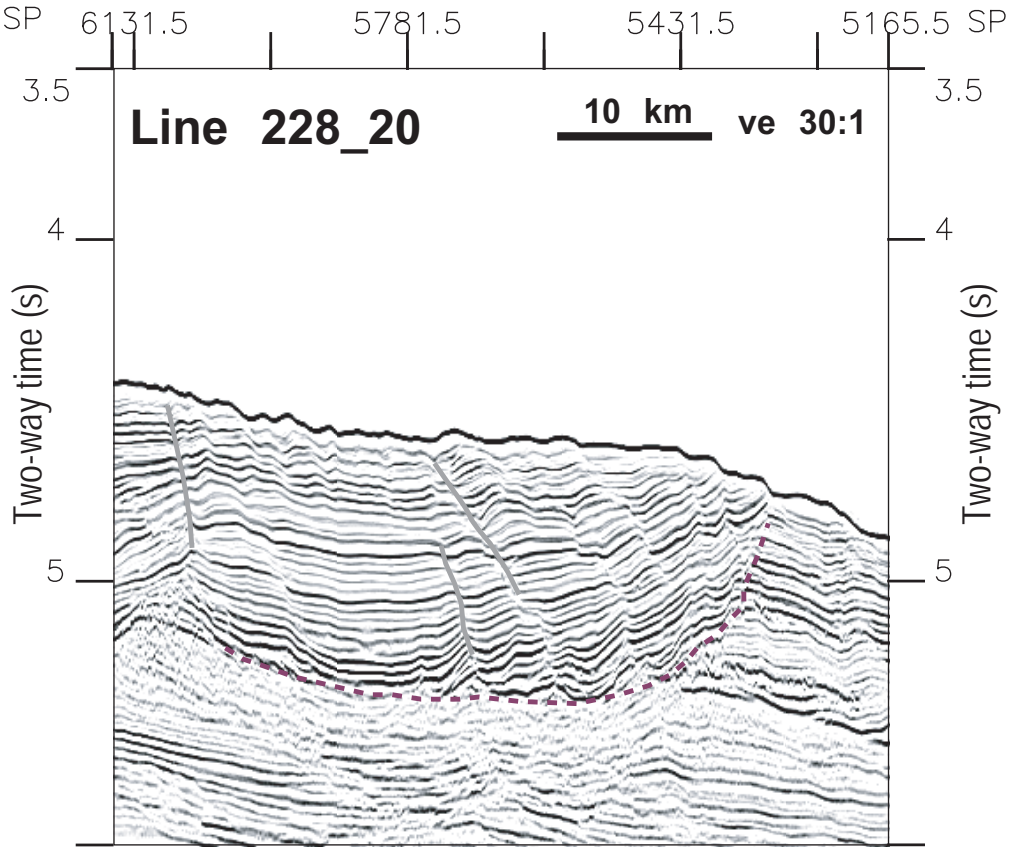


Figure 4.32: Reflector offsets along this low-angle surface (dashed form line) are interpreted as out-of-plane slumping. The surface is, in part, controlled by the location of the bottom simulating reflector which marks the change in reflector amplitude at ∼5.2 s TWT.

with higher temperatures and biogenic silica advancing the transition. The primary controls on the distribution of the BSR is unclear for the extent of the margin. Production of biogenic silica is observed to be greater on the continental rise of Prydz Bay relative to the continental slope and shelf so changes in the BSR reflectivity down dip are expected, however, the controls along strike of the margin are unclear.

Volpi *et al.* [2003] recognise the BSR as a decollement surface for slumps and slides off the Antarctic Peninsula. Evidence of this is seen off west Wilkes Land also, where we see a coincidence of the BSR and a low-angle slump surface, Figure 4.32.

## 4.14 Depth Conversion and Horizon Extrapolation

The horizons interpreted in MCS data were converted from TWT to depth using smoothed stacking velocity grids, as discussed in Chapter 3. Although the velocity models are pri-

marily based on stacking velocities derived from semblance analysis, constraints from sonobuoy refraction velocities were considered where available.

The interpretation of post-rift sediment thickness provides a crucial constraint in the geometry of gravity models in Chapter 6. However, the constraints on this thickness are limited landward of the lower continental slope. Therefore, it is necessary to extrapolate the landward extent of the *tur* and *eoc* horizons to create complete gravity models and allow the free air edge-effect anomaly to be modelled. These horizons were extrapolated in depth, so as not to require depth conversion where any velocity model would be unconstrained. Some constraint on horizon geometry was provided by data from JNOC surveys off west Wilkes Land, however, the central Wilkes Land sector extrapolations are largely unconstrained. The landward geometry of sequences 1 and 2 can be constrained for east Wilkes Land, from Lines GA-228_25 to GA-229_06, using ATC82 (IFP) and L184 (USGS) survey data.

An assumed zero post-rift sediment thickness at the Wilkes Land coast line provides a further constraint. This assumption is valid as outcrop on this Antarctic margin sector comprises almost entirely cratonic metamorphic rocks. The geometry of the extrapolated sediment thickness and line drawings of the interpreted, depth converted horizons for GA-228 Lines GA-228_18 to GA-228_29 are illustrated in Figures 4.33 and 4.34. These depth-sections provide geometrical constraints for gravity modelling in Chapter 6.

## 4.15 Summary

Seismic reflection data have allowed the architecture of the Wilkes Land rifted margin to be imaged and interpreted. On the basis of seismic character and velocity structure the limits of unequivocal continental and oceanic crust, and an interleaving zone of continent-ocean transition have been mapped. However, the location of a COB within the transition zone remains equivocal, on the basis of seismic data alone it can not be further constrained.

Regional sediment isopachs indicate a massive sediment load on the Wilkes Land margin. Most of this sediment is interpreted to have been deposited during a period of massive continental erosion and sediment transport, in response to a period of long-lived polythermal glaciation. The distribution of sediment along the margin suggests deep-marine currents have also been important in sediment transport on the Wilkes Land margin.

Through correlation with data from the conjugate Australian margin, age constraints are placed on major unconformities recognised within the sedimentary sequence. Relative age constraints are also inferred on the basis of seismic interpretation. For example, the

evidence of extension and deformation at later times in the Adélie Rift Block relative to central and west Wilkes Land. However, to further constrain the age of breakup between Antarctica and Australia, and to attempt to locate the COB, magnetic anomaly data must be analysed and correlated to seismic reflection data.

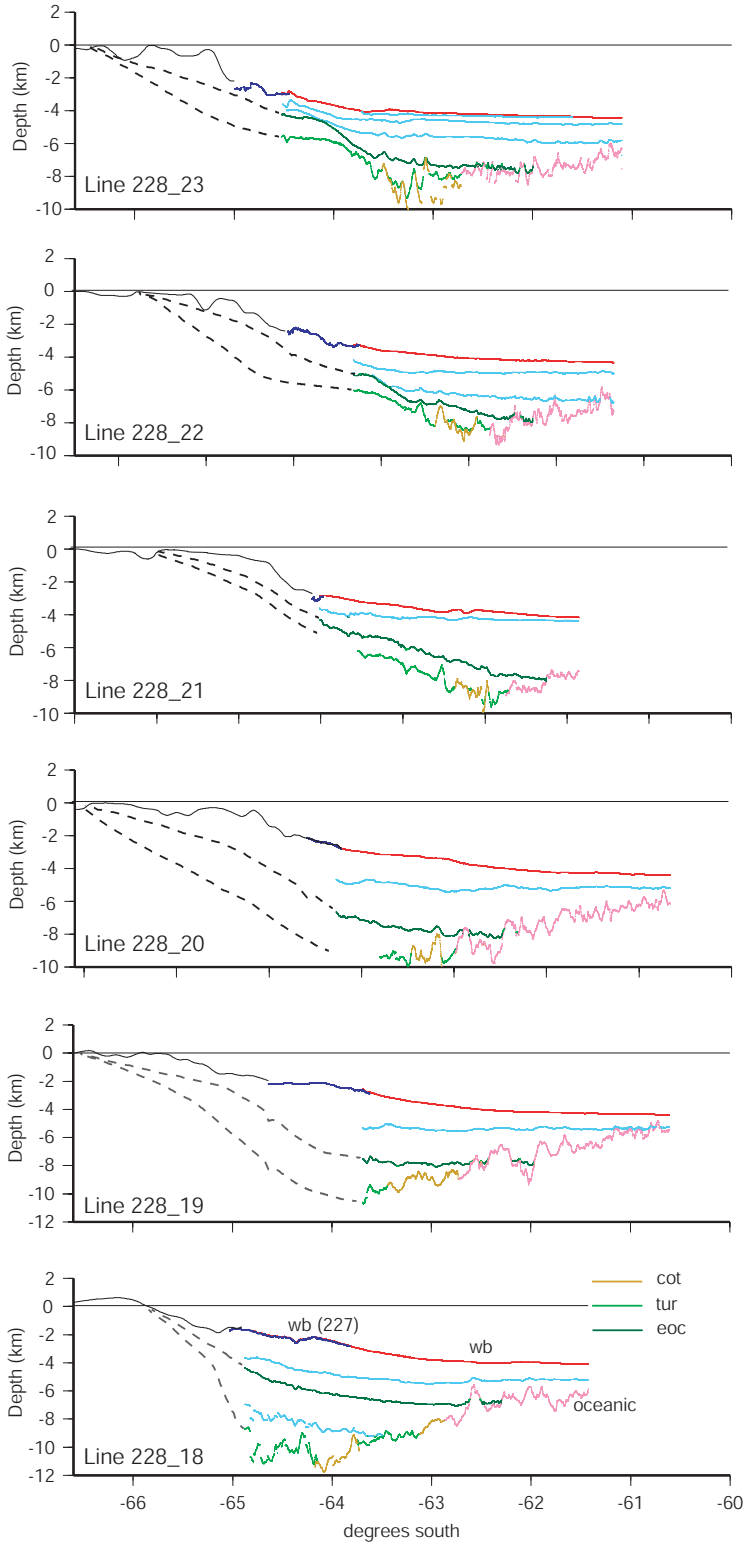


Figure 4.33: Line drawings of seismic reflection profiles GA-228_18 to GA-228_23 in depth. These sections provide constraints on the geometry of gravity models. Dashed black lines illustrate the extrapolated *eoc* and *tur* horizons.

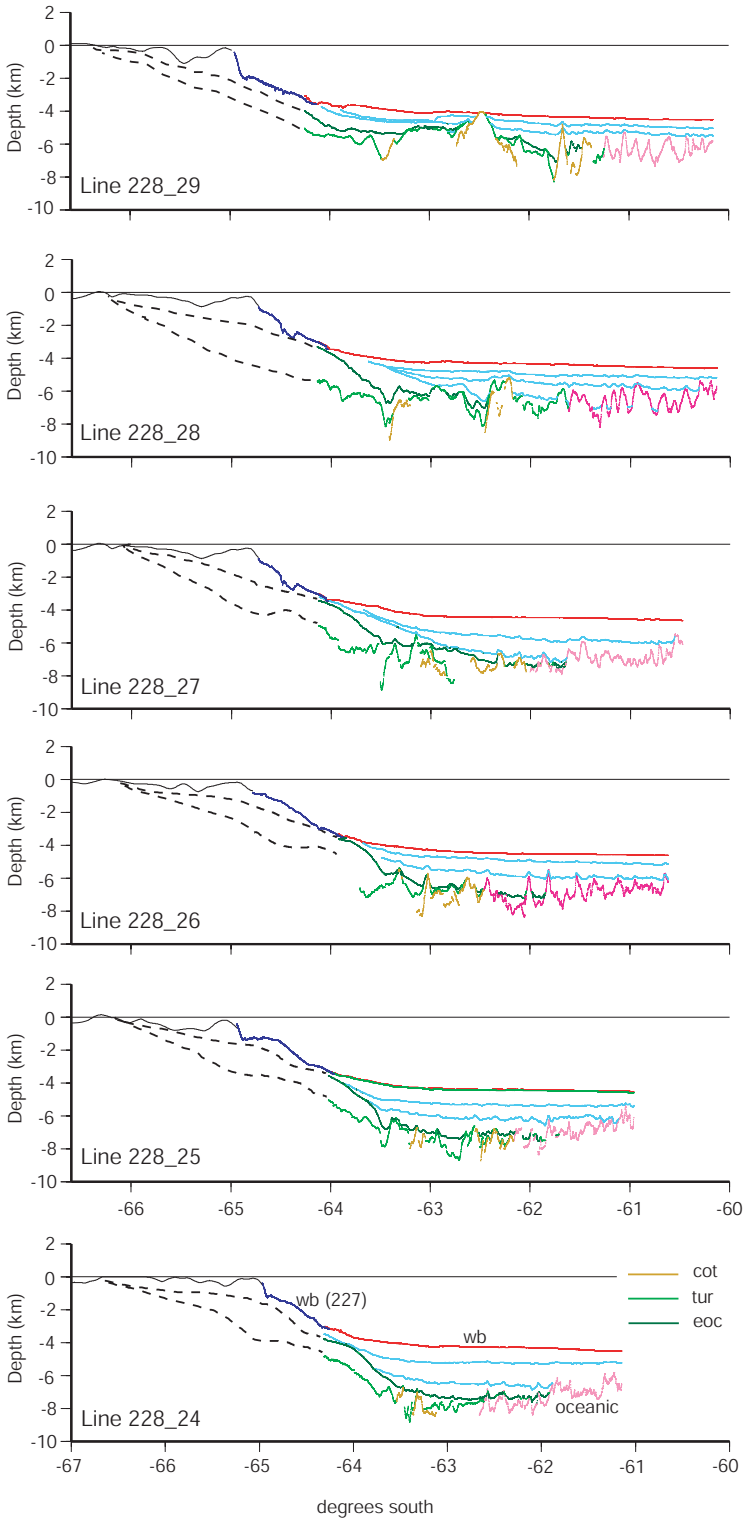


Figure 4.34: Line drawings of seismic reflection profiles GA-228_24 to GA-228_29 in depth. These sections provide constraints on the geometry of gravity models. Dashed black lines illustrate the extrapolated *eoc* and *tur* horizons.